

Visualization of cGMP signaling in the prostate

INAUGURAL DISSERTATION

submitted to the Faculty of Biology and Chemistry
in fulfillment of the requirements for the Doctoral degree (Dr. rer. nat)
of the Faculties of Medicine and Biology
of the Justus-Liebig-University Giessen

by

Robert Kügler

Meißen, Germany

Giessen (2018)

From the Institute of Anatomy and Cell Biology

Signaling group: Prof. Dr. Ralf Middendorff

Faculty of Medicine

Justus-Liebig-University

(External) Supervisor and Committee Member: Prof. Dr. Ralf Middendorff

(Internal) Supervisor and Committee Member: Prof. Dr. Adriaan Dorresteijn

Committee Member: _____

Committee Member: _____

Date of Doctoral Defense: __ / __ / ____

This study was funded by the Deutsche Forschungsgemeinschaft (DFG) Grant GRK 1871 and funding from Monash University, Australia, to the International Research Training Group (IRTG), a collaboration between Justus-Liebig-University Giessen and Monash University.

Project 6: “Hormonal regulation of cGMP pathways in the prostate - Impact for sperm transport”, R. Middendorff (Giessen), G. Risbridger, S. Ellem, R. Taylor (Monash)

“One, remember to look up at the stars and not down at your feet.
Two, never give up work. Work gives you meaning and purpose and
life is empty without it. Three, if you are lucky enough to find love,
remember it is there and don't throw it away.”

Stephen Hawking

Dedicated to my beloved ones

List of abbreviations

ANP	atrial natriuretic peptide
ArKO	estrogen-deficient aromatase knockout mouse
AROM ⁺	aromatase-overexpressing mouse
BNP	brain natriuretic peptide
BPH	benign prostatic hyperplasia
CNP	C-type natriuretic peptide
cGMP	cyclic guanosine monophosphate
DAB	3,3'-Diaminobenzidine
DAG	diacylglycerol
dNTP	deoxyribonucleotide triphosphate
DHT	dihydrotestosterone
GC-A	guanylyl cyclase type A
GC-B	guanylyl cyclase type B
G α / β / γ	G protein subunit α / β / γ
IP ₃	inositol-1,4,5-triphosphate
LUTS	lower urinary tract symptoms
MAPK	mitogen-activated protein kinase
MEM	minimum essential medium
MLC	myosin light chain
NO	nitric oxide
PBS	phosphate-buffered saline
PDE5	cGMP-specific phosphodiesterase type 5
PKC	protein kinase C
PKG I	cGMP-dependent protein kinase I
PLC	phospholipase C
RIMS	refractory index matching solution
sGC	soluble guanylyl cyclase
SMA	smooth muscle actin
SMC	smooth muscle cell
TUR-P	transurethral monopolar electroresection of the prostate

List of figures

Fig.1: Gross anatomy of the rat prostate	9
Fig.2: Gross anatomy of the human prostate	10
Fig.3: Noradrenaline mediated signaling pathways in prostatic SMCs.....	14
Fig.4: cGMP signaling pathway in prostatic SMCs	15
Fig.5: Dissection of the rat ventral prostate	27
Fig.6: Seeding template for human prostatic interstitial cells	30
Fig.7: General histology of the rat ventral prostate (serial sections).....	44
Fig.8: Virtual reconstructions of rat prostate glands.....	45
Fig.9: Virtual reconstruction of the mouse prostate glands	47
Fig.10: PDE5 expression within the rat prostatic vasculature	48
Fig.11: General histology of the human prostate.....	50
Fig.12: Visualization of human prostatic SMCs.....	51
Fig.13: SMCs of the human prostatic vasculature	52
Fig.14: Analysis of contractility of rat prostate glands.....	53
Fig.15: Analysis of contractions of rat prostatic ducts	54
Fig.16: Analysis of contractility of human prostate tissue	55
Fig.17: Analysis of contractions of prostatic vasculature in rats.....	56
Fig.18: Adult vs. postnatal architecture of the rat ventral prostate.....	58
Fig.19: PKG I regulation by testosterone deprivation in rats	59
Fig.20: cGMP-dependent Protein kinase I regulation in the prostate of ArKO, WT and AROM+ mice	61
Fig.21: cGMP-dependent Protein kinase I regulation in peri-glandular and vascular SMCs of ArKO, WT and AROM+ mice.....	62
Fig.22: Characteristics of human prostatic interstitial cells.....	63
Fig.23: qPCR of cGMP pathway components in human prostatic interstitial cells	64
Fig.24: Proliferation of prostatic SMCs in human BPH patient and rat prostate tissue	66

List of tables

Tab.1: Human-specific primer descriptions	31
Tab.2: Template for qPCR loading	32
Tab.3: Template for qPCR conditions.....	32
Tab.4: Hydrogel and buffer composition for tissue clearing.....	36
Tab.5: RIMS buffer composition for optical clearance enhancement.....	37
Tab.6: Lysis buffer for cell break down	39
Tab.7: Gel and buffer composition for gel electrophoresis.....	39
Tab.8: Buffer composition for nitrocellulose transfer.....	40

Contents

List of abbreviations.....	II
List of figures	III
List of tables.....	IV
Contents.....	V
1 Introduction	8
1.1 From gross anatomy to histology	8
1.1.1 The rodent prostate	8
1.1.2 The human prostate	10
1.2 Growing up: morphogenesis of the prostate.....	11
1.3 Neurophysiology of noradrenaline-induced SMC contractions.....	12
1.4 Cyclic guanosine monophosphate signal transduction in SMCs	14
1.4.1 General consideration.....	14
1.4.2 PKG I, a key protein for smooth muscle contractility.....	16
1.4.3 PDE5 and its role in the prostate	16
1.4.4 Further cGMP-specific PDEs	17
1.5 Prostate pathology	18
1.5.1 Prostate cancer.....	18
1.5.2 Benign prostatic hyperplasia	20
2 Aim of the study.....	22
3 Materials & Methods.....	23
3.1 Materials.....	23
3.1.1 Devices	23
3.1.2 Kits	23
3.1.3 Consumables.....	24
3.1.4 Reagents	24
3.1.5 Inhibitors.....	26
3.1.6 Primary antibodies.....	26
3.1.7 Secondary antibodies.....	26

3.2	Methods	27
3.2.1	Tissues and Cells	27
3.2.1.1	Rodent prostate	27
3.2.1.2	Human prostate	28
3.2.1.3	Human interstitial cells	29
3.2.2	Cell culture	29
3.2.2.1	Dihydrotestosterone treatment	30
3.2.3	Real-time PCR	31
3.2.3.1	Purification of total RNA	31
3.2.3.2	First-strand cDNA synthesis	31
3.2.3.3	Primer design	31
3.2.3.4	Real-time PCR set up and conditions	32
3.2.4	(Immuno-) Histochemistry	33
3.2.4.1	Fixation and slicing	33
3.2.4.2	Azan trichrome stain	33
3.2.4.3	Immunostaining	34
3.2.5	CLARITY	35
3.2.6	Time-lapse imaging	37
3.2.7	Western Blot	38
3.2.8	Statistical analysis	41
4	Results	43
4.1	Localization of SMCs in acini and ducts of the rat ventral prostate	43
4.2	The architecture of prostatic SMCs in rat and mouse	43
4.2.1	3D reconstruction of rat prostate tissue	43
4.2.2	3D reconstruction of mouse prostate tissue	46
4.3	Prostatic vasculature in rats	48
4.4	SMCs of the human prostate	49
4.5	The 3D architecture of SMCs in the human prostate	50
4.6	Vasculature of the human prostate	52
4.7	Functional analysis	53
4.7.1	Contractility of rat prostate acini	53
4.7.2	Contraction of rat prostatic ducts	54
4.7.3	Contractility of the human prostate	55

4.7.4	Vascular contractions	56
4.8	Hormonal influences on prostatic musculature	57
4.8.1	Postnatal development of SMC architecture in rats	57
4.8.2	Castration-induced androgen deprivation in rats.....	59
4.8.3	Genetically modified mouse models	60
4.8.3.1	Aromatase models affecting both, estrogens and androgens.....	60
4.8.3.2	Localization of prostate structures showing hormone-induced PKG I regulation.....	61
4.8.4	Hormonal regulation of cGMP pathway components in men.....	63
4.8.4.1	Characterization of human prostatic interstitial cells	63
4.8.4.2	Testosterone treatment of human prostatic interstitial cells	64
4.9	Visualization of SMC proliferation.....	65
5	Discussion	67
5.1	SMCs of the human and rodent prostate	67
5.2	Localization of key proteins of the cGMP pathway.....	69
5.3	Visualization of SMC function and relaxation for BPH treatment	70
5.4	Hormonal influences on the cGMP pathway	72
5.4.1	Effects of hormonal changes due to prostatic postnatal development	72
5.4.2	Hormone deficiency-induced regulation of the cGMP pathway in rat prostate	73
5.4.3	Testosterone deficiency-induced regulation of the cGMP pathway in humans.....	75
5.5	SMC proliferation in BPH tissue	77
6	Summary	78
7	Zusammenfassung	79
8	Acknowledgment	81
9	Declaration/Selbstständigkeitserklärung.....	83
10	References	84
11	Publications, talks and posters	102
11.1	Paper	102
11.2	Talk.....	102
11.3	Poster	102

1 Introduction

The prostate form part of the accessory male sex glands and is widely conserved among all mammals. During ejaculation the prostate secretes a clear and slightly alkaline (pH 7,29) fluid in the urethra that is expelled to the seminal fluid (Ross and Pawlina 2016; Hayward and Cunha 2000). Various studies investigated the chemical composition of the prostate secretory material. Prostate secretion mainly consists of immunoglobulins, prostaglandins, carbohydrates, citrate, polyamines, proteins, acid phosphatase and ions like Zinc (Costello and Franklin 2016; Bistulfi et al. 2016; Attiga et al. 2000).

1.1 From gross anatomy to histology

1.1.1 The rodent prostate

The rodent prostate is divided into four different zones according to their location around the urethra, described as ventral, lateral, dorsal and anterior lobes (Fig.1) and invested in a thin membrane (Knoblauch and True L. 2011). The prostate lobes do not entirely encircle the urethra and consist of epithelium-lined acini surrounded by stromal matrix. Loosely embedded, the collagenous extracellular matrix contains fibroblasts, blood vessels, wandering connective tissue cells, nerve terminals, lymphatics as well smooth muscle cells (SMC) that enclose each prostatic acinus (Jesik et al. 1982).

The two ventral lobes of the rat prostate are attached to the ventral aspect of the urethra. A layer of connective tissue and a series of ducts lined with columnar epithelium drain into the urethra (Cunha et al. 1987). All (2-3) ducts are longitudinally folded with numerous closely packed layers of smooth muscle cells, alternating a longitudinal and circular arrangement and interspersed by small capillaries between the duct wall and the surrounding SMCs (Ichihara et al. 1978). Together both ventral lobes represent the largest part of the rat prostate that requires half of the entire prostate mass. Acini of the ventral lobes show typically a large degree of infolding.

The lateral prostate is localized directly beneath the seminal vesicle, which is partially overlapping the ventral lobes and dorsally blended into the dorsal lobes. 5-7 ducts are connecting the lateral lobe with the urethra, surrounded by a thick stroma. Acini of the lateral prostate show a moderate epithelial infolding.

The dorsal prostate is found just behind the attachment of the seminal vesicle and inferioposterior to the bladder. 5-6 ducts are forming a complex and extensively arborized ductal network. Compared to other lobes epithelial infoldings are reduced (Hayashi et al. 1991).

The anterior lobes, also known as coagulating glands, are directly attached to the lesser curvature of the seminal vesicles. In contrast to the other lobes, the anterior prostate is more elongated and tubular with a papillary growth pattern. Its epithelium is cuboidal to columnar and filled with eosinophilic cytoplasm (Ittmann 2017).

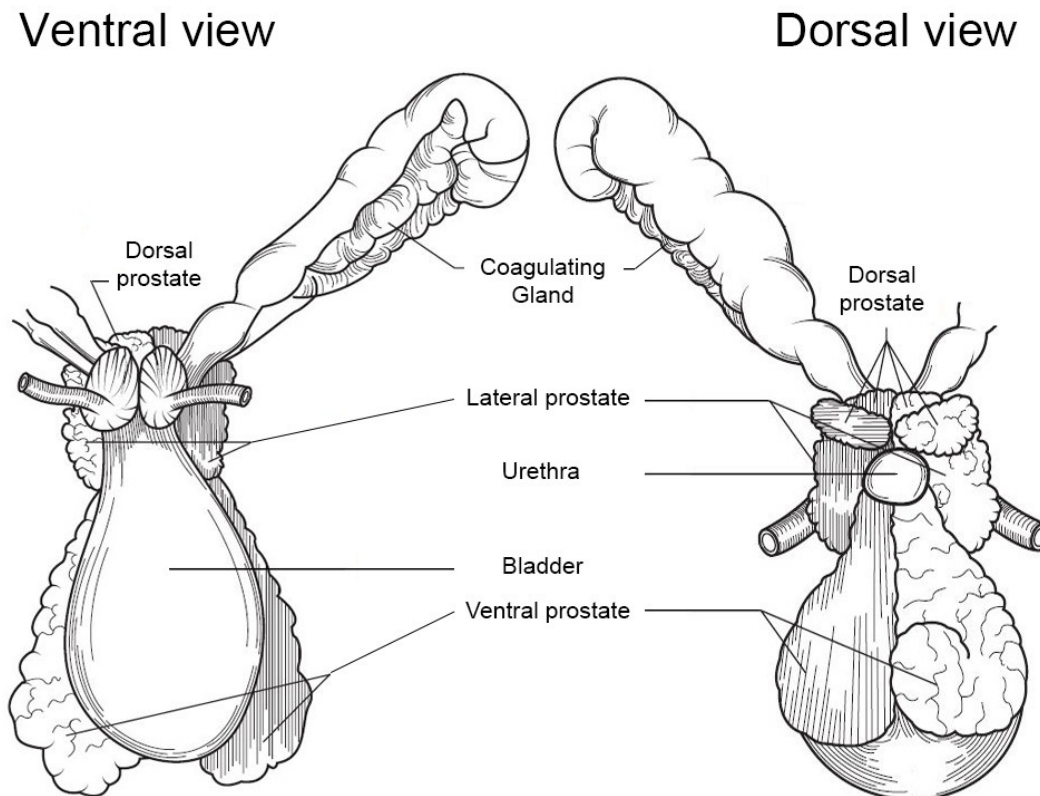


Fig.1: Gross anatomy of the rat prostate.

View in ventral and dorsal orientation. Modified from Prins and Lindgren 2015.

1.1.2 The human prostate

Considered to be the largest accessory sex gland of the reproductive tract, the prostate is mostly described to equal a walnut in form and shape, although spherical and quadrangular forms could also be found. The human prostate encloses the prostatic part of the urethra completely, inferior to the bladder. The gland consists of four different zones: central, transition and peripheral zone, enclosed by the anterior fibromuscular stroma (Fig.2). Approximately 30 to 50 tubuloalveolar glands that enter 15 to 30 excretory ducts are embedded mainly in the furrows lateral to the colliculus seminalis. Each zone exhibits a typical histology and function.

The cone-shaped central zone has its wider portion at the base of the prostate and contains around 25% of the prostate mass. This zone is found to be widely resistant to carcinoma and inflammation.

70% of the prostate mass is concentrated in the peripheral zone that ranges from the lateral to the posterior part of the prostate and surrounds the central zone. The peripheral zone is the main site of origin for prostate carcinomas.

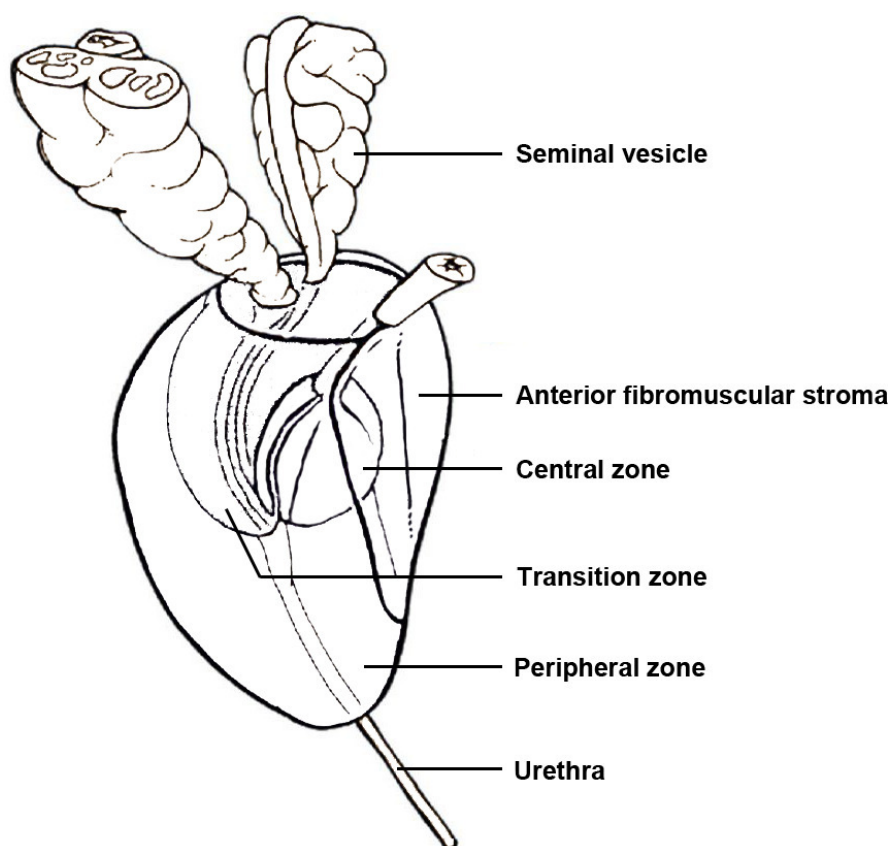


Fig.2: Gross anatomy of the human prostate.

View in sagittal orientation. Modified from Wein et al., 2011.

The transition zone occupies only 5% of the prostate tissue. Due to its close proximity to the urethra, the transition zone is capable to compress the urethra that causes painful bladder outlet obstructions, in case of benign prostatic hyperplasia (Ross and Pawlina 2016; Aumüller et al. 1979).

Human prostatic glands and ducts are lined by three types of glandular epithelium: luminal, basal and neuroendocrine cells. The fibromuscular stroma consists of numerous smooth muscle cells, interspersed with fibroblasts, nerve fibers and blood vessels. In contrast to the thin fibromuscular stroma in the rodent prostate, the human prostatic stroma is much more distinctive (Ittmann 2017).

1.2 Growing up: morphogenesis of the prostate

Because development is a continual process and not a series of defined stages, it is difficult to determine the exact time point of certain developmental stages during puberty. However, puberty is usually linked to changes in gross anatomy and/or histology, as well as hormonal changes, which is indeed very specific for men and rats (Wistuba et al. 2003). In both, the embryologic prostate develops from the endodermal urogenital sinus, different to other reproductive organs such as epididymis or seminal vesicles that originate from the mesodermal Wolffian duct (Prins and Lindgren 2015; Wolfertstetter et al. 2013). In first place dihydrotestosterone (DHT) is the predominant androgen responsible for the normal prostate development, proven by administration of 5- α reductase inhibitors, which results in malformations and abnormal prostate growth (Bowman et al. 2003; Imperato-McGinley et al. 1986). During the early stages of differentiation, estrogen action was found to be present in developing stromal cells as well as glandular epithelium (Prins et al. 1998).

Prenatally the rat prostate develops in three defined stages, known as bud stage, bud-tubular stage and acino-tubular stage. At the bud-tubular stage (around embryonic day 16), myofibroblasts of mesenchymal origin are already present co-expressing vimentin and α -smooth muscle actin (SMA). These early myofibroblasts are also visible in the human prenatal prostate (around weeks 23-25) and supposed to be precursors of smooth muscle cells and fibroblasts, the two most dominant cell types of the prostatic stroma (Shaw et al. 2008; Bierhoff et al. 1997). The last stage just finishes at postnatal day 28, reasonable for the rudimentary developed prostate at birth (Picut et al. 2018). After completion of the acino-tubular stage, prostate glands are histologically identical compared to adult ones and even

start secretion. The last step in prostate development is characterized by an overall growth in size until it reaches adult size around postnatal day 43 to 46, which continues even after sexual maturity (Dreef et al. 2007).

Development of the human prostate starts earlier compared to rat, during the 2nd trimester of pregnancy and is almost finished at birth. Human prostate glands even start secretion prenatally. Initial secretion occurs at gestational week 14 and is triggered by androgens, primarily in the peripheral zone, whereas the central zone undergoes squamous metaplasia. Primordia of the prostate gland appear at gestational weeks 10 to 12, forming epithelial outgrowths (prostatic buds) The surrounding stroma differentiate from mesenchymal cells and form a lamina propria of the primitive glands (Kellokumpu-Lehtinen 1985). The fetal prostate consists of five anatomical lobes described as anterior, posterior, middle and two lateral lobes until gestational week 20. Shortly after two lobes regress and the remaining three major prostate zones continue to develop (Lowsley 1912). All zones undergo squamous metaplasia of the tubule epithelium until birth, mediated by in utero estrogens. Due to the fact, that the human prostate is well-developed at the time of birth, postnatal changes are mainly observed during puberty, in which a rapid growth of the prostate occur caused by a pubertal surge in testosterone production (Picut et al. 2018).

The dorsolateral aspect of the urogenital sinus will develop the dorsal and lateral lobes. In contrast, the anterior prostate emerges from four large buds that grow cranially into the mesenchyme of the seminal vesicle (Cunha et al. 1987).

Prostatic ducts of the human fetus grow fast in length and branching, starting at gestational week 10. Within only three weeks, approximately 70 primary ducts emerge and secretion begins. For some time after birth, the second period of ductal growth occurs during puberty, similar to glandular development (Brechka et al. 2016; Cunha et al. 1987).

1.3 Neurophysiology of noradrenaline-induced SMC contractions

Numerous fibers of the autonomic nervous system permeate the prostate. In human, the innervation is ensured by the plexus prostaticus, which originates from the plexus hypogastricus inferior. The extensive nerve supply of the human prostate exhibits the greatest density of nerve fibers in the proximal central aspect, followed by the distal prostate and anterior capsule, whereas the innervation of the periphery is very sparse (Chapple et al. 1991).

Long postganglionic nerve fibers follow and innervate prostatic blood vessels. Smooth muscle cell innervation is mediated by short postganglionic fibers. Cell bodies within the ganglia of those fibers are in close proximity to the prostate, characteristic for male accessory glands in contrast to other organs, innervated by the sympathetic adrenergic nerve system (Spring-Mills and Hafez 1980).

In both, men and rodents the two divisions of the autonomic nervous system play its own role during normal prostate physiology. Stimulation of the cholinergic parasympathetic system mediates secretion of the prostatic fluid, whereas the noradrenergic sympathetic division is responsible for the expulsion of the fluid into the urethra (Prins and Lindgren 2015; Marinese et al. 2003). The sympathetic catecholamine noradrenaline operates as a neurotransmitter and activates $\alpha 1$ -adrenoceptors for smooth muscle contraction during emission (Tong et al. 1996; Lepor et al. 1990).

To ensure contractions in prostatic SMCs, polymerized actin needs to be available as filaments that anchor to the cell membrane and myosin light chain (MLC) need to be phosphorylated. MLC phosphorylation is increased by activation of MLC kinase or inhibition of MLC phosphatase (Somlyo et al. 1999).

Activation of $\alpha 1$ -adrenoceptors triggers three well-known signaling cascades: calcium, protein kinase C and Rho kinase-mediated ones (Fig.3). In addition, $\alpha 1$ -adrenoceptors stimulation releases receptor-associated, heterotrimeric G proteins from their receptors. G proteins typically contain a larger $G\alpha$ subunit, next to its smaller β and γ subunits.

The $G\alpha$ subunit is responsible for the activation of GTPase RhoA and phospholipase C (PLC) that mediates the formation of the second messengers inositol-1,4,5-triphosphate (IP_3) and diacylglycerol (DAG) via hydrolyzation of phosphatidylinositol-4,5-bisphosphate (Somlyo and Somlyo 2000). IP_3 , on the one hand triggers a massive intracellular increase of Ca^{2+} (by the opening of Ca^{2+} channels in the sarcoplasmic reticulum) that binds to Ca^{2+} dependent calmodulin, which is necessary for the calmodulin-dependent MLC kinase to increase the MLC phosphorylation (Hennenberg et al. 2014). DAG, on the other hand induces MLC phosphorylation by activating isoforms of protein kinase C (PKC) that inhibit MLC phosphatase. The third way of action uses RhoA and Rho kinase for inhibition of MLC phosphatase that finally causes SMC contraction (Christ and Andersson 2007).

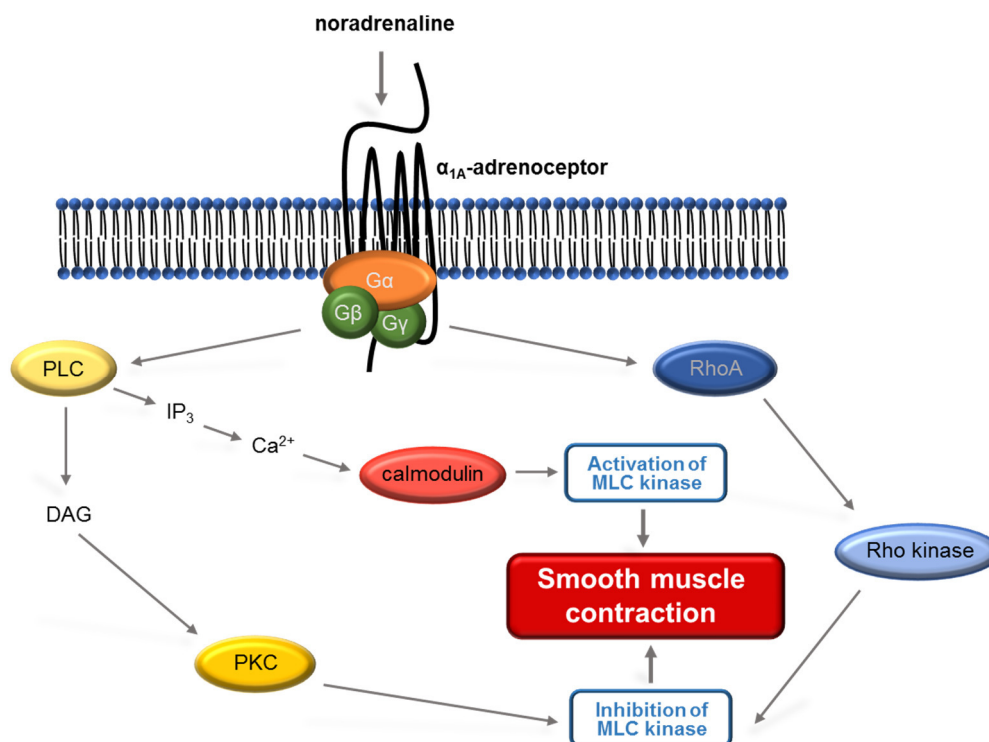


Fig.3: Noradrenaline mediated signaling pathways in prostatic SMCs.

Activation of α_1 -adrenoceptors mediates smooth muscle contraction by one of three well-known signaling pathways: protein kinase C (PKC), Rho kinase or calcium. (DAG) diacylglycerol; ($G\alpha,\beta,\gamma$) G proteins subunit α , β , γ ; (IP_3) inositol-1,4,5-trisphosphate; (MLC) myosin light chain; (PLC) phospholipase C; (RhoA) ras homolog gene family, member A. Modified from Hennenberg et al., 2014.

1.4 Cyclic guanosine monophosphate signal transduction in SMCs

1.4.1 General consideration

The importance of signaling pathways using cyclic guanosine monophosphate (cGMP) as second messenger is clearly stated among various investigations, facing certain aspects of prostate pathology (Peak et al. 2016; Liu et al. 2016; Peixoto and Gomes 2015; Lythgoe and McVary 2013). Amongst others cGMP pathways are involved in neurotransmission, smooth muscle contractility as well as proliferation (Hofmann et al. 2006). Within the prostate, cGMP is produced by natriuretic peptide membrane receptors with guanylyl cyclase (GC) activity, known as GC-A and GC-B (Fig.4).

Binding of the cardiac hormones atrial natriuretic peptide ANP or BNP to GC-A respectively CNP to GC-B activates the synthesis of cGMP. In addition a soluble form of GC (sGC) exists, using nitric oxide (NO) for activation that is generated by NO synthases. In either case, guanosine triphosphate is converted to guanosine monophosphate by reduction of pyrophosphate (Wedel and Garbers 2001).

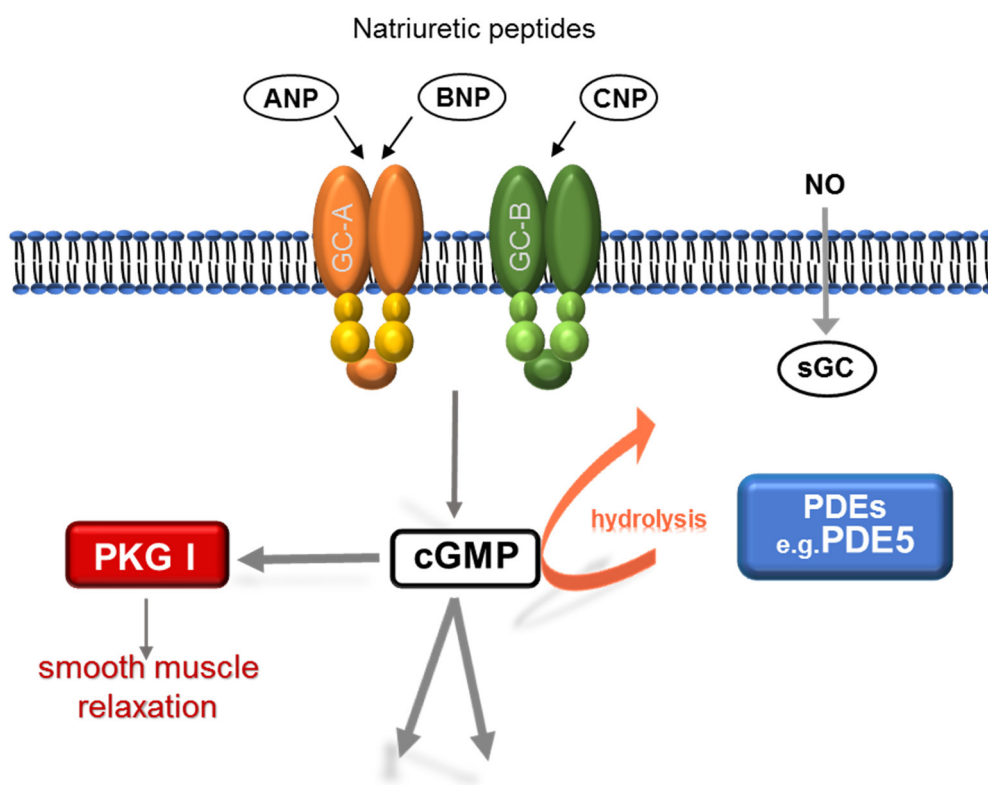


Fig.4: cGMP signaling pathway in prostatic SMCs.

The second messenger cGMP is produced by one of three types of guanylyl cyclase (GC). sGC uses nitric oxide (NO) to induce cGMP synthesis while GC-A and GC-B are activated by binding of natriuretic peptides (ANP, BNP, CNP). The intracellular amount of cGMP is regulated by hydrolysis of phosphodiesterases (PDEs). cGMP activates the cGMP-dependent protein kinase I (PKG I) to mediate smooth muscle relaxation.

The amount of intracellular cGMP is regulated by phosphodiesterases (PDE), with PDE5 representing a crucially implicated subtype, that mediates cGMP degradation over hydrolysis (Ghofrani et al. 2006). Finally, contractions of SMCs are initiated via activation of the cGMP-dependent protein kinase I (PKG I), one of the cGMP target proteins (Müller et al. 2011).

It is assumed that PDE5 expression is directly influenced by androgens (Seftel 2005). Upregulation of PDE5 expression was found together with a downregulation of PKG I protein level in Leydig cells of the rat testis after two weeks of testosterone treatment (Andric et al. 2010). These observations were only visible in treated animals but lack significant results at the cellular level. Therefore, cell culture experiments would have provided a system that is less influenced by other regulatory factors or cellular structures.

1.4.2 PKG I, a key protein for smooth muscle contractility

Usually, protein kinases modulate their targets by catalyzing the transfer of phosphates to certain amino acids such as serine, threonine or tyrosine that induce conformational changes or changes of the target function (Roskoski 2015). They are highly ubiquitous, vary in function and target over 30% of all cellular proteins (Tulis 2017).

The cGMP-dependent protein kinase I, in particular, belongs to the serine/threonine kinase family and is targeted with high affinity by cGMP. PKGI consists of three functional domains. The C-terminal catalytic domain comprises the MgATP- and peptide binding pocket. The N-terminal domain features a leucine-isoleucine zipper motif, while the regulatory domain contains tandem cGMP-binding sites (Fiedler et al. 2006).

However, the exact mechanism of action that finally results in smooth muscle relaxation after activation of PKG I is still unclear (Haynes and Cook 2006). It seems plausible, that stimulation of PKG I maintain the opening of large conductance Ca^{2+} activated K^+ channels or ATP-sensitive potassium channels (Beech 1997; Alioua et al. 1995). Both events may lead to hyperpolarization of the cell membrane and closure of voltage-gated Ca^{2+} channels. Furthermore, intracellular levels of Ca^{2+} in vascular smooth muscle cells are regulated by another PKG I action, which lead to phosphorylation of the sarcoplasmic reticulum protein phospholamban (Cornwell et al. 1991). All of this events would finally prevent the phosphorylation of MLC, a classic signaling pathway of noradrenaline-induced contractility, as described earlier (Haynes and Cook 2006).

1.4.3 PDE5 and its role in the prostate

PDEs consist of 11 families of enzymes that are able to break phosphodiester bonds. PDE5 is described as cGMP-specific phosphodiesterase (McAllister-Lucas et al. 1993). Regulating the intracellular level of cGMP, PDE5 is essential for various physiological processes and therefore plays a key role as a target enzyme for the treatment of lower urinary tract symptoms (LUTS) and benign prostatic hyperplasia (BPH) (Lin et al. 2013). Nowadays PDE5 inhibitors, namely tadalafil are approved for BPH treatment. Knowledge about the mechanism of action of PDE5 inhibition is primarily investigated for smooth muscle tone reduction in case of treatment for erectile dysfunction, pulmonary hypertension and BPH (Gacci et al. 2016; Uckert et al. 2008). PDE5 inhibitors induce smooth muscle relaxation through blocking the degradation of cGMP, which leads to an increase of intracellular cGMP. This in turn,

activates a cascade of enzymes including PKG I and results in prostatic SMC relaxation, as described earlier. Especially the duration of cGMP action is regulated by PDE5, which plays an important role in the modulation of oxygenation, inflammation, proliferation and nerve activity, besides smooth muscle relaxation (Kügler et al. 2018; Gacci et al. 2016; Juilfs et al. 1999). In addition, vascular SMC relaxation may improve blood flow to the lower urinary tract (Carson et al. 2014).

In both, rodent and human prostate tissue, the exact localization of PDE5 is still under discussion. Early studies of the human prostate state PDE5 expression to be present in glandular and subglandular areas of the transition zone, predominantly in glandular regions and less in stromal parts (Uckert et al. 2006; Uckert et al. 2001). Later investigations of the transition zone suggest PDE5 localization in smooth muscle cells of the prostate glands, co-localized with its substrate cGMP (Uckert et al. 2013; Giuliano et al. 2013), but not in the epithelium (Fibbi et al. 2010). Furthermore, PDE5 expression in the human prostatic vasculature is shown for the endothelial and smooth muscle layer of the vesicular-deferential artery (Morelli et al., 2011). PDE5 localization in rat prostate is even more controversial. Some reveal PDE5 immune reactivity exclusively within the fibromuscular stroma (Zhang et al. 2015), in contrast to findings that show the gland epithelium positively stained together with their surrounding SMCs (Wang et al. 2015b). Expression of PDE5 in rat prostatic blood vessels is reported for vascular SMCs embedded into the tunica media (Peuler and Phelps 2015). However, none of the previous studies had focused on PDE5 expression in SMCs of the prostatic ducts alone, separated from those of the prostate glands. Taken this into account could be a crucial factor in BPH treatment, especially since a typical negative side effect of other BPH therapeutics, such as α 1-adrenergic blockers, is abnormal and decreased ejaculation (Kügler et al. 2018; Kaplan 2009; Chapple 2004).

1.4.4 Further cGMP-specific PDEs

Apart from PDE5, PDE6 and PDE9 also specifically hydrolyze cGMP with high affinity. PDE6 plays an important role as a key component in the visual transduction cascade by regulating the amount of cGMP in rod and cone photoreceptor cells of the retina. This was demonstrated by mutations of the PDE6 β gene in mouse rod cells that causes an intracellular increase of the cGMP level of those cells (Wen et al. 2014; Bowes et al. 1990). Interestingly, PDE6 knockout mice develop fully functional retina and reproduce normally (Zhang et al. 2014). Outside the retina, subtypes of the PDE6 are present in lung and its vasculature, as well

as human embryonic kidney (Murray et al. 2003). In addition, PDE6 expression found in human alveolar epithelial cells could provide a potential target for the treatment of idiopathic pulmonary fibrosis (Nikolova et al. 2010).

PDE9 targets cGMP with the highest affinity among all PDE families. Until now only one isoform, PDE9 α is known. Knockout of PDE9 in mouse resulted in a reduction of the body weight, body fat and insulin resistance. Inhibition of PDE9 increases the cGMP level in the central nervous system together with an increased learning and memory capability (Deninno et al. 2009; van der Staay et al. 2008; Liu et al. 2008). Other tissues that express PDE9 are kidney, lung, liver and heart (Keravis and Lugnier 2012). In isolated myocytes of the human heart, PDE9 was found to regulate cGMP signaling apart from the nitric oxide pathway and is considered as a possible target in case of stress-induced heart diseases (Lee et al. 2015).

1.5 Prostate pathology

1.5.1 Prostate cancer

Prostate cancer is noticed to be the second most frequent cancer among men worldwide (Bruinsma et al. 2017). Estimates state that 1.1 million new cases have occurred in 2012 with the highest incidence rates in developed countries such as Australia/New Zealand, Northern America and Europe (Torre et al. 2015). Predictions for 2030 expect that the global incidence of prostate cancer will increase by 1.7 million and death increase by 0.5 million (Ferlay et al. 2010). Due to this, prostate cancer represents tremendous health and economic burdens (Wang et al. 2018).

In most cases (around 70%) prostate cancer develops from the peripheral zone. Approximately 10-20% emerges from the transition zone and only 1-5% arises from the central zone (Pizzuto et al. 2018). On a cellular basis, it is widely accepted that adenocarcinoma of the prostate arises from the epithelia of the glands. The prostatic epithelium consists of basal and luminal cells, interspersed with some neuroendocrine cells and is surrounded by stroma cells, such as (myo-) fibroblasts, smooth muscle cells, vascular endothelial cells or nerve fibers that transmit signals for epithelium regulation (Tyekucheva et al. 2017). Studies in mouse suggested at least three different prostate epithelial progenitor populations but were not able to clarify which one induces prostate cancer (Ousset et al. 2012; Wang et al. 2009). Apart from the proliferative epithelial component of the gland, stromal cells are more and more suspected to contribute to carcinogenesis and cancer progression

(Tuxhorn et al. 2002b; Olumi et al. 1999). However, inflammatory myofibroblastic tumors of the prostate are extremely rare as only two cases have been reported since 2012 (Zeng et al. 2018).

Another rare type of prostate cancer is known as (intra-) ductal carcinoma, a malignant epithelial proliferation that arises from primary periurethral prostatic ducts (Böttcher et al. 2018; Baig et al. 2015). Ductal carcinomas are reported to be quite aggressive due to high Gleason score, advanced tumor stages, biochemical relapse and distant metastasis (Chen et al. 2015; Kimura et al. 2014; Watts et al. 2013).

Non-metastasized cancer is often removed by either radical prostatectomy or radiation therapy. Common long-term side effects of both therapies are incontinence and impotence, often treated with PDE5 inhibitors (Prins and Lindgren 2015). Apart from that, administration of the PDE5 inhibitor sildenafil was observed during growth and metastasis of human prostate cancer cells, inoculated in a nude mouse model. Even daily sildenafil administration did not promote primary tumor growth or metastasis (Qian et al. 2003). However, the cGMP producing enzyme sGC was also shown to mediate prostate cancer cell proliferation, regulated by androgens (Cai et al. 2007). Because cGMP signaling pathways are known to regulate cell proliferation and therefore contribute to tumor development, therapeutics based on cGMP pathway components might not be a rewarding option (Bian and Murad 2014).

Other strategies to slow cancer development are associated with regulation of sex hormones. Androgen deprivation therapy initially stops the progression of prostate cancer, but often turns into an androgen-independent disease that progress after 12 to 36 months (Green et al. 2012; Crawford et al. 1989). There is also strong evidence of estrogens been involved in carcinogenesis and cancer progression, mediated by in situ estrogen production and estrogen receptor signaling (McPherson et al. 2010; Ricke et al. 2008). However, regulation of the intra-prostatic androgen and estrogen level may interact with certain cGMP pathway components, influencing the efficacy of those potential treatment targets.

1.5.2 Benign prostatic hyperplasia

Second to prostate cancer, benign prostatic hyperplasia (BPH) represents the other main growth disorder in the prostate affecting approximately 50% of men at the age of 60, up to 80% of men at the age of 80 or older and is often associated with painful bladder outlet obstructions (van Asseldonk et al. 2015). The transition zone is reported as the main site of origin for prostatic hyperplasia, whereas the central zone is considered to be BPH resistant (Prins and Lindgren 2015). However, prostatic enlargement is a true hyperplastic and not a hypertrophic process, which means a net increase in cell number, not cell size (McNeal 1990). This increase in cell number is assumed to be a result of epithelial and stromal proliferation respectively impaired programmed cell death that finally cause cellular accumulation (Roehrborn 2008). In primarily small-resected glands a predominance of the fibromuscular stroma was clearly shown (Shapiro et al. 1992). Another study demonstrated that the relative amounts of SMCs and fibroblasts in the human prostate are increasing with old age and presence of BPH (Sensibar et al. 1999). This study also revealed a BPH-related increase of growth rate in cultured human prostate SMCs which might reflect programmed cellular responses to hormones and growth factors.

It is widely accepted, that (active) smooth muscle tone plays a major role in the pathophysiology of BPH (Roehrborn and Schwinn 2004). Muscle tone in the prostate is regulated by the adrenergic nervous system. It is suggested that the overactivity of the autonomic nervous system contributes to BPH development (McVary et al. 1994). Further studies on receptor binding demonstrated α 1adrenoceptor to be the most abundant adrenoceptor subtype present in the human prostate (Yamada et al. 1994; Lepor et al. 1993). Treatment of BPH using α 1-adrenergic blockers has proven to be a potent strategy to mediate urethral pressure reduction and to increase urine flow rate. Alpha blockers such as prazosin or doxazosin act as inverse agonists to inhibit α 1-receptors and finally reduce smooth muscle tone of the prostate and bladder neck (Kaplan 2008). But treatment with alpha blockers is associated with common side effects like disturbed ejaculation. Therefore, PDE5 inhibitors represent a potent therapeutic alternative (Kügler et al. 2018). PDE5 inhibitors such as sildenafil or tadalafil mediate reduction of detrusor muscle overactivity in the bladder neck as well as relaxation of prostatic SMCs by increasing intracellular cGMP (Filippi et al. 2007; Roehrborn 2004). In addition, vascular smooth muscle relaxation through PDE inhibition might also contribute to BPH treatment by improved blood flow (Carson et al. 2014).

Apart from humans only dogs and some primates are known to develop naturally occurring BPH (Christensen 2018). Therefore plenty of strategies are pursued to induce BPH in rats such as inbreeding of Wistar-Kyoto rats or administration of inflammatory substances like formalin, testosterone, sulpiride or even specific microbial strains as inflammation promotes the establishment of BPH. (Da Silva et al. 2018; Wang et al. 2015c; Chung et al. 2015).

However, BPH development and maintenance is furthermore associated with the occurrence of sex steroid hormones and their receptors. Androgens are in focus of interest for clinical investigations because they are considered to be involved in proliferation, differentiation, morphogenesis and functional maintenance (Wen et al. 2015). Steroid metabolism in the prostate is ensured by 5α -reductase (type II), which catalyzes the reduction of testosterone to the more potent dihydrotestosterone (DHT). 5α -reductase inhibitors are another option for BPH treatment, mediating a decrease of DHT serum level together with slow progression of clinical BPH (Parsons 2010). Other than androgens, there is increasing evidence of estrogens to be effecting important mechanisms that contribute to prostatic cell growth while the molecular mechanisms for estrogen action during BPH pathophysiology remain unclear (Lee and Kuo 2017; Nicholson and Ricke 2011).

2 Aim of the study

This study aims to reveal the cellular localization of cGMP pathway components with special focus on the cGMP degrading protein PDE5 as well as the cGMP target protein PKG I. Comparisons between rat, mouse and human prostatic tissue attempt to validate possible similarities and/or differences. For this purpose, classical immunostaining will be combined with a modified approach, based on the novel CLARITY method to gain a better understanding of the prostatic architecture.

A subsequent step will be the visualization of cGMP effects. Time-lapse imaging will be used to illustrate prostatic contractility in rat and human tissue. It is planned to investigate possible regulatory effects of the PDE5 inhibitor sildenafil in this experimental setup.

Finally, attempts will be made to analyze the underlying mechanisms and therapeutic relevance of hormone regulation in cGMP pathways, involving experiments on both, rodents and humans. For this, histological investigations will use castrated rats as well as mouse models that contain a genomic aromatase knockout or aromatase overexpression. In addition, age-dependent changes will be tested by postnatal and adult rats. For comparisons with rodent tissue, testosterone effects on isolated and cultured interstitial cells of the human prostate will be analyzed

3 Materials & Methods

3.1 Materials

3.1.1 Devices

Agarose gel electrophoresis system	PeqLab, Erlangen, Germany
Automated cell counter TC 10	Bio-Rad, Munich, Germany
Centrifuge 5804 R	Eppendorf, Hamburg, Germany
Confocal laser scanning microscope LSM 710	Zeiss, Munich, Germany
Elisa Reader	Dynatech, Denkendorf, Germany
Fluorescence microscope, Axioskop 2 plus	Zeiss, Munich, Germany
High-temperature Incubator	Heraeus, Hanau, Germany
iCycler IQ™ Real-time PCR detection system	Bio-Rad, Munich, Germany
Microscope AxioStar plus	Zeiss, Munich, Germany
Microtome, RM2255	Leica, Wetzlar, Germany
Nanodrop 2000 Spectrometer	Thermo Scientific, Waltham, USA
Nuaire™ Bench Class II together with Nuaire™ DH Autoflow CO ₂ Air Incubator	IBS Integra Bioscience, Fernwald, Germany
Polyacrylamide gel electrophoresis system	Hofer, San Francisco, USA
Power supply	Hofer, San Francisco, USA
Safety Cabinet	Koettermann, Uetze, Germany
SonoPlus mini 20 ultrasonic homogenizer	Bandelin, Berlin, Germany
Spectrophotometer, Biophotometer	Eppendorf, Hamburg, Germany
Transillumination microscope BX50WI	Olympus, Tokio, Japan

3.1.2 Kits

Amersham™ ECL WB detection system	GE Healthcare, Freiburg, Germany
Bio-Rad protein assay	Bio-Rad, Munich, Germany
EnVision ⁺ System, Peroxidase (DAB) kit	DAKO, Hamburg, Germany
GeneAmp® RNA PCR kit	Applied Biosystems, Darmstadt, Germany
Horseradish peroxidase labeled polymer	DAKO, Hamburg, Germany
iScript™ cDNA synthesis kit	Bio-Rad, Munich, Germany
Platinum® SYBR® Green qPCR SuperMix-UGD	Invitrogen, Karlsruhe, Germany
RNeasy Micro kit	Qiagen, Hilden, Germany
RNeasy Mini kit	Qiagen, Hilden, Germany

3.1.3 Consumables

Amersham™ Hybond™ -nitrocellulose membranes	GE Healthcare, Freiburg, Germany
Automat Star coverslips	Engelbrecht, Edermünde, Germany
Blue tack	Bostik, Wauwatosa, USA
Cell culture plates (6 well, 24 well, 96 well)	Greiner bio-one, Frickenhausen, Germany
Cell Scraper	BD Falcon, Heidelberg, Germany
Cell star tubes (25 ml, 50 ml)	Greiner bio-one, Frickenhausen, Germany
Delta T dish	Bioptechs, Buttlar, USA
Eppendorf tubes (0.5 ml, 1.5 ml, 2 ml)	Eppendorf, Hamburg, Germany
Filter tips	Eppendorf, Hamburg, Germany
Flasks (T75, T175)	Greiner bio-one, Frickenhausen, Germany
Parafilm	Bemis NA, Neenah, USA
PCR tubes (0.2 ml)	Eppendorf, Hamburg, Germany
Pipettes (10 µl, 20µl, 100 µl, 1000µl)	Gilson, Middleton, USA
Serological pipettes (5 ml, 10 ml, 25 ml, 50 ml)	BD Falcon, Heidelberg, Germany
SuperFrost® Plus microscope slides	R. Langenbrinck, Emmendingen, Germany
X-ray films	Fuji, Tokio, Japan

3.1.4 Reagents

2,2'-Azobis(2-methylpropionamide) dihydrochloride	Sigma-Aldrich, Steinheim, Germany
3,3'-Diaminobenzidin (DAB)	Merck, Darmstadt, Germany
4',6-Diamidin-2-phenylindole (DAPI)	Merck, Darmstadt, Germany
Acrylamide solution, Rotiphorese Gel 30	Roth, Karlsruhe, Germany
Agarose	PeqLab, Erlangen, Germany
Ammonium persulfate (APS)	Roth, Karlsruhe, Germany
AmpliTaQ DNA polymerase	Applied Biosystems, Darmstadt, Germany
Aniline blue	Merck, Darmstadt, Germany
Azocarmine	Chroma, Stuttgart, Germany
Bisacrylamide	Roth, Karlsruhe, Germany
Boric acid	Roth, Karlsruhe, Germany
Bovine serum albumin (BSA)	Sigma-Aldrich, Steinheim, Germany

Bromophenol blue	Sigma-Aldrich, Steinheim, Germany
Calcium chloride	Merck, Darmstadt, Germany
Di-sodium hydrogen phosphate	Roth, Karlsruhe, Germany
Dithiothreitol (DTT)	Invitrogen, Karlsruhe, Germany
DNAase-1	Applied Biosystems, Darmstadt, Germany
Ethanol	Riedel de Haen, Seelze, Germany
Ethylenediaminetetraacetic acid (EDTA)	Roth, Karlsruhe, Germany
Glacial acetic acid	Merck, Darmstadt, Germany
Glucose oxidase	Sigma-Aldrich, Steinheim, Germany
Glycerol	Roth, Karlsruhe, Germany
Glycerine	Roth, Karlsruhe, Germany
Hepes	Sigma-Aldrich, Steinheim, Germany
Hematoxylin	Merck, Darmstadt, Germany
Histodenz	Sigma-Aldrich, Steinheim, Germany
Hydrochloric acid	Merck, Darmstadt, Germany
Hydrogen peroxide	Roth, Karlsruhe, Germany
Isopropanol	Sigma-Aldrich, Steinheim, Germany
Magnesium chloride	Merck, Darmstadt, Germany
Methanol	Fluka, Buchs, Switzerland
Minimal essential medium (MEM)	Gibco, Invitrogen, Karlsruhe, Germany
TEMED	AppliChem, Darmstadt, Germany
Nickel sulfate	Merck, Darmstadt, Germany
Noradrenaline	Sigma-Aldrich, Steinheim, Germany
Normal goat serum	Sigma-Aldrich, Steinheim, Germany
Page ruler™ Plus	Thermo Fisher Scientific, Waltham, USA
Paraformaldehyde (PFA)	Roth, Karlsruhe, Germany
Phosphotungstic acid	Riedel de Haen, Seelze, Germany
Picric acid	Fluka, Buchs, Switzerland
Ponceau S solution	Sigma-Aldrich, Steinheim, Germany
Sigma Marker™ wide range	Sigma-Aldrich, Steinheim, Germany
Skimmed-milk	Roth, Karlsruhe, Germany
Sodium chloride	Roth, Karlsruhe, Germany
Sodium dodecyl sulfate	Roth, Karlsruhe, Germany
Sodium deoxycholic acid	Sigma-Aldrich, Steinheim, Germany

Sodium hydroxide	Merck, Darmstadt, Germany
Sodium azide	Sigma-Aldrich, Steinheim, Germany
Thimerosal	Sigma-Aldrich, Steinheim, Germany
Tris	Roth, Karlsruhe, Germany
Tri-sodium citrate dehydrate	Merck, Darmstadt, Germany
Triton X-100	Sigma-Aldrich, Steinheim, Germany
Tween 20	Sigma-Aldrich, Steinheim, Germany
Western blocking reagent	Roche, Mannheim, Germany
Xylene	Roth, Karlsruhe, Germany
β -mercaptoethanol	Sigma-Aldrich, Steinheim, Germany

3.1.5 Inhibitors

Aprotinin (trypsin inhibitor)	Roth, Karlsruhe, Germany
Leupeptin (protease inhibitor)	Roth, Karlsruhe, Germany
Phenylmethanesulfonyl fluoride (serine protease inhibitor)	Sigma-Aldrich, Steinheim, Germany
Sildenafil (PDE5 inhibitor)	Pfizer, New York, USA

3.1.6 Primary antibodies

Anti-calponin-1	Rabbit monoclonal	Epitomics, California, USA
Anti-Ki67	Rabbit polyclonal	Novocastra, Newcastle, UK
Anti-PDE5	Rabbit polyclonal	Laurinda Jaffe, University of Connecticut Health Center, Farmington, USA
Anti-PKG I	Rabbit polyclonal	Enzo Life Sciences, Lörrach, Germany
Anti-sGC (β 1)	Rabbit polyclonal	CAYMAN, Ann Arbor, USA
Anti-SMA	Mouse monoclonal	Sigma-Aldrich, Steinheim, Germany
Anti-vinculin	Mouse monoclonal	Sigma-Aldrich, Steinheim, Germany
Anti- α -tubulin	Mouse monoclonal	Sigma-Aldrich, Steinheim, Germany

3.1.7 Secondary antibodies

Goat-anti-mouse IgG	Pierce, Bonn, Germany
Goat-anti-rabbit IgG	Pierce, Bonn, Germany
Cy3 anti-rabbit IgG	Jackson ImmunoResearch, Grove, USA
Alexa Fluor 488 anti-mouse IgG	Thermo Fisher Scientific, Waltham, USA

3.2 Methods

3.2.1 Tissues and Cells

3.2.1.1 Rodent prostate

Male Wistar rats were housed at the animal facilities of the Justus-Liebig University Giessen, with access to food and water ad libitum. Rats were anesthetized with 5% isoflurane and sacrificed via cervical dislocation. According to age, animal groups were divided into adult (older than 2 months) and postnatal (day 4 to 6 after birth) rats. Subsequent preparation of the prostatic ventral lobes was performed within the next 1 to 2 hours (Fig.5). The urogenital tract containing bladder, prostatic urethra, seminal vesicles, ductus deferens and the entire prostate was removed from the rat torso and transferred to minimal essential medium (MEM) for further dissection. Removal of fat and the thin prostatic capsule was necessary to distinguish between the four different prostate lobes (Fig.5A). Ventral prostatic ducts which drain into the ventral aspect of the urethra were severed in close proximity to the urethra (Fig.5B). Distal prostate glands were separated (Fig.5C) and dissected from connective tissue. Glands and ducts were finally embedded for anatomical investigations or prepared for time-lapse imaging studies.

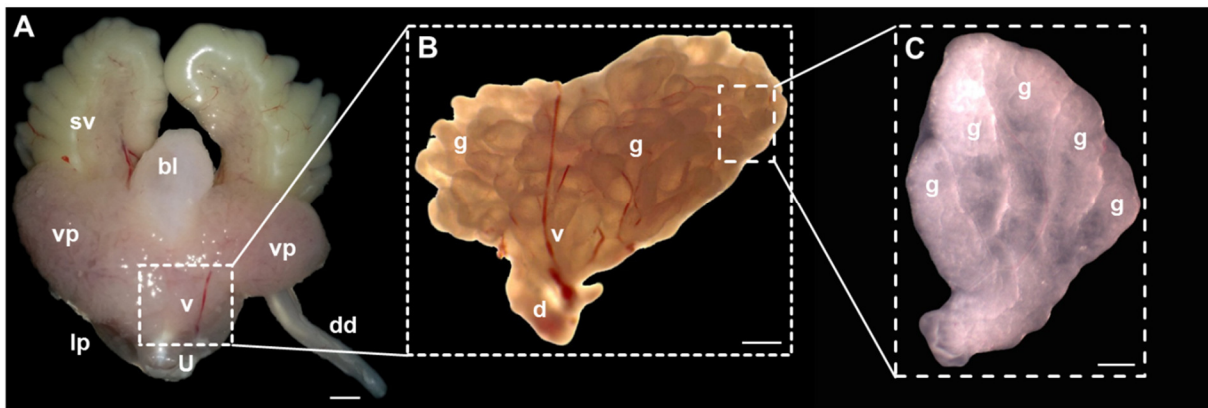


Fig.5: Dissection of the rat ventral prostate.

A: Ventral view of the lateral (lp) and ventral (vp) prostatic lobes which drain into the urethra (u) beneath the bladder (bl), seminal vesicle (sv) and ductus deferens (dd). **B:** Magnification of the left ventral lobe, highlighting prostatic ducts (d), glands (g) and blood vessels (v). **C:** Magnification of five adjacent prostatic glands. Scale bars (A) 2mm, (B) 1mm, (C) 0,5 mm

In addition, paraffin-embedded and frozen prostate tissue of genetically modified adult mice was obtained from the animal facilities of the Monash University Melbourne. The first mouse model in this study contained an aromatase knockout (ArKO) through targeted disruption of the *cyp19* gene, leading to an estrogen-deficiency in these mice. By breeding of male and female mice heterozygous for *cyp19*, homozygous aromatase $+/+$ or $-/-$ offspring was

produced. Day of birth was defined as day 0. Genotyping of male offspring was performed using tail DNA for PCR analysis (Bianco et al. 2006).

The second mouse model in this study showed overexpression of aromatase (AROM⁺) in most organs such as brain, testis, prostate, heart and liver (Jazbutyte et al. 2012). For this a purified expression vector for human P450 aromatase (pUBC-AROM) was constructed, using the pRC/CMV plasmid as backbone. The cytomegalovirus promoter of the vector was replaced by a 1.0-kb ubiquitin C promoter and raised on FVB/N background (Bell et al. 2014; Li et al. 2001).

Tissue collection, housing and transport followed the guidelines for animal care and were approved by the committee for laboratory animals of Justus-Liebig-University Giessen (rats: JLU no. 469_M, 510_M, 527_AZ and 580_M; mice: MARP/2011/070/BC, PC1-N18/11 and PC1-N52/13).

3.2.1.2 Human prostate

Human tissue samples originated from patients aged between 60 to 79 years (medium 71.7 ±6.5 years) which underwent either transurethral monopolar electroresection of the prostate (TUR-P) for BPH treatment or radical prostatectomy (RP) in case of prostate cancer at the Department of Urology, Pediatric Urology and Andrology of the Justus-Liebig-University Giessen.

None of the patients received any previously recorded hormone therapy. Tissue samples from TUR-P were collected periurethral, while tissue samples from radical prostatectomy originated from the peripheral aspect of the prostate. Biopsies were stored for a short time (up to 1 hour) in minimal essential medium at 4 °C before being dissected into sections thinner than 0.5 mm allowing transillumination to perform time-lapse imaging and anatomical investigations.

All patients gave written informed consent before surgery. Usage of human prostate tissue was approved by the ethics committee of the Medical Faculty, Justus-Liebig-University Giessen (ethical vote 49/05, 2005)

3.2.1.3 Human interstitial cells

A total of 6 human interstitial cell lines were isolated from prostate tissue of 3 different cancer patients (105 R, 107 R, 128 R), who underwent radical prostatectomy. With the permission of all patients, tissue samples of each prostate were dissected from 2 different regions located proximal respectively distal to the carcinoma area.

Patients gave written informed consent before surgery. Use of human prostate tissue was approved by the ethics committee at Monash University (2004/145).

3.2.2 Cell culture

A testosterone-enriched medium was used to isolate human prostatic interstitial cells and subsequently stored in dimethyl sulfoxide (DMSO) at liquid nitrogen. Frozen cell lines were brought up to cell culture by slowly disperse toxic DMSO, starting at passage 4 to 5 in T75 flasks. All cells were cultured at 37 °C, under 5% O₂ and 5% CO₂ in 15ml testosterone-enriched cell growth medium with FCS. The medium was renewed every 2 to 3 days. If cell growth reached at least 90% confluency, cells were reseeded in T175 flasks. Next time when cell growth reached total confluency, cells got passaged.

Passaging always included the following steps. First, the old growth medium was exhausted, followed by a washing step with 10ml PBS+EDTA for 5 min at room temperature (RT). After aspirating the PBS, 2 ml of trypsin (0,1%) was added and incubated for 5min at 37 °C. Trypsin was neutralized by adding of 5 ml medium with FCS and this cell suspension was then transferred into a 15 ml tube and spun down at 1000 rpm for 5 min at RT. The supernatant was aspirated and the remaining cell pellet was resuspended into 6 ml medium. After cell counting with the help of a TC 10 automated cell counter (Bio-Rad, Munich, Germany), the cell suspension was split in half and added to 17ml medium within two new T175 flasks, containing at least 1x10⁶ cells.

Tissue collections, cell isolation as well as all necessary cell culture experiments were performed at the facilities of the Department of Anatomy and Developmental Biology, Monash University, Melbourne, Australia.

3.2.2.1 Dihydrotestosterone treatment

Cell culturing continued until cell lines reached passage 7 to 8, containing a minimum of 6×10^6 cells per cell line. The day before DHT treatment, all cells were trypsinized and counted. Cells were resuspended in phenol red-free medium that contained no testosterone to avoid false responses. 2 ml phenol red-free medium together with 5×10^5 cells within each well were seeded in triplicates (Fig.5). Cells were allowed to recover under normal culturing conditions overnight.

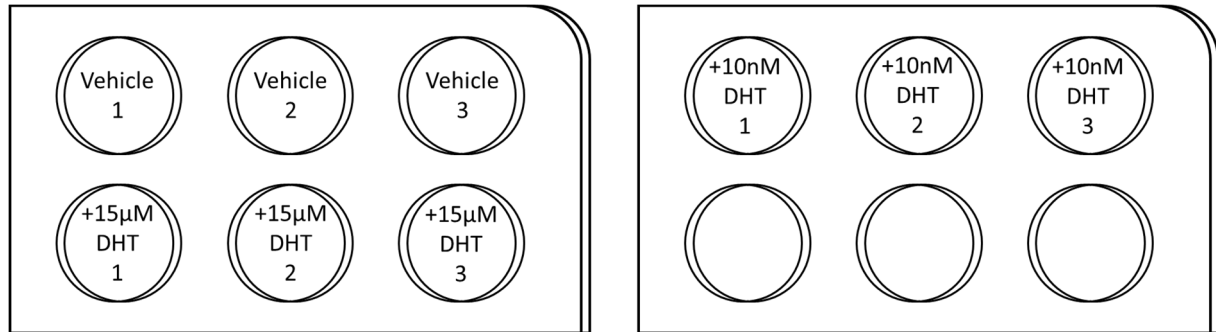


Fig.6: Seeding template for human prostatic interstitial cells.

All cell lines (total of 6) were seeded as triplicates into 6-well plates and allowed to regenerate overnight before treatment with DMSO (vehicle control), 15 μ M DHT or 10 nM DHT started.

In addition, a 96-well plate was seeded with 5×10^3 cells per well from all investigated cell lines (10 replicates) for later immunohistochemistry. The following day medium was exchanged by 1.9 ml fresh phenol red-free medium. To get a final concentration of 15 μ M DHT, 100 μ l of a 300 μ M DHT stock solution was added to each well, respectively 100 μ l of a 1 μ M DHT stock solution to reach a final concentration of 10 nM DHT. For vehicle control a stock solution of 300 μ l DMSO dissolved in 700 μ l medium was produced and 100 μ l of it was added to each vehicle replicate, resulting in 15 μ M final concentration. DHT incubation took 24 hours under normal culturing conditions, as described earlier (see 3.2.2 cell culture).

After 24 hours the medium was aspirated and pure PBS was added to wash the remaining cells on the bottom of the wells. PBS from all triplicates of one experimental setup was aspirated. Subsequently, cells of all three replicates were resuspended in 500 μ l of mercaptoethanol solution (1%) with the help of a cell scraper, collected in 1.5 ml tubes and finally stored at -80°C .

3.2.3 Real-time PCR

3.2.3.1 Purification of total RNA

Isolation of total RNA from all collected cells was performed using the RNeasy Mini Kit (Qiagen, Hilden). In a first step, lysed cells were spun down with 10,000 rpm. The supernatant was exchanged with 70% ethanol, mixed and transferred to an RNeasy spin column. Washing and RNA purification proceeded according to manufacturer's instructions until RNA was eluted into 40 μ l RNase free water. Samples were stored again at -80 °C.

3.2.3.2 First-strand cDNA synthesis

According to the amount of RNA of each sample, measured by NanoDrop system (Thermo Scientific, Waltham, USA), 500 ng of RNA was incubated on 65 °C together with 50 ng/ μ l Random Hexamer and 10 mM dNTPs for 5 min to remove secondary structures. The solution was allowed to cool down and incubated with 1 μ l RNaseOUT Recombinant RNase Inhibitor at 25 °C for 5 min. Superscript III Reverse Transcriptase was used for cDNA synthesis. For this step, the samples were incubated within the thermocycler at 50 °C for 1 hour. The reaction was inactivated by heating up to 70 °C for 15 min. All samples were diluted (1:10) in 200 μ l nuclease free water and stored at -20 °C.

3.2.3.3 Primer design

Except for α -SMA, all primers were self-designed by using the following procedure. For each gene listed below (Tab.1) the complete nucleotide sequence was searched online from the NCBI database.

Tab.1: Human-specific primer descriptions.

Gene name	Primer position	Primer sequence	Annealing temp	PCR product length [bp]	Origin
sGC (β 1)	1470	(fwd) 5'-TGCTGGCCAGGTTCAAGTAG-3'	59,96	142	self designed
	1611	(rev) 5'-TGTTCCGGCTTGTGAGGTTGA-3'	59,82		
PDE-5	2835	(fwd) 5'-TATGCCTAGTTTCTTACACACTGTC-3'	58,6	190	self designed
	3024	(rev) 5'-GTGCTAACAGTGGATGTTGTTGAT-3'	59,78		
PKG I	1330	(fwd) 5'-GTTGGAGGTTTCGGACGAGT-3'	59,97	118	self designed
	1447	(rev) 5'-GGATGTGCTCCTGCTGCTT-3'	60,04		
α -SMA	537	(fwd) 5'-TGTAAGGCCGGCTTTGCT-3'	59,57	112	Madar et al. 2009
	648	(rev) 5'-CGTAGCTGTCTTTTGTCCATT-3'	59,5		

The official NCBI homepage also provides a free online *Basic Local Alignment Search Tool* (BLAST) that was used to either test potential primer sequences or design them, featuring the

following characteristics, ordered by importance. Chosen primers were able to detect all splicing variants of a certain gene, without detecting further nucleotides and had a product length around 150 bp, a melting temperature close to 60 °C, a self-complementary factor below 5 as well as a GC percentage around 50%. Primers were ordered from Eurofins MWG-Biotech (Ebersberg). A stock solution of 200 pM/μl was produced for usage in real-time PCR.

3.2.3.4 Real-time PCR set up and conditions

The polymerase chain reaction, short PCR enables to multiply a DNA sequence of interest, targeted by specific primer pairs. DNA replication is achieved by exposing the reactants to cycles of repeated heating and cooling which control temperature-dependent reactions, necessary to melt and replicate DNA. In case of real-time or quantitative PCR (qPCR), products are additionally labeled with fluorescence markers, to quantify the amplified amount of DNA copies. The number of cycles is counted in which the detectable fluorescence of an amplified PCR product that exceeds the background fluorescence and printed as Ct value.

Power SYBr Green PCR Master Mix was produced and incubated with triplicates of the cDNA templates. qPCR was always performed with the following composition.

Tab.2: Template for qPCR loading.

Component	Volume [μl] for 1 sample
Power SYBR Green Master Mix	12.5
10μM fwd primer	0.5
10μM rev primer	0.5
Template	5
Water	6.5
Total	25

The amplification for all genes of interest used the following conditions.

Tab.3: Template for qPCR conditions

Heating step 2 to 4 were repeated for 50 cycles.

Temperature [°C]	Duration [sec]
95	600
95	20
60	20
72	20
50	30
20	∞

} 50 Cycles

To compare Ct values of the genes listed in Table 1, values were normalized by using the Δ Ct-method (Huggett et al. 2005). The expression ratio is calculated, relative to a second (housekeeping) gene, which is typically constitutive and widely expressed in all cells.

$$\text{Ratio (relative expression)} = 2^{-\Delta Ct} = 2^{-(Ct \text{ gene of interest} - Ct \text{ housekeeping gene})}$$

The experimental setup for this investigation used *Glyceraldehyde 3-phosphate dehydrogenase* (GAPDH) as a housekeeping gene. GAPDH catalyzes the sixth step of glycolysis and is therefore constantly expressed at high levels among most tissues.

3.2.4 (Immuno-) Histochemistry

3.2.4.1 Fixation and slicing

Prostate tissue samples, originating from human, rat or mouse were fixed in Bouin solution (picric acid, acetic acid and formaldehyde) for 24 hours, followed by an ascending alcohol series for dehydration. Tissues were embedded in paraffin and allowed to harden completely before slicing. Using a RM2255 microtome (Leica, Wetzlar, Germany), slicing thickness was set to 5 μ m.

In addition, previously seeded human prostate interstitial cells were equally fixed with Bouin solution. After a short-term incubation for roughly 15 min, Bouin was washed off with pure PBS.

3.2.4.2 Azan trichrome stain

Trichrome stains are highly approved to analyze the general histology of the investigated tissue. For the purpose of this study, the Azan stain after Heidenhain was performed, resulting in a dark red staining of cell nuclei, whereas collagen is colored in blue.

After deparaffining in descending alcohol series, cell nuclei of investigated rodent and human tissue sections were stained with acetocarmine solution at 56 °C for no longer than 15 min, under visual control. Phosphotungstic acid binds the dye to the tissue, followed by a second step of staining with aniline blue, which marks collagen fibers. For long-term storage, tissue sections were dehydrated in isopropanol (and xylene) and finally embedded in mounting medium (Eukitt; Fluka, Buchs, Switzerland), protected by Automat Star coverslips (Engelbrecht, Edermünde, Germany).

3.2.4.3 Immunostaining

Paraffin-embedded prostate tissue sections from human, rat and mouse were investigated by immune reactive staining with a special focus on smooth muscle cells. At first, sections were deparaffinized in descending alcohol series, including a step of incubation in 1.2% H₂O₂ (dissolved in methanol) to block endogenous peroxidase activity. Primary antibodies for α smooth muscle actin (SMA, mouse monoclonal, 1:1000; Sigma-Aldrich, Steinheim, Germany), PKG I (rabbit polyclonal, 1:1000, Enzo Life Sciences, Lörrach, Germany) and PDE5 (rabbit polyclonal, 1:1000; gift from Laurinda Jaffe, University of Connecticut Health Center, Farmington, USA) were diluted in PBS with 0.2% BSA and 0.1% sodium azide and incubated at 4 °C overnight to ensure a slow penetration of the antibody into the tissue. Slides were transferred to humidity chambers for overnight incubation. Sections without primary antibodies served as negative control.

The following day, sections were washed several times in PBS before horseradish peroxidase-labeled polymer (DAKO, Hamburg, Germany) was added to each section at RT for 30 min. After washing with PBS and 0.1M PB, peroxidase activity was detected by DAB. The reaction was initiated by nickel-glucose oxidase amplification and stopped under visual control. For the purpose of storage, all sections were dehydrated by ascending alcohol series (and xylene) and mounted in Eukitt® Quick-hardening mounting medium (Merck, Darmstadt, Germany), protected by Automat Star coverslips.

In addition, immunofluorescence double staining from the same paraffin-embedded tissue sections were performed to co-localize two proteins of interest within identical smooth muscle cells. The procedure starts again by deparaffinization in descending alcohol series, including the incubation in 1.2% H₂O₂. But after washing in PBS, sections needed to be transferred into 2% normal goat serum for 1 hour at RT to block unspecific binding sites. Primary antibodies for SMA (1:1000) and PDE5 (1:1000) were diluted in PBS with 0.2% BSA and 0.1% sodium azide and applied to tissue sections for overnight incubation in humidity chambers at 4 °C. Sections without primary antibodies served as negative control.

After a short washing step in PBS the following day, sections were incubated with fluorescence-labeled secondary antibodies (Cy3 anti-rabbit IgG, 1:500; Jackson ImmunoResearch, West Grove, USA respectively Alexa Fluor 488 anti-mouse IgG, 1:500; Thermo Fisher Scientific, Waltham, USA) together with 4',6-Diamidino-2-phenylindol

(DAPI, 1:1250; Merck, Darmstadt, Germany) for 1 hour at RT. Including this step, all following steps were performed in darkness to avoid a loss of fluorescence caused by UV from daylight. Staining procedure ends by washing of the tissue sections in PBS, followed by mounting under coverslips with buffered glycerol for long-term storage at 4 °C.

Apart from prostate tissue sections, immunostaining of cultured human prostatic interstitial cells was performed by using a DAB Kit (DAKO, EnVision⁺System, Peroxidase, Hamburg, Germany) which follows the same principles as described earlier. Bouin-fixated cells were treated with 0.3% triton x-100 (Merck, Darmstadt, Germany) for 5 min at RT to permeabilize them. After short washing of each well with PBS, DAB detection was proceeded according to manufacturer's instructions, using primary antibodies for SMA (1:1000), PKG I (1:1000) and PDE5 (1:1000). DAB reaction was stopped with water under visual control. Cell nuclei were counterstained with hematoxylin (Merck, Darmstadt, Germany) for 10 sec and washed off with warm tap water. For short-term storage, cold water was added to each well, sealed by parafilm (Bemis NA, Neenah, USA) and transferred to stock at 4 °C.

Conventional light and fluorescence microscopy served for documentation of all performed stainings using an Axioplan 2 imaging microscope and Axiovision LE software (Zeiss, Munich, Germany).

3.2.5 CLARITY

CLARITY which is an abbreviation for Clear lipid-exchanged acrylamide-hybridized rigid imaging/immunostaining/*in situ* hybridization-compatible tissue-hydrogel, features an improvement of common histological techniques by generating three-dimensional (3D) images of whole tissues. The principle of this technique is to conserve biologic tissue by transforming it into a translucent hydrogel-tissue hybrid. Biomolecules were mounted in a hydrogel matrix to preserve their structural framework before unattached lipids will be washed away. Since this technique was developed for clearance of brain tissue, no protocol for prostate tissue of any species was available and had to adapt from instructions described by Chung and Deisseroth (2013).

The protocol was preceded with prostate tissue samples dissected from rodent ventral lobes or human prostate tissue, collected mostly periurethral.

Tissue sections of approximately 1 mm³ in size were fixed in 4% paraformaldehyde for 24 hours at 4 °C. To form a hydrogel mesh with the prostate tissue, incubation of hydrogel solution (Tab.4) for 24 hours at 4 °C was followed by its polymerization at 37 °C for 3 hours. Remaining hydrogel excess was carefully removed. In a subsequent step, tissue samples were incubated in clearing solution (Tab.4) for a minimum of 5 days under visual control to wash out most lipids. Removal of lipid components is crucial to avoid light scattering for optimal tissue opacity.

Tab.4: Hydrogel and buffer composition for tissue clearing.

Hydrogel solution components	Final concentration
Acrylamide	4%
Bisacrylamide	0.05%
2,2'-Azobis(2-methylpropionamide)dihydrochloride	0.25%

Clearing solution components	Final concentration
Sodium dodecyl sulfate (SDS)	10%
Boric acid	200 mM

Extensive washing steps with 0.1% PBS-Triton were performed before and after adding primary antibodies, targeting SMA (1:100), PKG I (1:100), PDE5 (1:100), calponin-1 (rabbit monoclonal, 1:100; Epitomics, California, USA), Ki67 (1:100, rabbit polyclonal, Novocastra, Newcastle, UK) as well as α -tubulin (mouse monoclonal, 1:100, Sigma-Aldrich, Steinheim, Germany) and fluorescence-labeled secondary antibodies (Cy3 anti-rabbit IgG, 1:200 and/or Alexa Fluor 488 anti-mouse IgG, 1:200). All antibodies (primary and secondary) were diluted in 0.1% PBS-Triton and incubated for at least 5 days at RT. Stainings were performed either as single antibody staining or double antibody staining in combination with SMA. In addition, staining with DAPI (1:400) allowed to distinguish between glandular epithelium and stromal smooth muscle cells.

Further 24 hours of tissue washing steps with 0.1% PBS-Triton were executed before the tissue was transferred into a refractory index matching solution (RIMS, Tab.5) for 24 hours at RT. RIMS buffer optically enhances clearance caused by closely approximated refractory indexes of the translucent sample and its embedding solution, which in turn facilitates light to pass through with neither refraction nor reflection.

Tab.5: RIMS buffer composition for optical clearance enhancement.

Refractory index matching solution components	Final concentration
Histodenz	88%
Tween-20	0.1%
Sodium azide	0.01%

Finally, samples were mounted in RIMS buffer on common slides. Because sample thickness could easily reach 2 mm, the gap between slide and coverslip was bridged by a ring of blue tack (Bostik, Wauwatosa, USA).

Documentation of all samples was performed on a LSM 710 Confocal Laser Scanning Microscope (Observer.Z1, Zeiss, Munich, Germany), capturing z-stacks with a slice distances between 1.5 to 5 μm .

Z-stacks were reconstructed using the open source program *ImageJ* 1.50e (public domain software, NIH, USA, download at <http://imagej.nih.gov/ij>). The integrated program tool “3D projects” provides a simple setup for interpolated 3D reconstructions and offers the opportunity for automatic contrast enhancement, if necessary.

3.2.6 Time-lapse imaging

For the purpose of functional investigations, time-lapse imaging was performed in combination with transillumination microscopy to visualize relevant drug effects of the PDE5-inhibitor sildenafil on smooth muscle cell contractility. The total tissue of the periurethral or peripheral aspect of the human prostate respectively, glands and duct of the rat ventral lobes were embedded in a collagen suspension to ensure tissue immobilization. Collagen was collected from tails of adult rats and suspended in 10x DMEM/F12 (Gibco, Invitrogen, Karlsruhe, Germany), together with 0.1% glacial acetic acid, 0.5 M sodium hydroxide and 1 M HEPES. Prostate samples were placed inside the viscous collagen solution and mounted at the bottom of a Delta T dish (Bioptechs, Buttlar, USA). At 37 °C collagen was polymerized and covered by 1 ml MEM for optimal tissue supply.

Time-stack recording was performed using a BX50WI transillumination microscope (Olympus, Tokio, Japan) equipped with UMPlan Fl 10x/0,5 W and UMPlanFl 20x/0,5 W objectives that were attached to a Till-Imago QE CCD camera (Photonic, Gräfelfing, Germany). Camera input was recorded by TillVision software (Version 4.0, Photonic).

Pictures were taken automatically every 2 sec to produce virtual time-stacks. The temperature was set constantly to 34 °C during the whole recording time.

Experimental set up always included the following drugs and durations. During the first 30 min, spontaneous contractility was observed which and used as positive control, followed by 15 min treatment with the PDE5 inhibitor sildenafil (5 µM, Pfizer, New York, USA). To proof for tissue vitality, any response to noradrenaline (10 µM, Sigma-Aldrich, Steinheim, Germany) a neurotransmitter of α 1-adrenoceptor from the prostatic autonomic nervous system was recorded for additional 15 min. All investigated substances were directly dripped into MEM. In a final step, histological determination of all observed tissues was confirmed by paraffin-embedded azan stainings.

Digital time-stack processing used ImageJ 1.50e (public domain software, NIH, USA, download at <http://imagej.nih.gov/ij>) to visualize smooth muscle cell contractions. Regions of interest were defined for contractile areas and followed over time. The built-in tool “Reslice” translated all contractions into visible peaks on a fixed timescale. Contrast enhancement was adjusted if necessary to improve the final outcome. Contraction frequency could then easily calculated as the number of peaks over time. First 10 min of spontaneous contractions, respectively first 4 min after drug addition were taken as residence time and excluded from calculations. Sample recordings without any visible drug response were excluded from statistics.

3.2.7 Western Blot

Next to immunostaining, the protein level of certain cGMP pathway components was additionally analyzed from tissue homogenates of the rat and mouse ventral prostate. Western Blot protocol was preceded as described by (Müller et al. 2011)) with only slight modifications.

In the first step of protein isolation, rodent prostate tissue was transferred into lysis buffer, followed by tissue break down with the help of a SonoPlus mini 20 ultrasonic homogenizer (Setting: pulse 0,005s, time 1min, Am 90%, Bandelin, Berlin, Germany). Since prostate tissue reveals high protease activity, protein isolation was performed on ice. Cell debris was homogenized in lysis buffer (Tab.6) and centrifuged at 3000 x g for 8 min at 4 °C. The

remaining pellet was discarded. The supernatant, containing total isolated proteins was frozen with liquid nitrogen and stored at -80 °C.

Tab.6: Lysis buffer for cell break down.

Lysis buffer components	Final concentration
Tris/HCL (pH 7.5)	50 mM
Sodium chloride	150 mM
EDTA	5 mM
Triton X-100	1% (w/v)
Sodium deoxycholic acid	5% (w/v)
Phenylmethanesulfonyl fluoride (PMSF)	2 mM
Aprotinin	1 mM
Leupeptin	1 mM

For measurement of total protein concentration, a Bradford protein assay (Bio-Rad, Munich, Germany) was used. Coomassie Brilliant Blue G-250 dye binds to proteins which in turn shift its absorbance maximum for an acidic solution from 465 nm to 595 nm. Detection of final protein concentration was measured at 595 nm by a microplate reader. Bovine serum albumin (3 to 18 µg/µl) served as standardized control.

Equal amounts of protein samples were transferred to 3x SDS gel loading buffer (Tab.7) and denatured at 104 °C for 2 min. SDS binds to the hydrophobic regions of proteins which turn the protein charge into a constant negative state and enables the separation of proteins according to their molecular weight during gel electrophoresis. SDS polyacrylamide gels (10%) run in a SE 600 vertical electrophoresis system (Hoefer Scientific Instruments, MA, USA), firstly with 13 W for 1 hour to concentrate all proteins within each sample and secondly with 17 W for 2 hours to separate protein samples. The protein ladder wide range (Sigma-Aldrich, Steinheim, Germany) and/or Page ruler™ Plus (Thermo Fisher Scientific, Waltham, USA) were used to estimate protein length.

Tab.7: Gel and buffer composition for gel electrophoresis.

3x gel loading buffer components	Final concentration
Tris	375 mM
Dithiothreitol (DTT)	200 mM
Sodium dodecyl sulfate (SDS)	15% (w/v)
Glycerin	20% (v/v)
Bromphenol blue	0.6 mg/ml

Gel running buffer components	Final concentration
Tris	25 mM
Glycine	192 mM
Sodium dodecyl sulfate (SDS)	0.1% (w/v)

Resolving gel buffer components	Final concentration
Tris	375 mM
Sodium dodecyl sulfate (SDS)	0.1% (w/v)

Resolving gel (10%) components	Final concentration
4x Resolving gel buffer (pH 8.5)	15 ml
Acrylamide solution (30%)	20 ml
Distilled water	24,7 ml
Ammonium persulfate (10%)	0.25 ml
Temed	0.05 ml
Total volume	60 ml

Stacking gel buffer components	Final concentration
Tris	500 mM
Sodium dodecyl sulfate (SDS)	0.1% (w/v)

Stacking gel components	Final concentration
4x Stacking gel buffer (pH 6.8)	5 ml
Acrylamide solution (30%)	2.6 ml
Distilled water	12.275 ml
Ammonium persulfate (10%)	0.1 ml
Temed	0.025 ml
Total volume	60 ml

Separated proteins were transferred to Amersham™ Hyperbond™ - ECL nitrocellulose membranes (GE Healthcare, Freiburg, Germany) at 27 volts overnight. Next day incubation with Ponceau-S (Merck, Munich, Germany) for 10 min at RT was used to reveal the efficacy of protein blotting which was scanned for documentation. Membranes were subsequently incubated in blocking reagent (Roche, Mannheim, Germany) for 2 hours at RT.

Tab.8: Buffer composition for nitrocellulose transfer.

Blotting buffer components	Final concentration
Tris	100 mM
Glycine	193 mM

TBS-T components	Final concentration
Tris	20 mM
Sodium chloride	137 mM
Tween 20	0.05% (v/v)

After a few washing steps with distilled water, immunoblotting started using the following primary antibodies: α smooth muscle actin (SMA, mouse monoclonal, 1:1000; Sigma-Aldrich, Steinheim, Germany), PKG I (rabbit polyclonal, 1:1000, Enzo Life Sciences, Lörrach, Germany), PDE5 (rabbit polyclonal, 1:1000; gift from Laurinda Jaffe, University of Connecticut Health Center, Farmington, USA), sGC (rabbit polyclonal, 1:5000, CAYMAN, Ann Arbor, USA) and vinculin (mouse monoclonal, 1:6000, Sigma-Aldrich, Steinheim, Germany). Incubation took 1 hour followed by short washing with TBS-T (Tab.6), before horseradish peroxidase-conjugated secondary antibodies (goat-anti-mouse respectively goat-anti-rabbit IgG, 1:2000, Pierce, Bonn, Germany) were applied. All antibodies were diluted in antibody incubation buffer (90% TBS-T, 10% blocking buffer, 0.005% Thimerosal).

Protein signals were detected by chemiluminescence, using Amersham™ enhanced chemiluminescence reagent (GE Healthcare, Freiburg, Germany). Signal illumination was finally captured on x-ray film (Fuji, Tokio, Japan).

Membrane stripping followed directly after protein signal detection, to wash off any remaining antibodies. This procedure always started with the incubation in 5% skimmed-milk (Roth, Karlsruhe, Germany) which protects proteins from the subsequent washing step with 0.5 M sodium chloride/ 0.5 M acetic acid. After washing with distilled water and 1.5 M Tris membranes were either dried completely for long-term storage at 4 °C or reused for incubation with further primary antibodies following the previously described protocol.

For detailed comparisons of individual protein levels within each sample densitometric quantification was performed. Band intensity values were measured by ImageJ 1.50e (public domain software, NIH, USA, download at <http://imagej.nih.gov/ij>) and normalized to those of vinculin.

3.2.8 Statistical analysis

All final graphs and statistics were performed with the statistics program GraphPad Prism (version 6.02 for Windows, GraphPad Software, La Jolla, California, USA, www.graphpad.com). In detail, determination for normally distributed data was achieved with the Kolmogorov-Smirnov test. Data sets were analyzed using a one-tailed t-test in case of normal distribution, otherwise Mann-Whitney U test was performed.

For significance analysis of data produced by time-lapse imaging, only vital samples were included in statistics. Sample vitality was confirmed by any visible response to noradrenaline at the end of each time-lapse experiment. Data pairing was assumed for comparisons between calculated contraction frequencies before and after sildenafil addition. Values from all other investigations were treated as unpaired data.

4 Results

4.1 Localization of SMCs in acini and ducts of the rat ventral prostate

Prostatic ventral lobes in rats consist of numerous prostatic acini that drain into the urethra by elongated prostatic ducts (Fig.7A). Secretion of the acini is mediated by glandular epithelium. Acini and ducts are loosely embedded in stromal connective tissue, interspersed with blood vessels (Fig.7B). Both prostatic structures are encircled with layers of SMCs, shown by immunostainings for smooth muscle actin (SMA). Interestingly, numerous layers of SMCs surround the proximal ducts, while prostate acini (Fig.7C) are encircled with only a thin layer of SMCs.

Independently of their individual localization within the prostate ventral lobe, all smooth muscle cells were found to express PDE5 and PKG I which represent two well-known enzymes, involved in the cGMP pathway for smooth muscle contractility (Fig.7D, E). Staining from serial cuttings therefore, offers the opportunity to compare the expression of several proteins within equal cellular structures. In contrast to SMCs, epithelial cells of prostatic ducts and glands lack any positive immunostaining for PDE5 and PKG I.

4.2 The architecture of prostatic SMCs in rat and mouse

4.2.1 3D reconstruction of rat prostate tissue

The development of a novel CLARITY protocol which is adapted for clearance of prostate tissue provided a totally new perspective of the anatomic architecture of prostatic SMCs. For the first time, the very tight arrangement of those SMCs could follow simultaneously over several anatomically intact prostate glands.

It was shown that SMCs surround prostatic acini neither evenly nor totally chaotic. In fact, peri-glandular SMCs rather form large bandage-like structures that tightly enclose the complete prostate gland, interrupted by roundish areas without SMCs (Fig.8A). SMCs follow various directions and partly overlap each other (indicated with white arrowheads). Larger areas that lack SMCs were commonly found at the tips and branchpoints of the acini (Fig.8A, indicated with white asterisks).

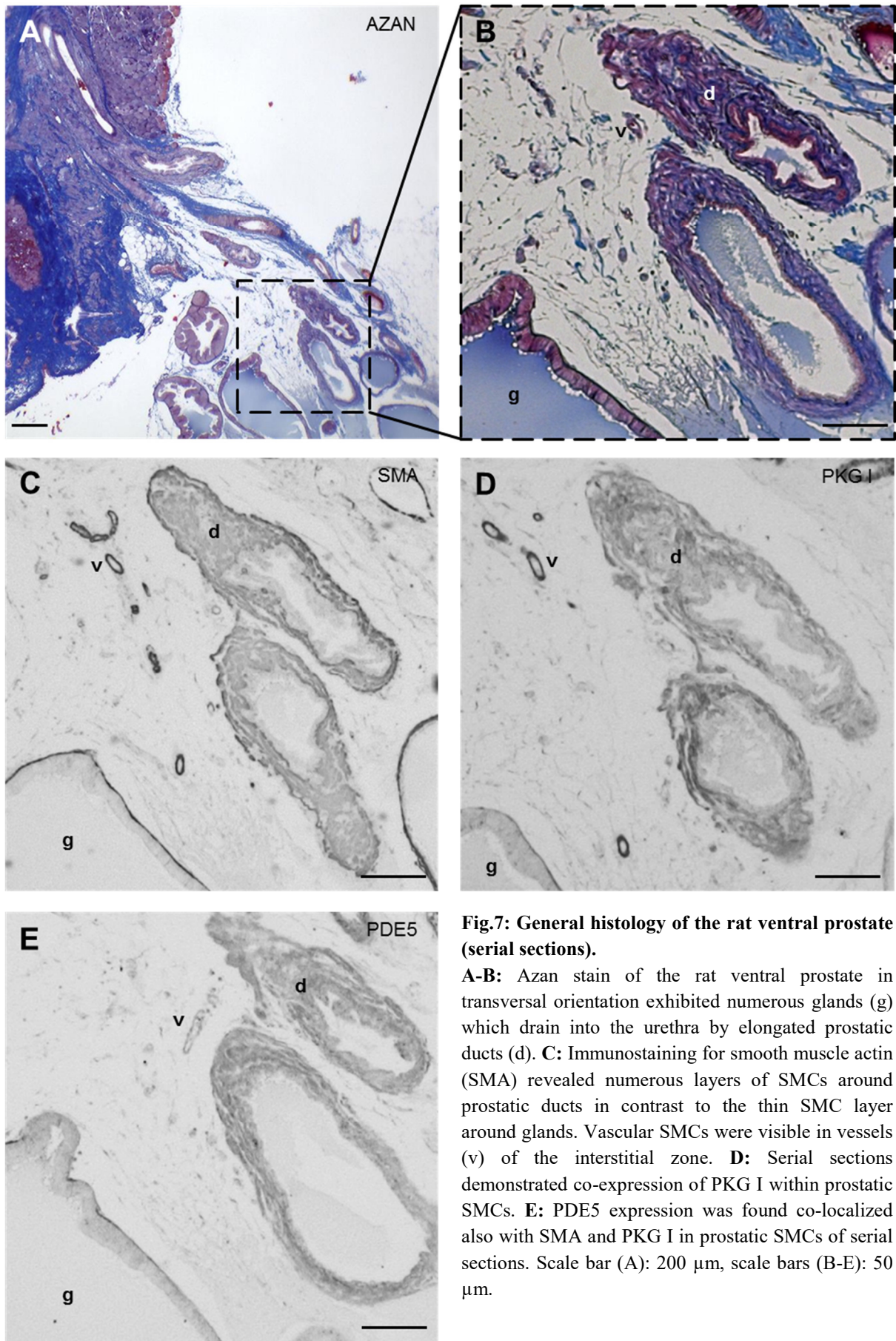


Fig.7: General histology of the rat ventral prostate (serial sections).

A-B: Azan stain of the rat ventral prostate in transversal orientation exhibited numerous glands (g) which drain into the urethra by elongated prostatic ducts (d). **C:** Immunostaining for smooth muscle actin (SMA) revealed numerous layers of SMCs around prostatic ducts in contrast to the thin SMC layer around glands. Vascular SMCs were visible in vessels (v) of the interstitial zone. **D:** Serial sections demonstrated co-expression of PKG I within prostatic SMCs. **E:** PDE5 expression was found co-localized also with SMA and PKG I in prostatic SMCs of serial sections. Scale bar (A): 200 μm , scale bars (B-E): 50 μm .

Expression of calponin-1, a protein crucial for smooth muscle contractility, was investigated in addition (Fig.8B). Although calponin expression was found to be less intense compared to smooth muscle actin in the rat ventral prostate, the same peri-glandular SMC localization was confirmed, highlighting elongated clusters of SMCs either overlapping each other (Fig.8B, indicated with arrowheads) or forming empty areas (Fig.8B, indicated with asterisks).

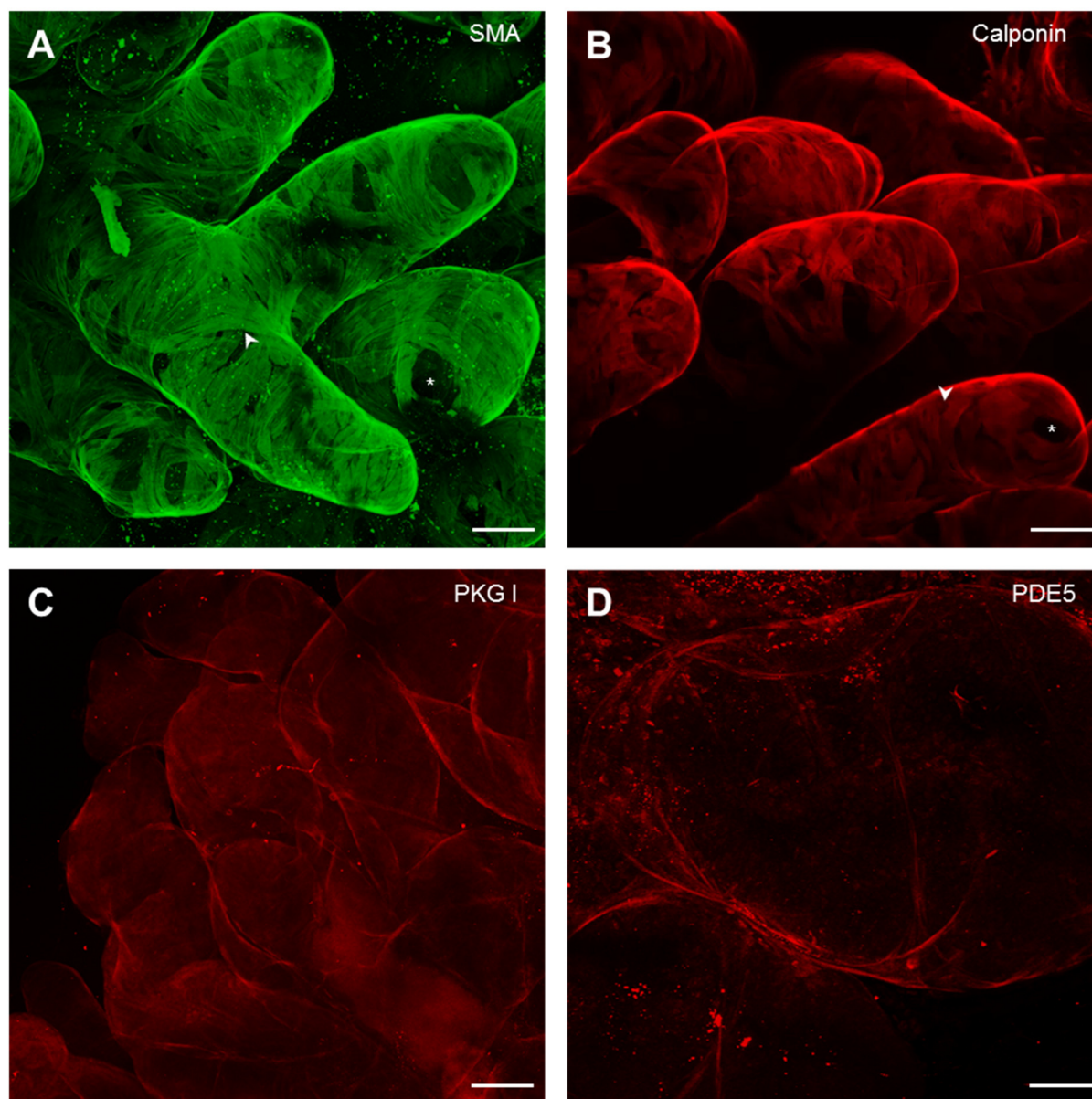


Fig.8: Virtual reconstructions of rat prostate glands.

A: Expression of SMA illustrates SMC architecture, forming bandage-like SMCs that overlap each other (arrowheads) or exhibit empty areas (asterisks). **B:** Expression of calponin confirmed SMC arrangement, which tightly encloses all prostatic acini. **C:** PKG I was found to be expressed without any distinct orientation around the whole prostate glands. **D:** Similar to PKG I localization, PDE5 was expression tightly around all prostatic acini. Scale bars (A-C): 75 μ m, scale bar (D): 20 μ m.

Similar to SMC location, PKG I expression was also found in a peri-glandular manner around the whole prostate glands but without any distinct orientation (Fig.8C). The same location pattern was observed in case of PDE5 expression in rat ventral prostate tissues (Fig.8D).

4.2.2 3D reconstruction of mouse prostate tissue

Acini of the mouse ventral prostate showed a similar organization of peri-glandular SMCs compared to rat. Tightly encircling all prostatic acini, SMCs form bandage-like structures which partially overlap or leave empty areas (Fig.9A-C).

Interestingly, co-localization of calponin and smooth muscle actin revealed structural differences between both SMC markers (Fig.9A-B). Most acini were found to express both SMC markers, except of only a few glandular parts which lack expression of either one of them (Fig. 9A-B, indicated with white arrows). Furthermore, smooth muscle actin expression seems to be enriched in certain cells and therefore highlights individual bandage-like SMC structures, while calponin was expressed equally through all glandular SMCs.

PDE5 expression from double staining with smooth muscle actin was found peri-glandularly but without any distinct orientation (Fig.9C, D). This finding confirmed the expression pattern already described for rat prostate glands (see Fig.8A). In addition, weak expression of PDE5 was also visible in SMCs of the vasculature (Fig.9D).

Although α -tubulin itself is a globular protein, forming microtubule cytoskeleton in eukaryotic cells, an antibody for α -tubulin could be used for reconstruction of the prostatic innervation network (Fig.9E). A dense network of autonomic nerve fibers was clearly visible, innervating the epithelium-enclosing SMC layer of the mouse prostate. Counterstaining with DAPI helped to reflect the general shape of the prostatic acini.

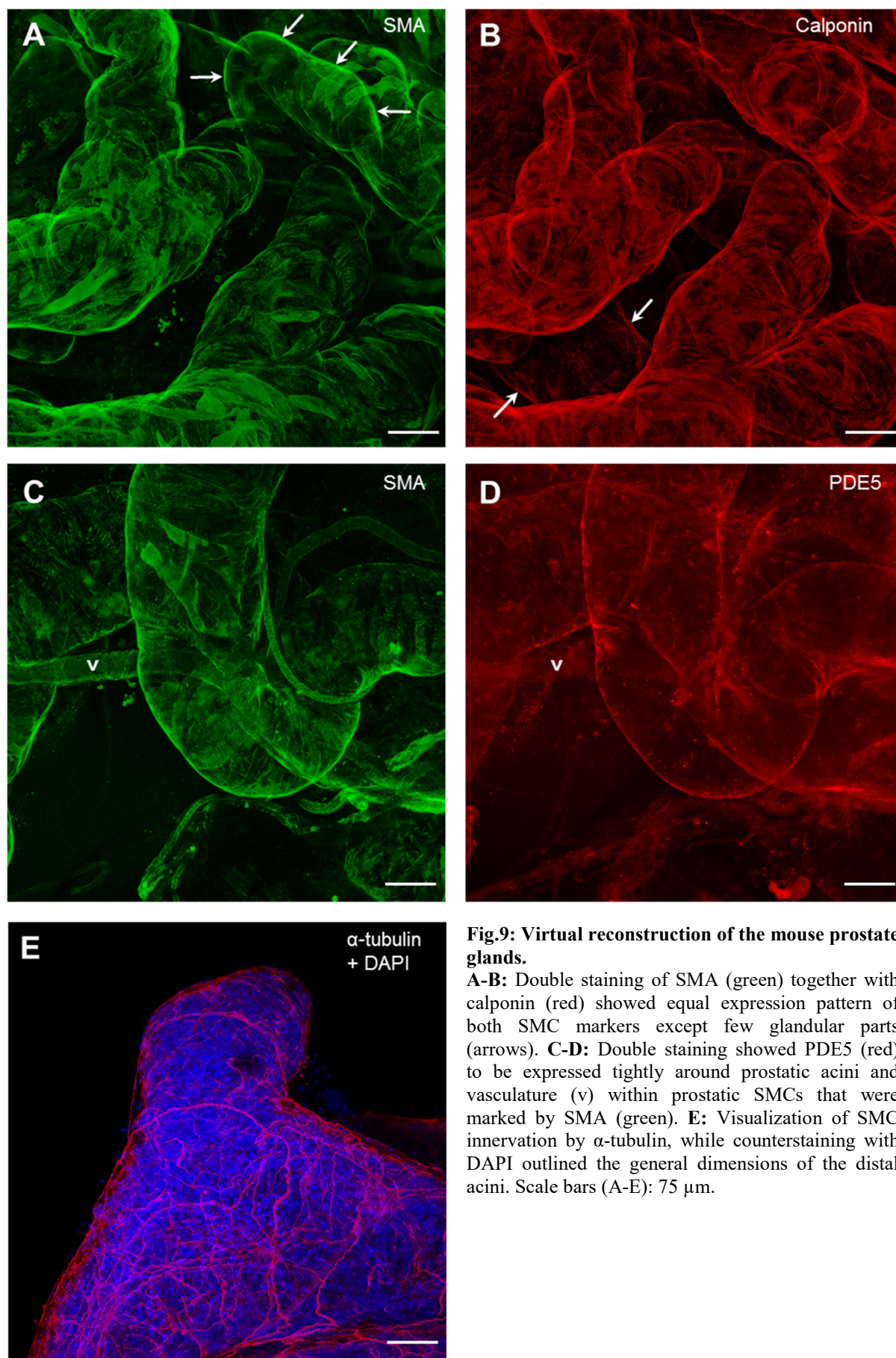


Fig.9: Virtual reconstruction of the mouse prostate glands.

A-B: Double staining of SMA (green) together with calponin (red) showed equal expression pattern of both SMC markers except few glandular parts (arrows). **C-D:** Double staining showed PDE5 (red) to be expressed tightly around prostatic acini and vasculature (v) within prostatic SMCs that were marked by SMA (green). **E:** Visualization of SMC innervation by α -tubulin, while counterstaining with DAPI outlined the general dimensions of the distal acini. Scale bars (A-E): 75 μ m.

4.3 Prostatic vasculature in rats

In order to investigate all structures of the rat ventral prostate that contain SMCs, the prostatic vasculature was investigated in addition to those SMCs located around acini and ducts. Numerous blood vessels supply the rat ventral prostate which consists of three major layers. The tunica intima forms the inner layer by endothelial cells, whereas the outer layer is known as tunica adventitia that contains connective tissue and nerve fibers. Between these two layers, an intermediate layer called tunica media is located. It is built up from SMCs and connective tissue. SMCs of the tunica media regulate blood flow by controlling the caliber of the blood vessels (Prins and Lindgren 2015).

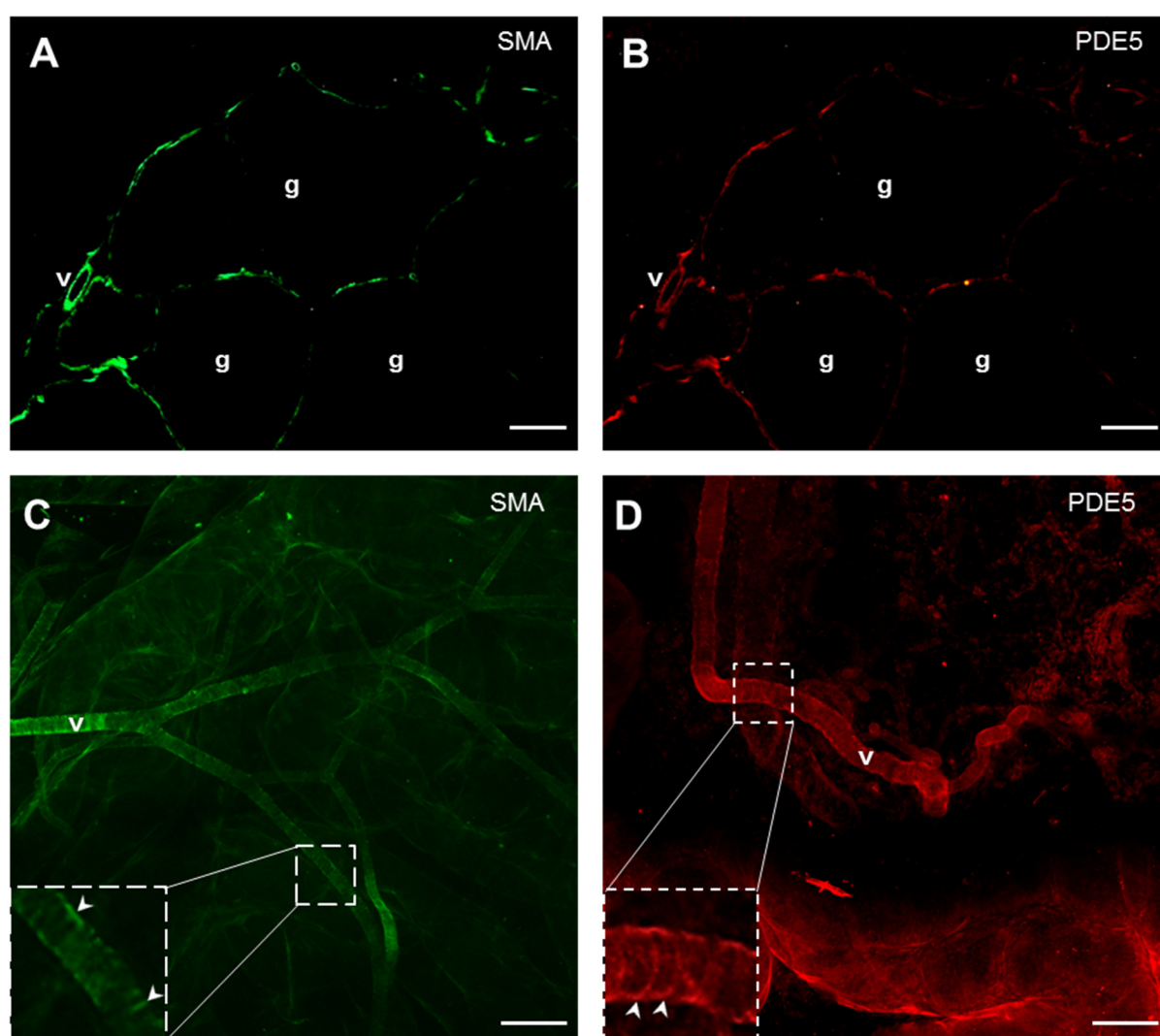


Fig.10: PDE5 expression within the rat prostatic vasculature.

A-B: Double staining on rat ventral prostate sections revealed PDE5 expression in SMCs of the vasculature (v) marked by SMA (green). PDE5 (red) expression in glandular SMCs (g) served as positive control. **C:** Three-dimensional orientation of vascular SMCs was visualized by CLARITY. SMA staining revealed numerous vascular branchpoints. Higher magnification demonstrated the circular orientation of SMCs in prostatic vessels (arrowheads). **D:** PDE5 expression in three-dimensional reconstructions of the rat prostate confirmed its localization within vascular SMC with circular orientation. Scale bars (A-B): 25 μ m, scale bars (C-D): 75 μ m.

Co-expression of PDE5 together with smooth muscle actin unequivocally revealed PDE5 to be expressed only in SMCs (Fig.10A-B). Localization of PDE5 expression within vascular SMCs was confirmed by CLARITY (Fig.10C-D) which gives an impressive insight of the three-dimensional architecture of the prostatic vasculature. The circular orientation of vascular SMCs was clearly visible (Fig.10C-D, indicated with white arrowheads) as well as several branchpoints.

4.4 SMCs of the human prostate

Tissue samples from biopsies donated by patients that underwent radical prostatectomy or transurethral resection were histologically investigated using classical AZAN and immunostaining. Comparisons to rodent prostate histology focused on prostatic smooth muscle cells and revealed some differences between those species. Although in all investigated species SMCs were found to be present in the stroma between prostatic glands and ducts, SMCs of the rodent prostate tightly enclose glands and ducts (see Fig.7C) whereas SMCs of the human prostate were found across the entire interstitial zone (Fig.11B, indicated with arrows) alternating with connective tissue (Fig.11A). Different to the rodent prostate in which prostate glands were loosely connected to each other, human prostate glands gain stability by a massive prevalence of connective tissue and SMCs (Fig.11A) throughout the prostatic stroma.

Proximal ducts in rodents were easily distinguishable from glands according to several SMC layers that surround the epithelial layer of the prostatic ducts, while glands were found to be encircled just by a thin SMC layer. In men, prostatic ducts were identified due to their elongated shape compared to prostate glands, often surrounded by numerous SMCs. However, a systematic analysis that helps to clearly distinguish between ductal and glandular SMCs would be of importance.

Within the human prostatic stroma, immunostaining for PDE5 showed expression of this cGMP-degrading enzyme only in SMCs (Fig.11C) while glandular epithelium cells lack any positive staining. According to previous findings in rat prostate, the cGMP target enzyme PKG I was also localized exclusively in SMCs of the human prostate (Fig.11D).

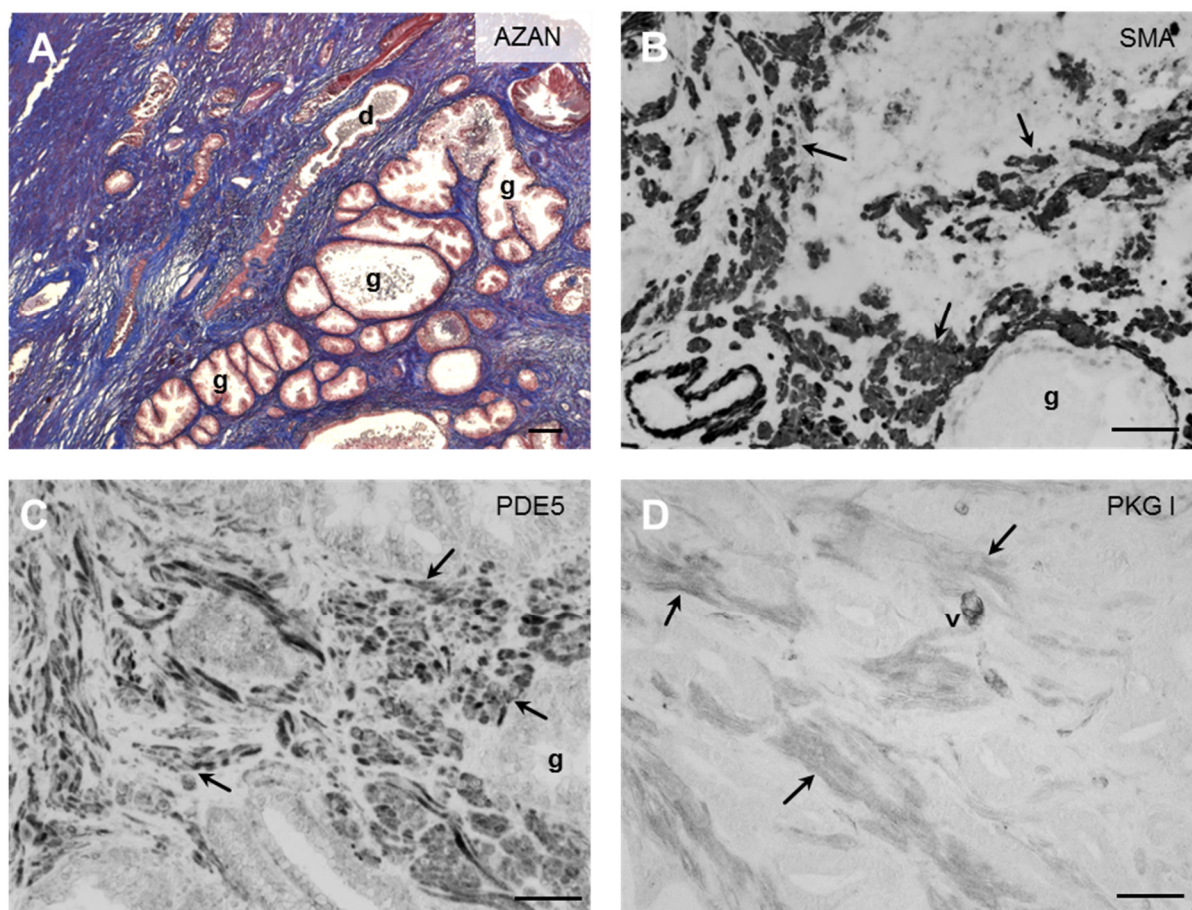


Fig.11: General histology of the human prostate.

A: SMCs were located in all parts of the prostatic interstitial zone and massively interspersed by connective tissue (blue). Elongated ducts (d) were visible in close proximity to prostate glands (g). **B:** Immunostaining for SMA confirmed SMCs (arrows) to be located across the entire interstitial zone. **C:** PDE5 expression was limited to SMCs only. **D:** Besides interstitial SMCs, PKG I was localized also within SMCs of the vasculature (v). Scale bars (A-D): 100 μ m.

4.5 The 3D architecture of SMCs in the human prostate

For the visualization of the SMC arrangement between individual prostatic glands, CLARITY was performed using human biopsy samples. Tissue samples were labeled with an antibody for smooth muscle actin together with DAPI. The distinct organization of interstitial SMCs was easily observable. SMCs were not only found directly surrounding the glandular epithelium but were also visible in all parts of the interstitial tissue (Fig.12A), alternating with connective tissue and extend between prostate glands (see Fig.11A).

In addition, cellular localization of PDE5 expression was investigated by co-localization of smooth muscle actin and PDE5 (Fig.12B-E). Immunofluorescence staining on paraffin-embedded tissue nicely revealed the expression of PDE5 within interstitial SMCs (Fig.12B-C), determined by smooth muscle actin.

To gain a more vivid impression of PDE5-expressing SMCs within the human prostate, CLARITY was performed as double staining with antibodies for PDE5 and smooth muscle actin. The PDE5 expression followed exactly the localization of elongated SMCs which either surround prostatic glands or stretch further through the stroma (Fig.12D-E). Interestingly, interstitial SMCs in close proximity to glands were commonly found in a longitudinal orientation, while those SMCs distal from glands were also oriented transversally of multiple directions (Fig.12D).

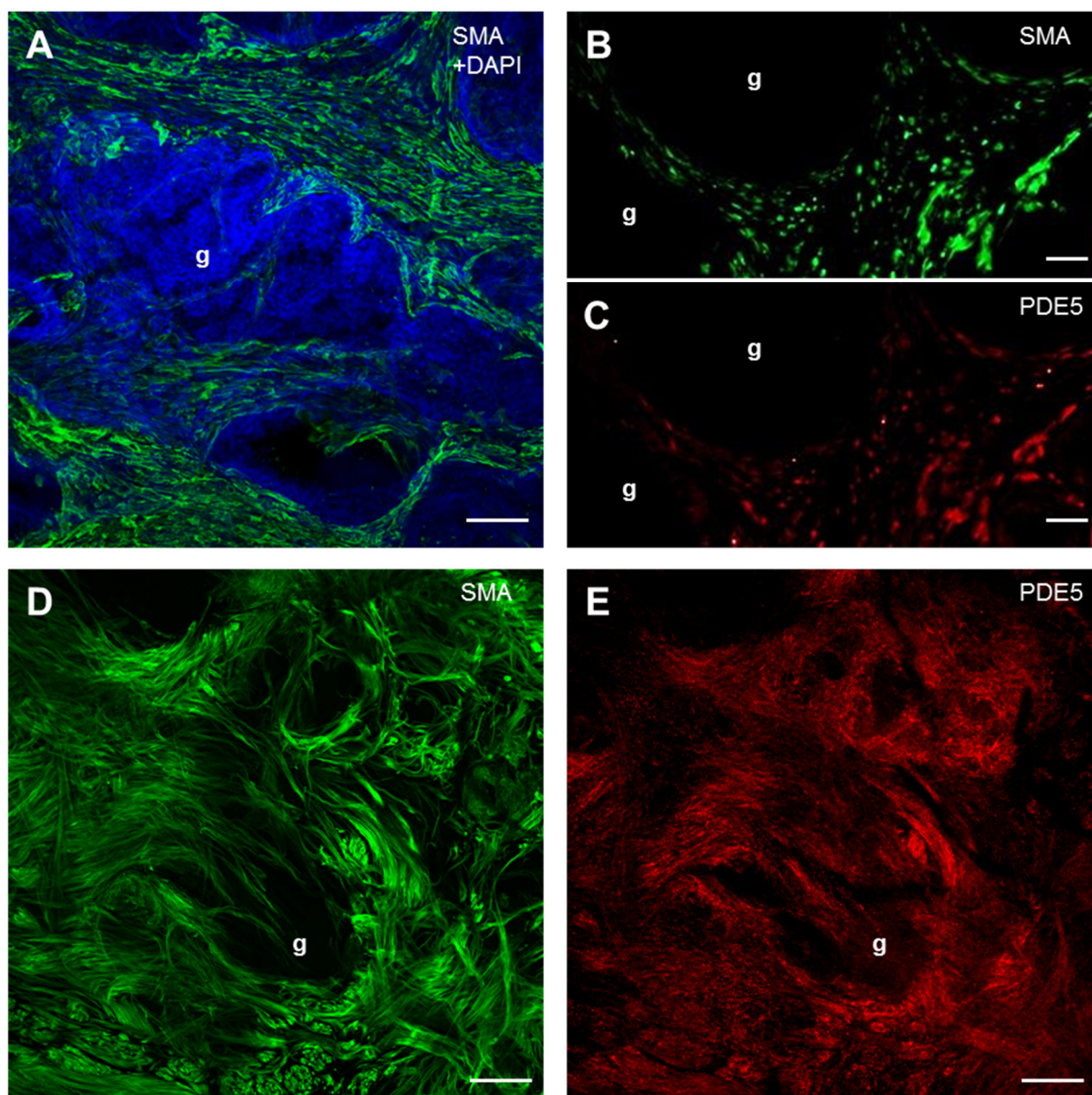


Fig.12: Visualization of human prostatic SMCs.

A: In the CLARITY approach from human prostate biopsies SMA (green) and DAPI (blue) were used to visualize SMCs that extend in all parts of the interstitial zone between prostatic glands (g). **B-C:** Double staining on paraffin-embedded human prostate biopsies revealed PDE5 (red) expression in interstitial SMCs which were localized by SMA (green) staining. **D-E:** CLARITY-based double staining visualized the three-dimensional architecture of PDE5 (red) -expressing human prostatic SMCs visualized by SMA (green). Scale bars (A, F, G): 75 μ m, scale bars (B, C): 25 μ m.

4.6 Vasculature of the human prostate

In paraffin embedded human tissue samples SMCs of the tunica media could be detected by positive immunostaining for smooth muscle actin (Fig.13A). Co-localization with PDE5 confirmed expression in vascular smooth muscle cells (Fig.13B) as already described in case of rat prostatic blood vessels (see Fig.10A-D) with exception of few interfering artifacts, presumably erythrocytes.

In a second approach, the differentiation status of vascular SMCs in comparison to interstitial SMCs was tested. CLARITY double staining for calponin (to detect more differentiated SMCs) and SMA (to visualize smooth muscle cells in general) revealed SMA expression in vascular smooth muscle cells (Fig.13C) but lacked expression of calponin within the same vessels (Fig.13D). Interstitial SMCs, however regularly showed co-expression of smooth muscle actin and calponin (indicated with white arrows). This in turn, suggests a more differentiated phenotype of interstitial SMCs compared to vascular SMCs (Fig.13C-E).

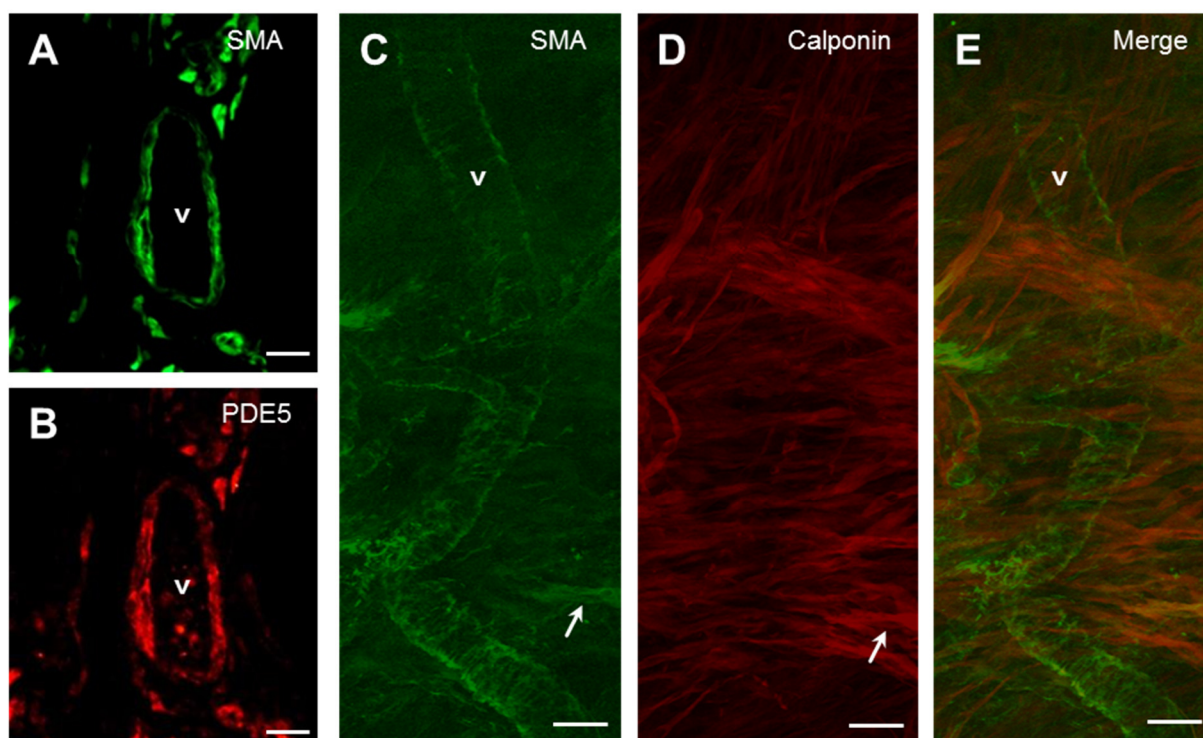


Fig.13: SMCs of the human prostatic vasculature.

A-B: Double staining on paraffin-embedded human biopsies of the prostate exhibited co-localization of PDE5 (red) within SMCs of the prostatic vasculature (v) labeled with antibody for SMA (green). **C-E:** Large vessel (v) of the human prostate that was cleared and stained with our CLARITY approach showed calponin (red) expression (marker for differentiated SMCs) exclusively in interstitial SMCs (arrows). Both, interstitial and vascular SMCs were capable of labeling with SMA, a general SMC marker. Scale bars (A-B): 10 μ m, scale bars (C-E): 25 μ m.

4.7 Functional analysis

4.7.1 Contractility of rat prostate acini

In order to investigate the functional mechanism of PDE5 action in the prostate, isolated acini of the rat ventral prostate were investigated using time-lapse imaging on transillumination microscopy. As described earlier (see Fig.8A) prostate acini in rat were found tightly encircled by SMCs. Spontaneous contractions of glandular musculature were visible along the wall of acini (Fig.14A) and exhibited a slightly irregular pattern (Fig.14B). However, the potency of contractions and contractile pattern did not differ (data not shown) among various parts of the gland. Time-lapse images of wall movements were treated as time stacks and translated into little peaks (Fig.14B, indicated with arrows) to follow them over time. Treatment with the PDE5 inhibitor sildenafil immediately resulted in a reduction of the contractile frequency (Fig.14B). Subsequent addition of noradrenaline confirmed tissue viability (not shown). Drug effect was proven to be statistically significant by analyzing a total number of 8 individual animals (Fig.14C).

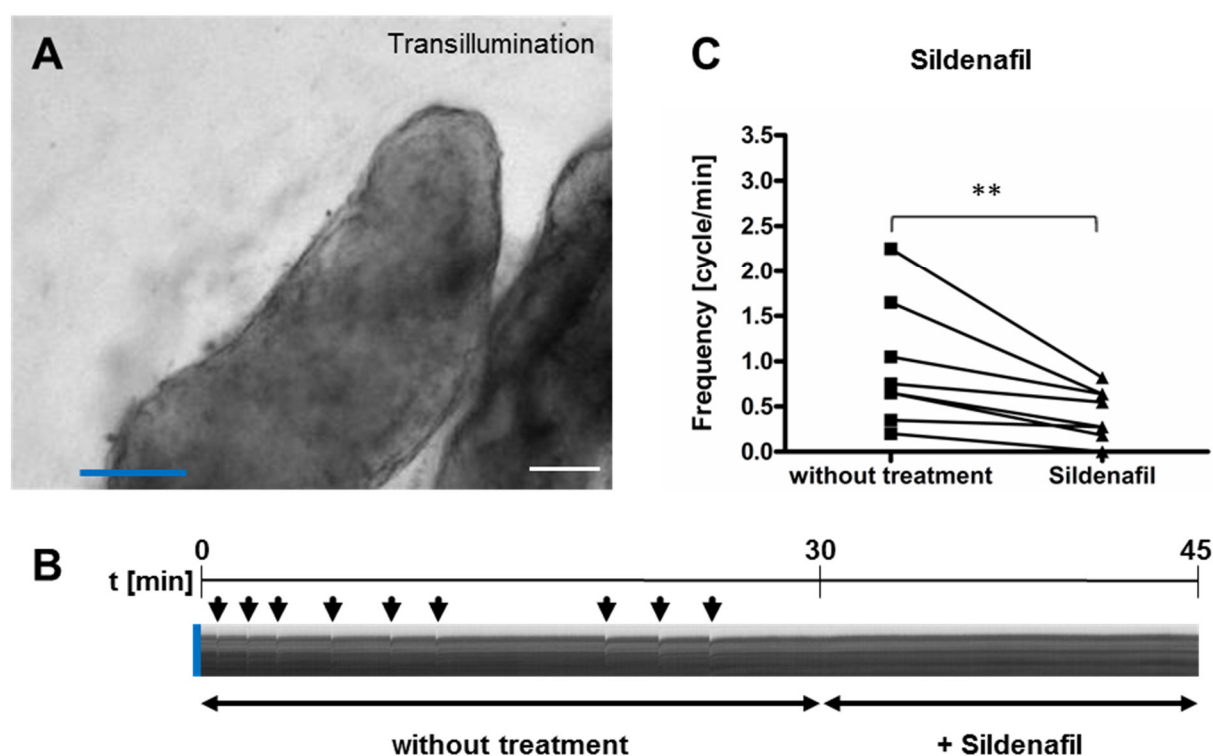


Fig.14: Analysis of contractility of rat prostate glands.

A: Freeze frame of single glands dissected from the rat ventral prostate. Blue line indicates the region of interest (ROI) from which wall movements were depicted. Scale bar (A): 100 μ m. **B:** Time stack originating from ROI in (A) with spontaneous contractions were visible as twitches (arrows) and stopped completely after addition of sildenafil. **C:** Paired, one-tailed t-test proved a highly significant reduction of the contractile frequency after addition of sildenafil (n=8, **p<0.01).

4.7.2 Contraction of rat prostatic ducts

Ducts of the rat ventral prostate which directly drain into the urethra were investigated regarding their response to the PDE5 inhibitor sildenafil. In contrast to acini, proximal prostatic ducts are surrounded by several layers of SMCs which is why ducts were analyzed separately to acini. For comparison of both structures, time-lapse imaging of the prostatic ducts used the same experimental set up as previously established for contractile recordings of prostatic acini.

Time-lapse imaging revealed no spontaneous contractions on prostatic ducts at any time (Fig.15C). Also, no detectable response was visible after treatment with sildenafil. However, the addition of noradrenaline to mimic sympathetic stimulation instantly caused a dramatic contraction of the whole duct (Fig15A-B).

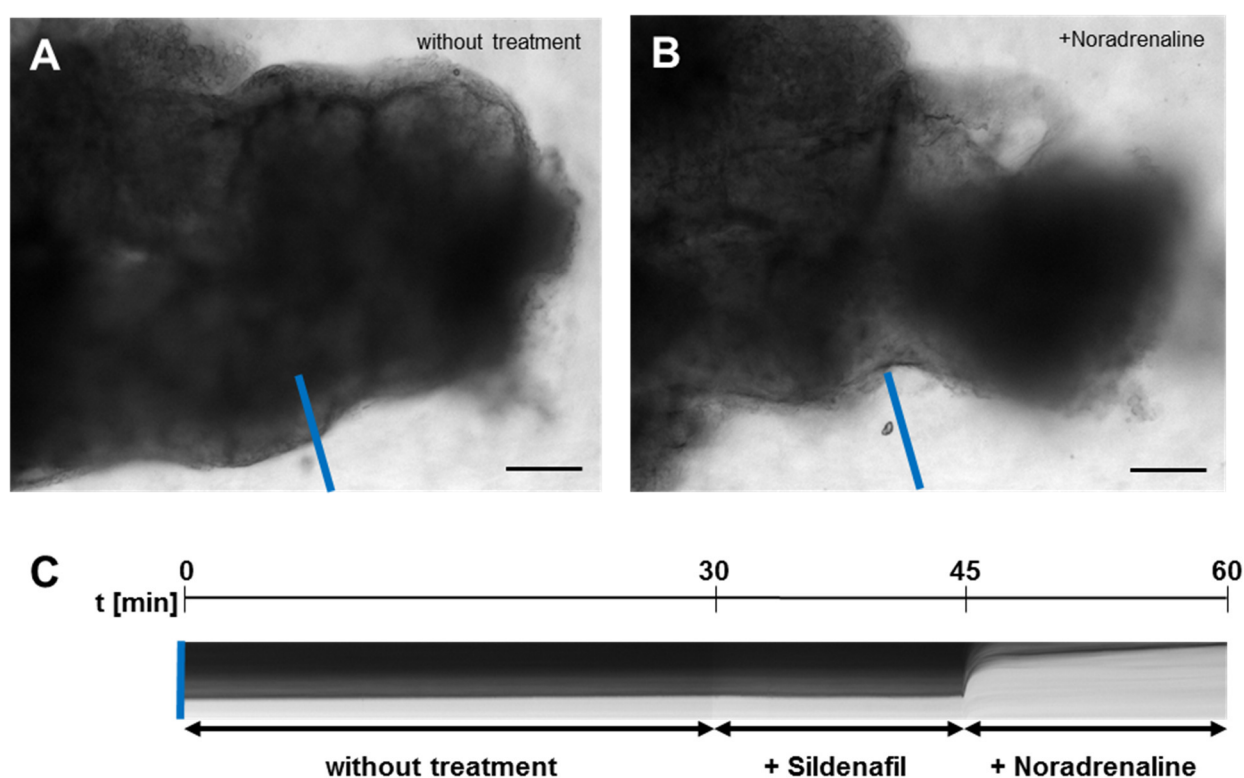
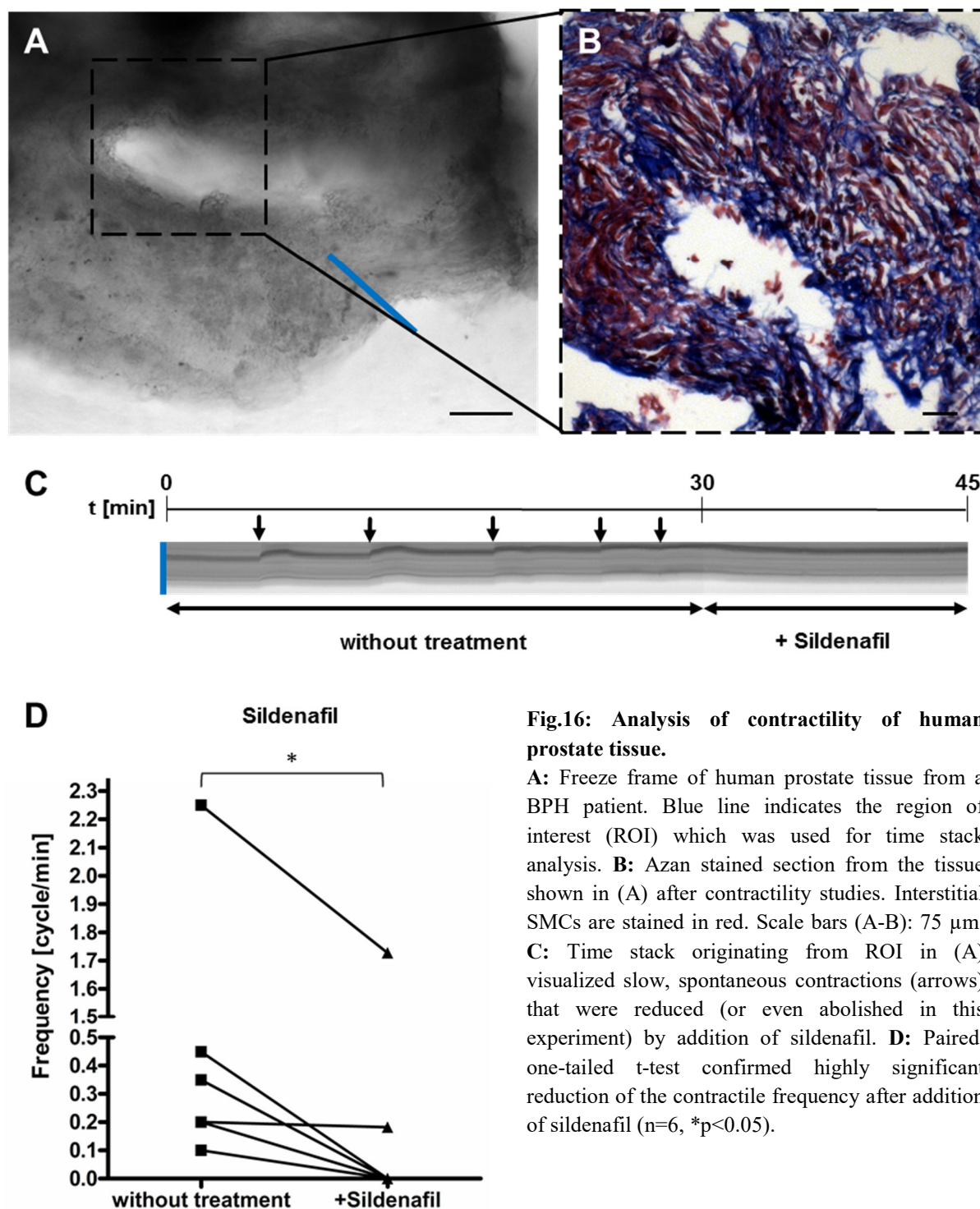


Fig.15: Analysis of contractions of rat prostatic ducts.

A: Freeze frame of untreated proximal duct from the rat ventral prostate. Blue line indicates the region of interest (ROI) from which movements of the interstitial zone were depicted. **B:** Freeze frame from identical duct as shown in (A). Addition of noradrenaline resulted in a dramatic contraction of the whole duct. Scale bars (A-B): 75 μm . **C:** Time stack, originating from the ROI visible in (A) and (B) as a blue line, showed no spontaneous contractions, neither under untreated conditions nor after addition of sildenafil. Addition of noradrenaline immediately caused a striking reduction of the ductal diameter.

4.7.3 Contractility of the human prostate

Comparison of human and rodent prostate anatomy shows obvious histological differences. Despite this, it should be tested whether PDE5 action in prostatic SMCs of both species was comparable. Therefore tissue sample from donors suffering of BPH or prostate cancer were analyzed for contractility. To ensure transillumination, tissue sections were sliced as thin as possible by hand in regions with visible prostate gland proportion.



Slow contractions occurred spontaneously in form of partial movements of the interstitial tissue. Contractility was visible in close proximity to prostate glands with a slightly irregular pattern. Regions with highest contractile activity were used to capture (Fig.16A) and translate tissue movements into countable peaks (Fig.16C).

Treatment with the PDE5 inhibitor sildenafil immediately reduced spontaneous contractions or even abolished those movements completely. With a total number of 6 cases, contractile reduction by sildenafil was statistically confirmed (Fig.16D).

Treatment with noradrenaline at the end of each experiment served as vitality control. All investigated human tissues were subsequently embedded in paraffin and stained with AZAN (Fig.16B) to visualize contractile structures.

4.7.4 Vascular contractions

In rats, arteries were regularly found directly attached to those proximal ducts of the ventral lobes that enter the urethra at its ventral aspect. Single blood vessels were dissected (Fig.17A) in order to observe any contractile response to sildenafil and noradrenaline. Due to the mechanism of normal blood vessel function, spontaneous contractions were not found for vascular SMCs as expected and therefore induced by noradrenaline.

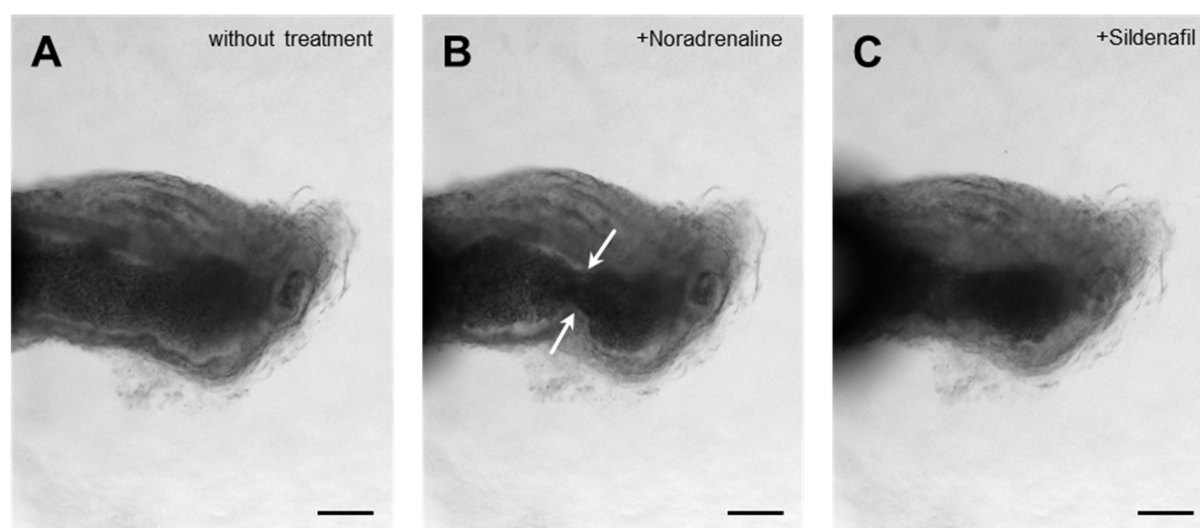


Fig.17: Analysis of contractions of prostatic vasculature in rats.

All freeze frames (A-C) represent different time points out of one single experiment. **A:** Large blood vessel originating from the proximal aspect of the rat ventral prostate without any treatment. **B:** Addition of noradrenaline caused circular compression of the vascular SMCs that reduced the vessel diameter (white arrows). **C:** Re-expanded vascular diameter after treatment with sildenafil. Scale bars (A-C): 50 μm .

In some cases, only short parts along the investigated vessels showed circular compression of the vascular musculature after noradrenaline addition (Fig.17B). This in turn, leads to a dramatic reduction of the vessel diameter in those arterial parts.

Sildenafil-treated vessels than reestablished their arterial diameter with a final dimension comparable to the untreated situation at the beginning of the experiment (Fig.17A, C).

4.8 Hormonal influences on prostatic musculature

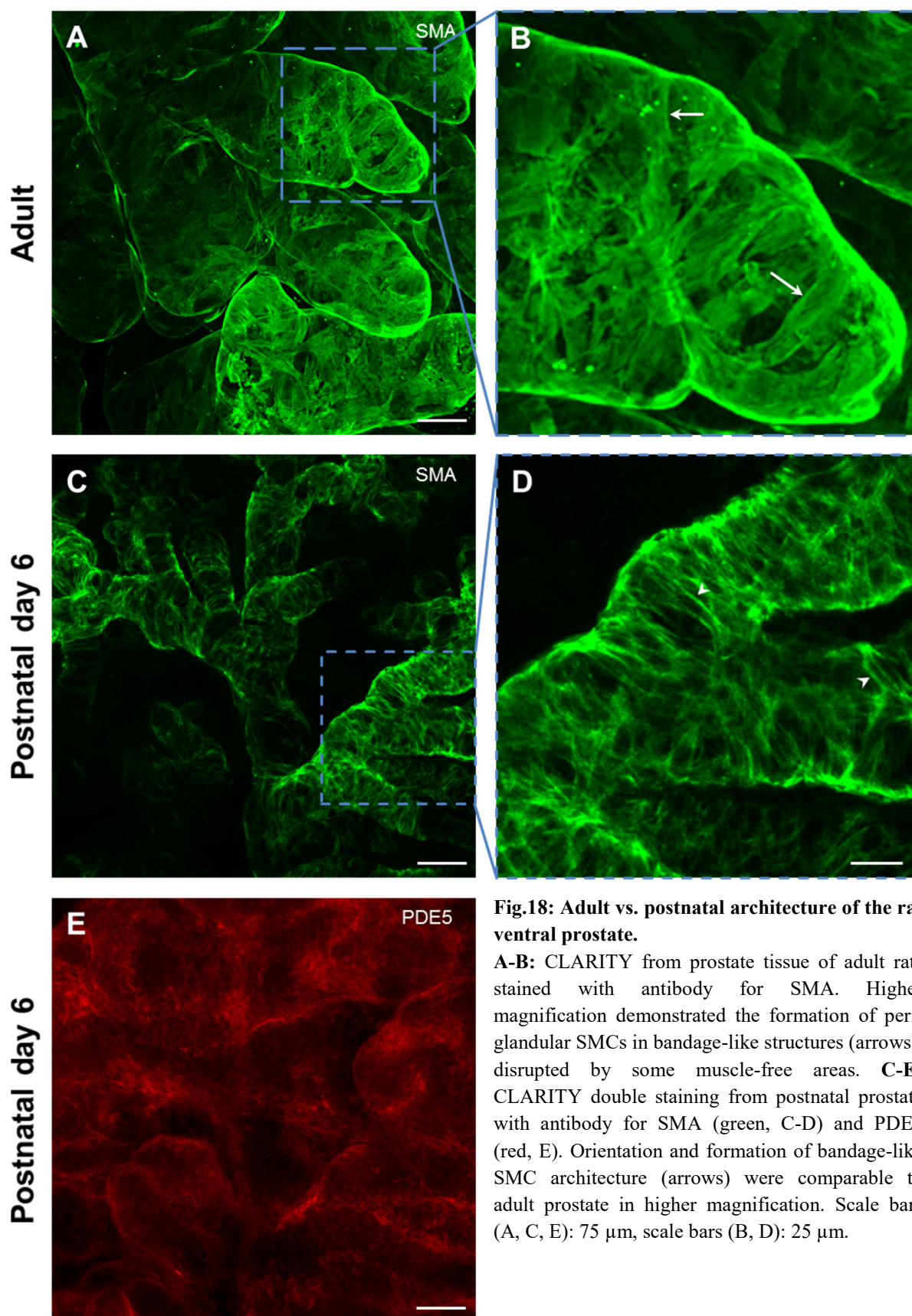
4.8.1 Postnatal development of SMC architecture in rats

Development and homeostasis of the prostate are highly androgen-dependent, similar to other organs of the male genital tract like testis or epididymis. Dynamics of serum testosterone levels are comparable in rats and men with very low levels shortly after birth and highest adult levels (Picut et al. 2018). Because of this contrasting situation, prostatic SMCs from adult rats were compared to those just reaching postnatal day 6 (6d).

In order to identify age-related differences in prostatic SMCs, acini from adult respectively 6d old rats were investigated using our three-dimensional CLARITY approach. Apart from the smaller size with fewer branches of the developing postnatal rat prostate, further histological changes were observed. The focus of this investigation was on age-related changes in the expression of smooth muscle actin and PDE5 within peri-glandular SMCs.

In adult rats, peri-glandular SMCs (stained with antibody for smooth muscle actin) were found tightly around prostatic acini forming large bandage-like structures (marked with arrows) which were disrupted by some empty areas (Fig.18A-B, see also Fig.8A). Comparison with the smooth muscle actin staining of the postnatal prostate acinus (6d) revealed SMCs to be similarly arranged and oriented (indicated with arrowheads) as observed in adult animals (Fig.18C-D). However, explicit differences in case of expression intensity were observable. While “bandages” around adult acini were visible as clear compact structure, those from postnatal rats showed highest smooth muscle actin expression along the edges of the “bandages” and weakened to the center (Fig.18C-D). This less distinct expression of smooth muscle actin in the postnatal prostate coincided with lower PDE5 expression obtained from identical peri-glandular SMCs. Localization of PDE5 exhibited a rather diffuse expression around most postnatal acini (Fig.18E-F) and thus reflected just barely the general architecture of peri-glandular SMCs. This contrasted previous described

PDE5 expression investigated in adult rats (see Fig.8D) which was localized tightly around prostatic acini.



4.8.2 Castration-induced androgen deprivation in rats

To get deeper insights how testosterone influences the cGMP pathway, a testosterone deprivation model was used to study possible changes of the rat ventral prostate. In detail, testosterone deprivation was ensured by castration of male Wistar rats, followed by treatment with defined amounts of testosterone to restore hormone cut-off.

Western blot analysis was used to determine the regulatory effect of increasing testosterone levels on the cGMP target protein PKG I (Fig.19). In prostate, highest PKG I level was found at vehicle control which represents a total loss of all testosterone resources. Interestingly, a correlation of increasing testosterone concentrations together with decreasing PKG I expression was clearly visible at the immunoblot. Protein kinase B (PKB) was used as a reference for another protein kinase that exhibited no differences in any treatment within the prostate.

Protein preparation of skeletal muscles and penis (further androgen-dependent organ of the genital tract) served as positive control and showed no differences in the expression of both protein kinases at any obtained testosterone treatment. This finding demonstrates the regulatory capacity of testosterone on PKG I expression within the rat prostate.

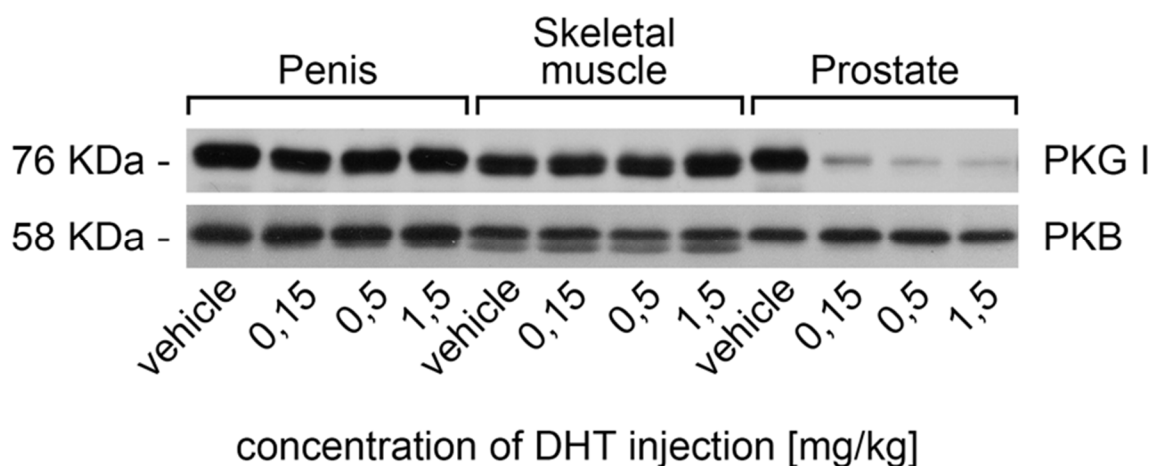


Fig.19: PKG I regulation by testosterone deprivation in rats.

Western Blot analysis of male Wistar rats after hormone cut-off (via castration) followed by artificial testosterone restoring. PKG I expression within the prostate decreased by increasing concentration of testosterone with highest amounts of PKG I at vehicle control. In penis (androgen-dependent organ of the male reproductive tract) and skeletal muscle (androgen-independent tissue) PKG I expression was found unchanged at any given testosterone condition. Protein kinase type B (PKB) served as positive control. Expression of PKB was not influenced by hormone cut-off or its restoring.

4.8.3 Genetically modified mouse models

4.8.3.1 Aromatase models affecting both, estrogens and androgens

Testosterone deprivation by castration showed visible regulatory effects on the expression of PKG I in the rodent prostate. Next step was to investigate how changes of estrogen potentially influence the cGMP pathway. For this purpose two different genetically modified aromatase mouse models were investigated, an estrogen-deficient aromatase knockout (ArKO) mouse, generated by targeted disruption of the *cyp19* gene (Bianco et al. 2006; Fisher et al. 1998) as well as an aromatase overexpression (AROM⁺) mouse, bearing the human ubiquitin C promoter/human P450 aromatase fusion gene (Ellem et al. 2009; Li et al. 2001). Aromatase in general, is responsible for the conversion of testosterone to estradiol via formation of an aromatic A-ring. The aromatase knockout (ArKO) maintain a complete lack of estrogen in mice, while serum testosterone levels increase up to 8 times the wild type (WT) level (Risbridger et al. 2003). Opposite hormonal serum levels are present in case of an overexpression of aromatase (AROM⁺) in mice which cause dramatically increased estrogen production by using up almost all produced testosterone (Li et al. 2001).

In a first step, tissue samples from the prostatic ventral lobe of ArKO, AROM⁺ and wild type mice were evaluated regarding changes in levels of the cGMP target protein PKG I using Western blot analysis (Fig.20A). In addition, cGMP-regulating enzymes PDE5 (degrades cGMP) and sGC (produces cGMP) were analyzed. Vinculin, a cytoskeletal protein served as a loading control and revealed no quantifiable difference between all three mouse groups (n=10).

Densitometric analysis revealed a significant increase of PKG I expression in AROM⁺ mice compared to wild type, while PKG I expression in ArKO mice was found to be downregulated (Fig.20B). This provides the first evidence for an estrogen-regulated enzyme involved in the cGMP pathway within the prostate.

Regarding PDE5, expression of this cGMP-degrading enzyme was found also significantly increased in AROM⁺ mice compared to ArKO mice (Fig.20C).

Despite a slight increase in AROM⁺ mice, respectively decrease in ArKO mice, comparison of sGC expression between all three mouse groups revealed no statistically significant differences (Fig.20D).

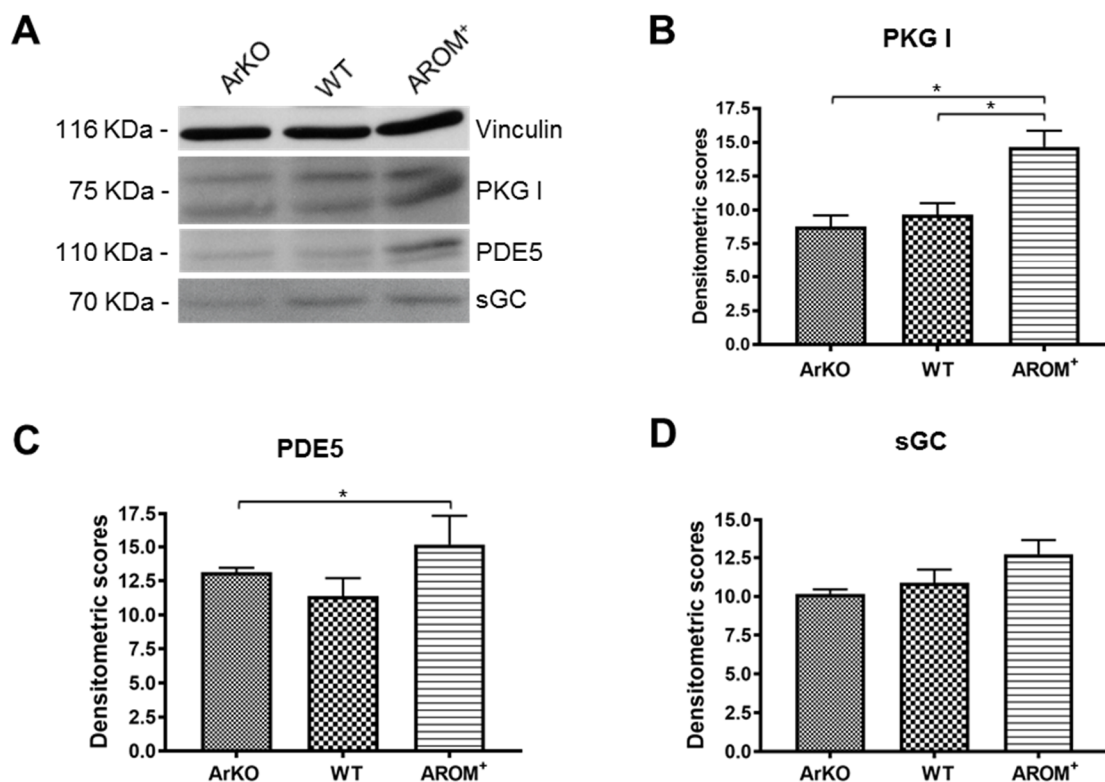


Fig.20: cGMP-dependent Protein kinase I regulation in the prostate of ArKO, WT and AROM⁺ mice.

A: Western Blot analysis of PKG I, PDE5 and sGC from prostate tissue of genetically modified mouse models containing an aromatase knock out (ArKO) or overexpression (AROM⁺). Vinculin served as loading control. **B-D:** Densitometric analysis based on the Western blot in (A). Statistics were performed with paired, one-tailed t-tests. PKG I was significantly upregulated in AROM⁺ mice compared to ArKO and WT (n=5, *p<0,05, B). PDE5 expression was also significantly higher in AROM⁺ mice compared to ArKO and WT (n=5, *p<0,05, C). Expression of sGC showed no significant differences (D).

4.8.3.2 Localization of prostate structures showing hormone-induced PKG I regulation

Paraffin-embedded prostate tissue sections originating from the ventral lobe of ArKO, AROM⁺ and wild type mice were stained immunohistochemically using a PKG I antibody. In all 3 groups of mice (n= 24) PKG I expression was clearly visible in vascular SMCs (Fig.21A, C, E). Striking differences were found in SMCs surrounding the glandular epithelium. While ArKO mice lack almost all peri-glandular PKG I expression, a considerable increase of PKG I around prostate glands was found in AROM⁺ mice compared to wild type.

To check whether the regulatory effect of hormones was simply caused by regulation of the number of SMCs, staining of serial sections of all investigated animals were performed using a smooth muscle actin antibody. Comparison of all three groups of mice revealed no visible difference in the amount of SMCs encircling the prostate glands (Fig.21B, D, F) which supports the assumption of a true hormone-dependent regulation of PKG I in prostatic SMCs.

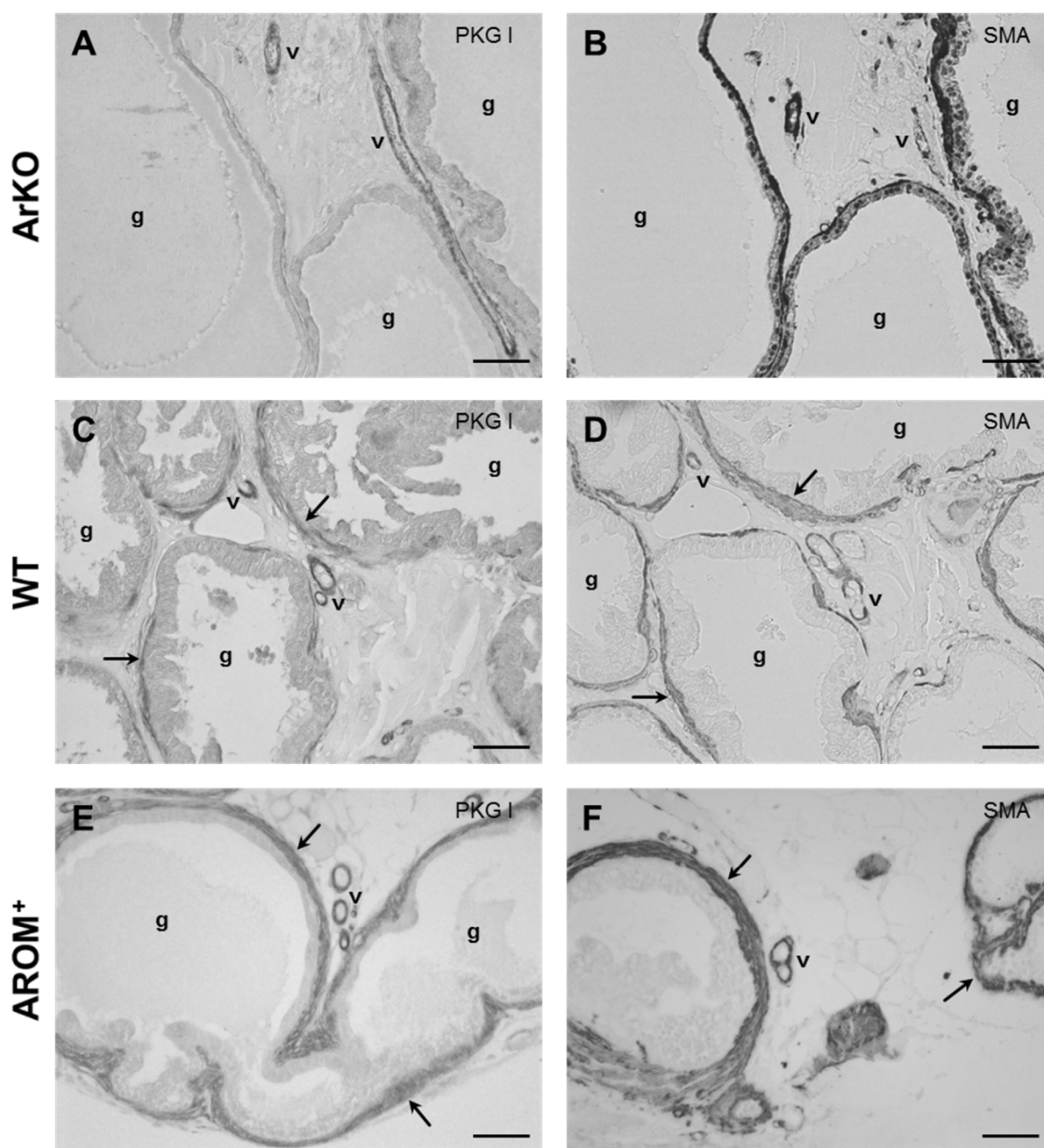


Fig.21: cGMP-dependent protein kinase I regulation in peri-glandular and vascular SMCs of ArKO, WT and AROM⁺ mice.

A-B (ArKO): Immunostaining for PKG I (A) demonstrated its expression in cells of the vasculature (v) but barely around prostatic glands (g) in mice containing an aromatase knock out. Corresponding serial section to (A) labeled for SMA (B) localized SMCs in vessels and around prostatic glands. **C-D (WT):** Striking expression of PKG I (C) in peri-glandular SMCs (arrows) and vascular SMCs of wild type mice. Corresponding serial section to (C) showed SMA (D) expression in both, peri-glandular and vascular SMCs. **E-F (AROM⁺):** Dramatic upregulation of PKG I (E) expression in peri-glandular SMCs of mice that showed an aromatase overexpression. Corresponding serial section to (E) labeled for SMA (F) demonstrated comparable expression as seen in WT (D) and ArKO (B). Scale bars (A-F): 50 μ m.

4.8.4 Hormonal regulation of cGMP pathway components in men

4.8.4.1 Characterization of human prostatic interstitial cells

Cultured human interstitial cells donated by Australian prostate cancer patients were used to investigate possible regulatory effects of testosterone on cGMP pathway components in human prostatic interstitial cells.

Untreated cells were analyzed by classic immunocytochemistry using antibodies for smooth muscle actin, PKG I, PDE5 (Fig.22A-C) and counterstained with hematoxylin to discriminate their phenotypic characteristics. First of all, the expression of smooth muscle actin was found in all cultured human interstitial cells (Fig.22A) with almost equal intensity levels independent of cellular shape or dimension. This finding suggests a mostly contractile phenotype of the investigated interstitial cells. However, it remains unclear whether the origin of these cultured cells were primarily SMCs or myofibroblasts or both.

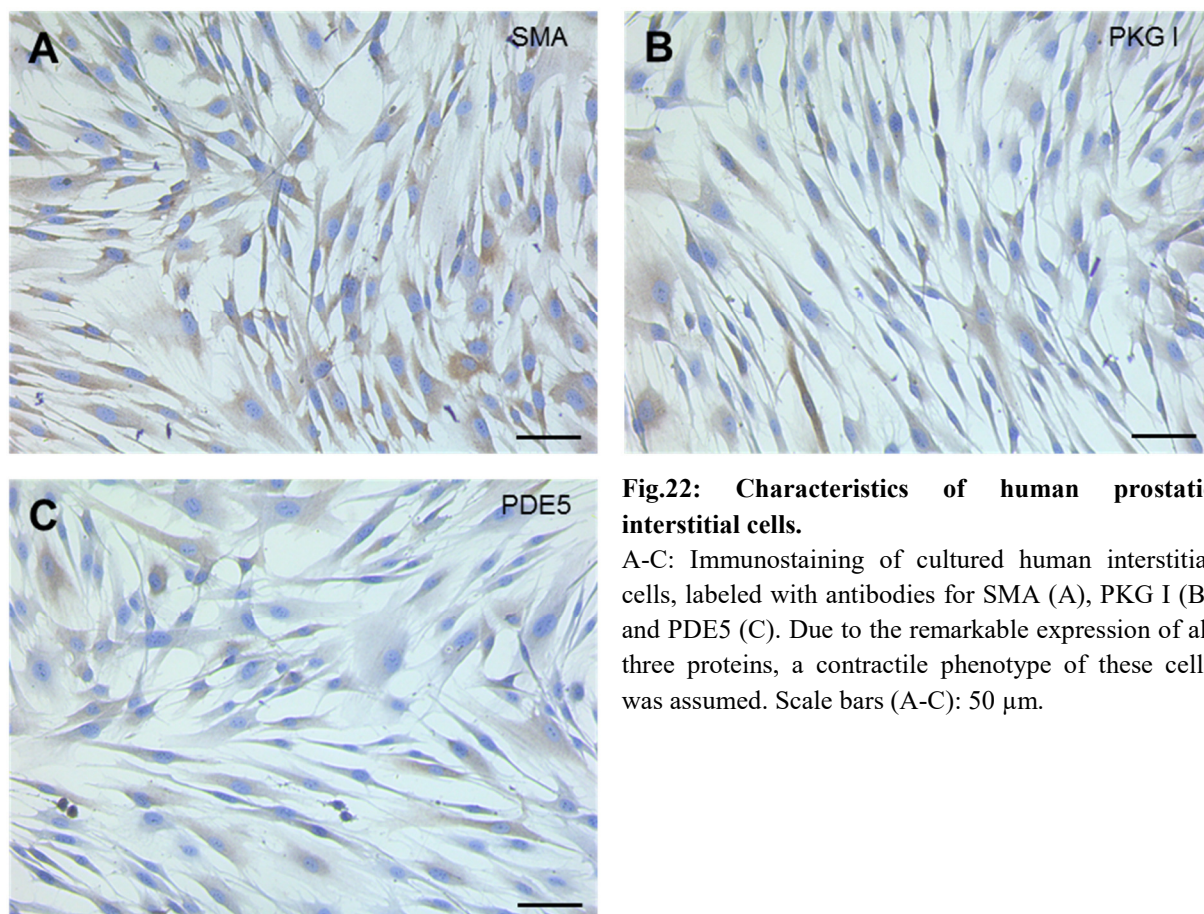


Fig.22: Characteristics of human prostatic interstitial cells.

A-C: Immunostaining of cultured human interstitial cells, labeled with antibodies for SMA (A), PKG I (B) and PDE5 (C). Due to the remarkable expression of all three proteins, a contractile phenotype of these cells was assumed. Scale bars (A-C): 50 μ m.

Furthermore, the cGMP target protein PKG I was shown to be expressed in almost all cultured cells with slight differences in intensity among cells of the same population

(Fig.22B). Finally, the cGMP degrading enzyme PDE5 was also found in most cultured interstitial cells (Fig.22C) with little exception of only a few enlarged cells. The visible expression of both cGMP pathway components, PKG I and PDE5 encouraged the suggested contractile phenotype of the investigated cultured human interstitial cells.

4.8.4.2 Testosterone treatment of human prostatic interstitial cells

In a second step, cultured human interstitial cells were treated with two different concentrations of dihydrotestosterone (DHT) to identify possible regulatory effects on certain cGMP pathway components.

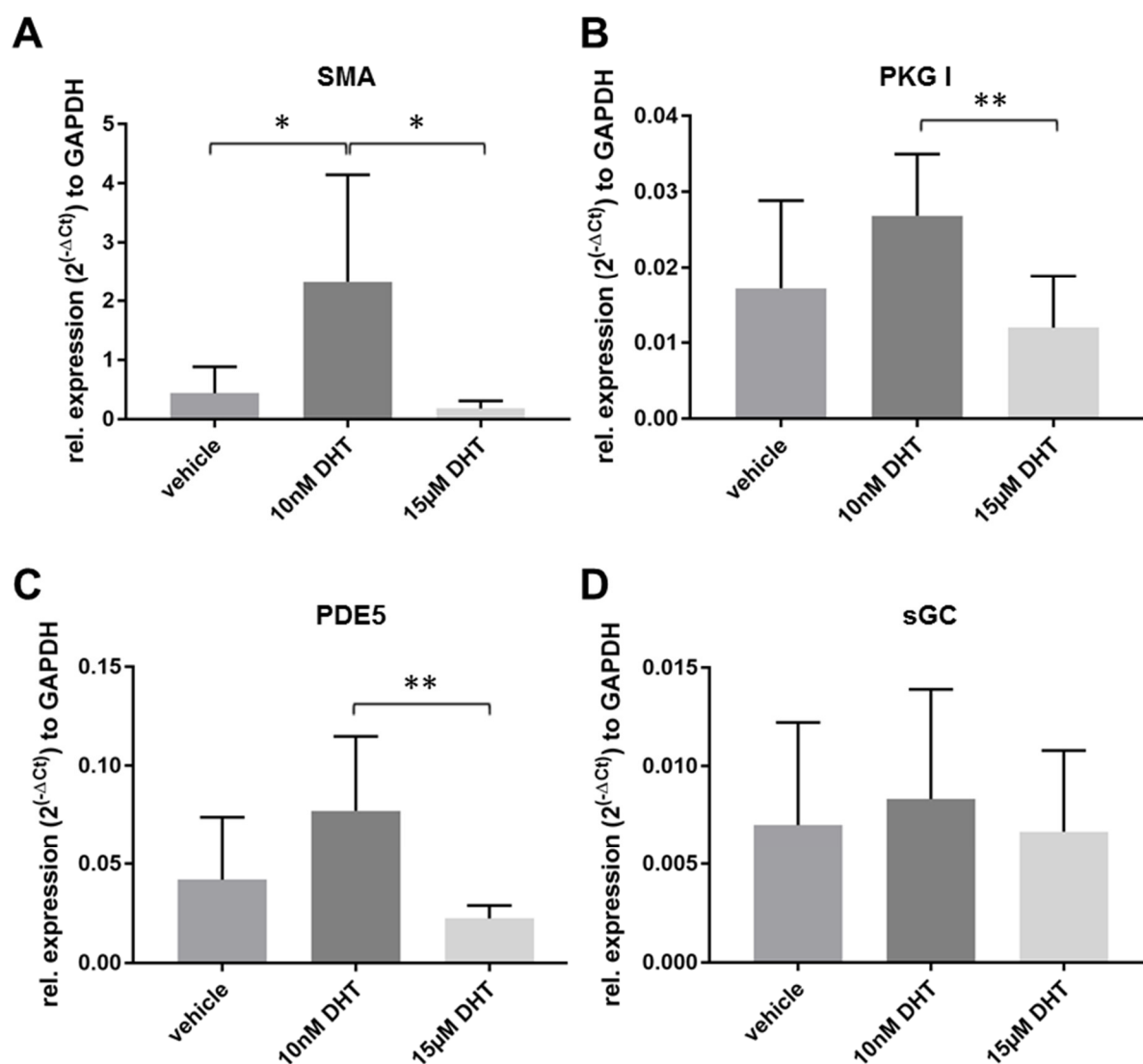


Fig.23: qPCR of cGMP pathway components in human prostatic interstitial cells.

A: Significant upregulation of SMA mRNA in case of DHT treatment with a low concentration of 10 nM compared to the superphysiologic concentration of 15 μM DHT and vehicle control. **B-C:** Expression (relative to the housekeeping gene GAPDH) of PKG I (B) and PDE5 (C) revealed upregulation of both mRNAs after treatment with 10 nM DHT. **D:** No statistical difference regarding the expression (relative to the housekeeping gene GAPDH) of sGC mRNA was found after both DHT treatments. All statistical analysis based on t-tests (paired, one-tailed) for comparisons between individual mRNA levels.

In detail, cells were pretreated with either a physiological (10 nM DHT) or superphysiological (15 μ M DHT) concentration of dihydrotestosterone. After 24 hours of incubation with DHT, cells were harvested in mercaptoethanol and processed for mRNA quantification via qPCR. A significantly increased mRNA level of smooth muscle actin was found (Fig.23A) in case of the cellular pretreatment with 10 nM DHT compared to 15 μ M DHT and vehicle control. This finding might indicate the increase to a rather pure contractile phenotype of those cultured interstitial cells pretreated with physiological DHT concentration.

This assumption was confirmed by the analysis of further mRNAs from muscle typical proteins, such as PKG I (cGMP target protein), PDE5 (degrades cGMP) or sGC (produces cGMP). Relative expression of PKG I was found significantly upregulated after pretreatment with the physiological concentration of 10 nM DHT (Fig.23B) compared to treatment with 15 μ M DHT. Similar to PKG I, relative expression of PDE5 revealed a significant upregulation (Fig.23C) in cells pretreated with the physiological DHT concentration in comparison to those receiving the higher dose.

Surprisingly, mRNA levels of the cGMP-producing enzyme sGC showed no significant differences (Fig.23C) in any case of DHT pretreatment. This in turn, might suggest that sGC is probably not affected by changing testosterone levels.

4.9 Visualization of SMC proliferation in BPH tissue

The current knowledge, whether or not prostatic SMC proliferation is active during pathologic benign prostatic hyperplasia (BPH) development is still rare. For this purpose, the three-dimensional CLARITY approach was used to check for potential SMC proliferation. Biopsies donated by BPH patients were investigated using a double staining protocol for smooth muscle actin and Ki67 together with the general nuclear marker DAPI (Fig.24A-B).

A proliferation was clearly visible in interstitial SMCs of human BPH tissue samples (Fig.24B). Identification of these proliferative SMCs was performed by co-localization with the expression of smooth muscle actin as well as the shape of the cell nuclei, characterized by a rather oval contour of those nuclei compared to round nuclei of epithelial cells.

Proliferative activity was detected also in nuclei of glandular epithelial cells (Fig.24B). In general, human BPH biopsies regularly showed more proliferating cells within the glandular epithelium compared to interstitial SMCs (Fig.24A).

Proliferation of peri-glandular SMCs (Fig.24C-D) was also visible in the ventral prostate of adult rats without enlargement disorder. In rat, immunostaining for Ki67 confirmed the previous impression from human BPH tissue and demonstrated an even higher amount of proliferative epithelial cells compared to proliferative peri-glandular SMCs.

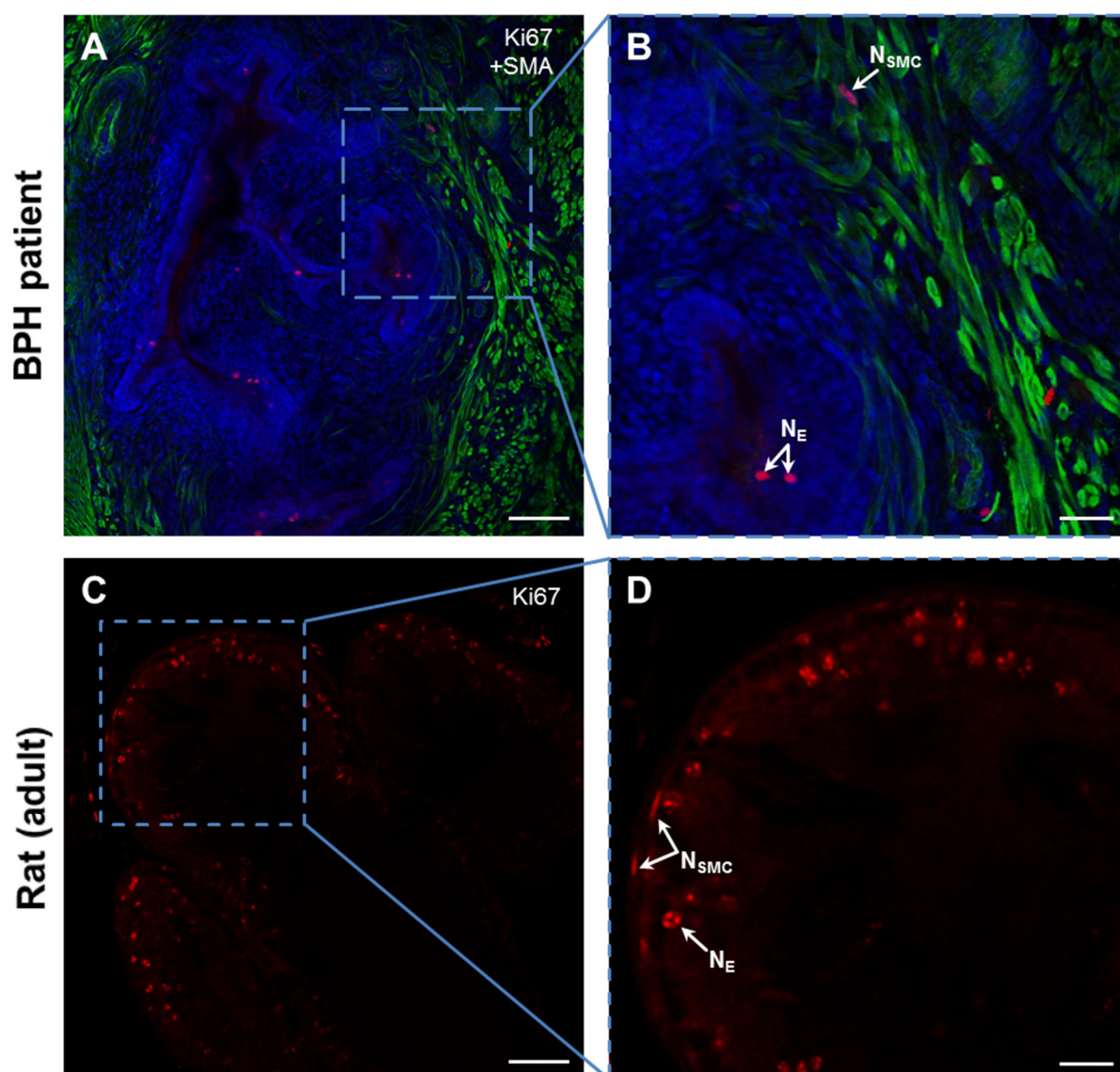


Fig.24: Proliferation of prostatic SMCs in human BPH patient and rat prostate tissue.

A-B: CLARITY double staining from human prostate biopsies of diagnosed BPH used SMA (green), Ki67 (red) and DAPI (blue) to visualize proliferating nuclei. Higher magnification revealed proliferation in oval-shaped nuclei of peri-glandular SMCs (N_{SMC}), apart from rather round-shaped nuclei of epithelial cells (N_E). **C-D:** Immunostaining of prostate tissue in adult rats without enlargement disorder showed proliferating nuclei of both cell types, glandular epithelium and peri-glandular SMCs. Scale bars (A, C): 75 μ m, scale bars (B, D): 25 μ m.

5 Discussion

In the present study PDE5 (degrades intracellular cGMP) was found to be expressed exclusively in SMCs of the vasculature and those surrounding prostatic glands and ducts. Within the rodent and human prostate, our three-dimensional approach (based on CLARITY) revealed in detail the cellular arrangement of PDE5-expressing SMCs around prostate glands. Inhibition of PDE5 using sildenafil resulted in significant reduction of the spontaneous contractility of human and rat prostate tissue by time-lapse imaging based on transillumination microscopy. Spontaneous contractions of prostatic SMCs were only found around prostate glands whereas prostatic ducts lacked any spontaneous contractions even though massive contractions of the whole duct could easily be induced by addition of noradrenaline. Testosterone deprivation due to aromatase overexpression (AROM⁺) in genetically modified mice mediated a striking upregulation of PDE5 and PKG I (target of cGMP action). In agreement, the aromatase knockout (ArKO) mice which lack estrogen production within the prostate (McPherson et al. 2001) showed the opposite effect. This hormone-dependent PKG I regulation was confirmed using castrated rats.

5.1 SMCs of the human and rodent prostate

The first part of this study focused on the general histologic description of smooth muscle cells present in mammalian prostate and continued with the cellular localization of certain enzymes involved in the cGMP pathway. Comparisons were made between rodents and humans that revealed species-dependent characteristics.

Using our new adapted three-dimensional CLARITY approach, the rat prostate glands (respectively acini) were found tightly enclosed by SMCs with orientation in multiple directions causing particular overlapping as well as some empty areas. The lack of SMCs regularly found at the tip of prostatic acini could possibly be explained as persisting voids that remain from the need of space during postnatal development of the ductal and glandular system. Cunha and colleagues localized (1987) the formation of new branchpoints at the distal tip of the ductal/glandular network. Therefore, it seems useful to induce development of new branches in parts of the distal tips in which the formation of those branches is not impeded by peri-glandular SMCs. In contrast to the peri-glandular/peri-ductal SMCs of the rat prostate, the human prostate possesses SMCs in all parts of the prostatic stroma alternated by connective tissue. The reason for this histological difference between both species might be a

result of the different gross anatomy found in both. Compared to the compactly organized human prostate glands, rodent acini were found rather loosely connected via sparse connective tissue.

However, transport of secretion might also be affected by different SMC locations. While bandage-like SMCs of the rodent prostate tightly encircle acini in various directions and thus possibly mediate a selective fluid transport by direct reduction of the acinus diameter, transport of secreted fluid in humans might function in a more indirect way. Due to the fact that SMCs were present in all parts of the human stroma, contraction of these interstitial SMCs may cause a reduction of the stromal tissue which in turn would drain nearby glands.

Former studies by Ishihara and colleagues (1978) showed proximal prostate ducts in rodents to be encircled by multiple layers of SMCs. It has been suggested that prostate ducts do not appear to secrete prostatic fluid but rather actively help to drain the acinus during ejaculation (Lee et al. 1990). This assumption could also be applicable for human prostate ducts and if so demonstrates the importance to distinguish between glands and ducts in case of investigations with a focus on certain drug effects or basic research.

Apart from prostate glands and ducts, SMCs are also important for the regulation of the blood flow as these cells determine the vascular diameter. In both rat and human, SMCs were clearly visible in circular orientation along the prostatic vascular system using antibodies that bind to smooth muscle actin. Double staining with an additional antibody for calponin performed in the present study revealed sparse expression of calponin in SMCs of human blood vessels compared to smooth muscle actin, while most interstitial SMCs expressed both muscle markers. Calponin, a troponin-T like protein binds to actin, myosin, Ca^{2+} -binding proteins and tropomyosin. Calponin inhibits the actomyosin ATPase and prevents the movement of actin filaments which indicates its important role in the Ca^{2+} -dependent regulation of actin-myosin interaction during smooth muscle contraction. (Liu and Khalil 2018; Kreipke and Rafols 2009; Birukov et al. 1991). Due to its expression in SMCs of the contractile phenotype, calponin is supposed to be a sensitive indicator for smooth muscle differentiation (Saboor et al. 2016; El-Mezgueldi 1996). A study in genetically modified mice that lack the *Cnn1* gene (encoding calponin isoform 1), confirmed the importance of calponin for vascular development as these mice showed an impaired blood vessel maturation (Yamamura et al. 2007). The lack of calponin in vascular SMCs of the human prostate

observed in the present study might be an indication for vascular remodeling, compared to the rather full developed SMCs of the surrounding stroma.

In contrast, peri-glandular SMCs of acini from the rat and mouse prostate express smooth muscle actin as well as calponin in comparable quantities. Double staining in mouse however, revealed few glands to share more calponin than smooth muscle actin which indicates a fully developed prostate. Furthermore, the general muscle cell marker smooth muscle actin was found to be enriched in some parts of the mouse acini which possibly demonstrate functional and/or anatomical differences along a single prostatic acinus, while calponin was found to be expressed with equal intensity in peri-glandular SMCs indicating differentiated SMCs to be developed equally in all parts of the mouse acinus.

Innervation of acinar SMCs in the mouse prostate was visualized by staining with α -tubulin using our CLARITY approach. α -tubulin clearly showed the distribution of the autonomic nervous system around prostatic acini. To estimate especially the amount of noradrenaline-containing nerve fibers, a double staining with antibodies for α -tubulin and the enzymes of catecholamine synthesis (such as tyrosine hydroxylase, aromatic L-amino acid decarboxylase or dopamine beta-hydroxylase) or use of the SPG (sucrose-potassium phosphate-glyoxylic acid) method (Gray et al. 2007; Fukuda et al. 1996) would be of interest.

5.2 Localization of key proteins of the cGMP pathway

Signaling pathways using cGMP are crucial to mediate smooth muscle relaxation beside many other important cell processes. PDEs are known to degrade cGMP via hydrolysis, with PDE5 representing a cGMP-specific member of the PDE family. Its precise histologic localization was therefore, one of the main aims for this study.

In men, PDE5 was shown to be present in SMCs of the prostate glands, ducts and vasculature. This was clearly visible by double stainings together with smooth muscle actin not only in classic two dimensional DAB stainings on serial sections but especially with our three-dimensional CLARITY approach. CLARITY broadened our understanding of the spatial arrangement and function of SMCs around mammalian prostate glands (Kügler et al. 2018). In rodents, investigations on prostatic blood vessels confirmed expression of PDE5 (exclusively) in vascular SMCs. In contrast, PDE5 was barely localized peri-glandularly around acini of rat and mouse prostate. In general, visualization of the complete vasculature was often limited since smaller capillaries lack measurable fluorescence. This could be

explained by the fact that in the present study only muscle markers were investigated and (smaller) capillaries do not contain SMCs (Townsend 2012). In addition, a methodological limitation might also involve problems of antibody staining, its detection by laser-scanning microscopy or the computer-based three-dimensional reconstruction of our CLARITY protocol.

Another important enzyme involved in the cGMP signaling pathway is the protein kinase PKG I that is known to mediate smooth muscle relaxation (Wolfertstetter et al. 2013; Francis et al. 2010; Schlossmann et al. 2003). Again PKG I expression was found only in SMCs within the prostatic vasculature and stroma of both, human and rodent prostate using classical immunostaining as previous studies showed before (Francis and Corbin 1994; Wolfe et al. 1989; Lincoln 1983). This SMC localization matches former investigations in rat lungs describing the expression of PKG I in SMCs of the airways and of the bronchial arteries but not in the lung epithelium (Zhan et al. 1999).

Interestingly, CLARITY-based immunostainings showed PKG I expression additionally around prostatic acini which might reflect a different subcellular distribution compared to structural proteins.

5.3 Visualization of SMC function and relaxation for BPH treatment

Smooth muscle tone can be separated into two compartments: neurogenic tone (mediated by the release of neurotransmitters like noradrenaline from the autonomic nervous system to ensure movement of the secreted fluid into the prostatic urethra during ejaculation) and myogenic tone (spontaneous rhythmicity of the prostatic tissue, stimulus-independent from the autonomic nervous system). While previous studies focusing on spontaneous contractile activity were performed in mostly guinea-pigs, the human prostate is only insufficiently described (Lee et al. 2017; Chakrabarty et al. 2015; Exintaris et al. 2009; Exintaris et al. 2006; Oh et al. 2003).

This study visualized the spontaneous contractile activity of SMCs surrounding the rat prostatic acini respectively SMCs present in the stroma of the human prostate. The frequency of spontaneous contractility was highly comparable between both species and varied between 0.1 to 2.3 cycles/ min. Based on time-lapse imaging, our approach provided rapid and reliable contraction analyses. Especially investigations of rat prostate were appropriate for this method

due to its translucent architecture. Since proximal ducts could easily be separated from their remaining glands within the distal aspect of the rat prostate, pharmacologic effects could be analyzed individually in isolated prostatic structures. Therefore, time-lapse imaging gave a much better understanding of how interstitial SMCs contract spontaneously compared to other experimental techniques like organ bath. Transillumination microscopy also allowed simultaneous determination of contractile frequencies at different sites of one individual gland, while organ bath recordings might only reflect a sum of several contractile parts of the investigated tissue. In contrast to complicated cinematographic approaches used in the past, today's modern digital image analyses are readily available and easy to handle for further statistical procedures (Mietens et al. 2014). In addition, time-lapse imaging is found to be less invasive in case of tissue preparation due to the experimental set up of the organ bath which can cause tissue damage while holding the tissue in place by clamps and/or applying pre-tension at the beginning of the organ bath experiment. Therefore time-lapse imaging is highly suitable for systematic molecular and drug analysis. However, spontaneous contractions of glandular SMCs probably provide a basal muscle tone, necessary for agitation of secreted fluid in the glandular lumen. This in turn, supports the assumption of prostatic pacemaker cells, generating nervous system-independent contractions which were suggested in human and guinea pig prostate (Nguyen et al. 2011).

Surprisingly, prostatic ducts were found to lack spontaneous contractile activity. The physiological function of ducts seems to rather be the guidance of secreted fluid and not secretion itself, highlighted by the powerful response after addition of noradrenaline. Furthermore, prostatic ducts showed no visible response to treatment with PDE5 inhibitors (sildenafil). The reason for this insensitivity to sildenafil was most certainly not the lack of PDE5 in those structures, as PDE5 expressing SMCs were clearly localized in multiple layers around all investigated ducts. Therefore PDE5 action in peri-glandular SMCs possibly differs from those cells around prostate ducts. It could be that PDE5 in ductal musculature maintains a basic tension to facilitate rapid catecholamine-induced contractions during emission (Kügler et al. 2018).

In contrast to prostatic ducts, glands of the prostate clearly showed a visible response to treatment with sildenafil. In both, man and rat prostate, spontaneous contractile activity was significantly reduced after the addition of sildenafil. For the first time, sildenafil action was cinematographically visualized on living prostate tissue. This indicates sildenafil treatment to

be only effective in glandular SMCs and not interfering with ductal SMCs. It would be of interest to investigate to what extent other cGMP specific PDEs, such as PDE6 or PDE9 contribute to prostatic contractility. Systematical testing of further PDE inhibitors respectively a combination of different PDE inhibitors would extend our knowledge about the physiology and function of the ductal network in the prostate.

In parallel with investigations on glandular and ductal SMCs, the musculature of the prostatic blood vessels was tested by time-lapse imaging regarding any visible response to treatment with sildenafil. Noradrenaline-induced contractions in prostatic vasculature were found to be abolished by incubation with sildenafil. Studies on vasoactive effects of sildenafil revealed the prostatic blood flow to be increased by approximately 75% which can be seen as a consequence of increased vascular SMC relaxation (Haaga et al. 2007). Another organ bath study which focused on human penile blood flow demonstrated sildenafil-induced inhibition of noradrenergic contractions together with an inhibition of smooth muscle contraction on precontracted vessels (Medina et al. 2000). All of these findings point to the assumption that an increased intraprostatic blood flow would probably enhance the effectiveness of medical treatment.

5.4 Hormonal influences on the cGMP pathway

5.4.1 Effects of hormonal changes due to prostatic postnatal development

Besides inhibition of single cGMP pathway components, numerous components were tested regarding their regulation by sex hormones. Natural changes in testosterone serum levels occur during postnatal development and were therefore investigated first. In both men and rats, testosterone shows very low levels shortly after birth and increases constantly until adulthood (Picut et al. 2018). Due to this fact, comparative investigations on rat prostate tissue from two different ages (postnatal day 6 and adult) exhibited postnatal prostate to be less distinct and organized regarding their typical architecture of PDE5 expressing SMCs. It is a matter of fact that organogenesis including SMC development is linked directly or indirectly to androgens through specific developmental genes (Francis and Swain 2017; Marker et al. 2003) which would explain the less distinct SMC organization of postnatal animals found in this study. It would be interesting to investigate fetal SMC organization around prenatal day 17 on which testosterone level is typically increased (Chen et al. 2009; Habert and Brignaschi 1991).

5.4.2 Hormone deficiency-induced regulation of the cGMP pathway in rodent prostate

A more direct way to study the influence of sex hormones was to manipulate its production in vivo. The first of those studies focused on testosterone deprivation within the rat prostate caused by a complete testis removal (castration). Castrated animals showed upregulation of PKG I protein which was diminished by subsequent treatment with testosterone and therefore indicates a direct correlation between serum testosterone level and the amount of intracellular PKG I. Different to other androgen-dependent organs (e.g. penis) of the male genital tract, the prostate highly reacts to changing hormonal conditions. But how could this sensitivity to testosterone be explained? Experiments with chemical testosterone deprivation investigated in various organs of the rat genital tract confirmed PKG I to be androgen-regulated only in the prostate and suggested that in this reproductive organ, suppression of PKG I represent a mechanism involved in androgen-controlled balance between proliferation, differentiation and apoptosis (Müller et al. 2011; Sampson et al. 2007; Rommerts et al. 1988). This upregulation of PKG I protein could be relevant in patients undergoing androgen deprivation therapy which is routinely used for the treatment of prostate cancer. Parallel development of prostate cancer and prostatic enlargement due to BPH is widely reported. Therefore, SMC relaxation due to PKG I upregulation by androgen deprivation therapy could be comparable to BPH treatment with sildenafil that likewise reduces prostatic smooth muscle tone (Dai et al. 2016; Miah and Catto 2014; Alcaraz et al. 2009). In this regard, it would be interesting to test for additional effects of regular BPH medications like PDE5 inhibitors in combination with androgen deprivation therapy.

Other animal models used for the investigation of possible hormone-regulated effects on the cGMP pathway in the prostate contained genetic modifications resulting in overexpression or loss of aromatase gene (AROM⁺, ArKO) which determines the producible amount of estrogen and testosterone. Histological and molecular analysis of AROM⁺ mice confirmed previous findings in rats in which reduced serum testosterone mediates upregulation of PKG I protein. Furthermore, these animals also showed an upregulation of PDE5 expression which counteracts the cGMP-induced muscle relaxation. It is currently not clear which of both cGMP pathway components, PKG I or PDE5 contributes more to the overall prostatic SMC contractility. This could be clarified in detail by time-lapse imaging or organ bath studies using those genetically modified animals. In this regard, it could also be tested whether the increased prostatic PDE5 expression reduces sildenafil effectiveness. However, the amount of produced cGMP seems to be non-hormonally regulated as the expression of the cGMP

generating enzyme sGC (β 1) always equals wildtype mice. Nevertheless, it could be that cGMP production is still affected by sex hormones in case of a regulation by other cGMP generating enzymes such as GC-A and/or GC-B which needs to be investigated in further studies.

Systematical analysis of the prostatic histology from estrogen deficiency (ArKO) mice revealed the peculiar finding that PKG I expression is exclusively hormone-regulated in peri-glandular SMCs but not in vascular SMCs. This observation could be a result of different developmental steps during differentiation of both SMC types. Even though SMCs possess a mesenchymal origin, mature peri-glandular SMCs differentiate out of mesenchymal myofibroblasts (Shaw et al. 2008; Wong et al. 2003), while the recruitment and differentiation of vascular SMCs during angiogenesis starts from pericytes (Wang et al. 2015a). In detail, pericytes are recruited from either the vessel wall or the surrounding mesenchymal precursor cells and differentiate into vascular SMCs (Yao et al. 2014; Gerhardt and Betsholtz 2003; Dorresteijn 1990). Different to vascularization, many important steps during prostate development are mediated by androgens and estrogens (Cunha 1994) which could explain the hormonal sensitivity of peri-glandular SMCs. Moreover, studies in rats and humans already demonstrated some controversial properties that separate vascular SMCs from other types of SMCs. Saboor and colleagues e.g. investigated in detail the histologic expression of the neuronal stem cell marker nestin in lungs of mice and men and found nestin solely localized in pulmonary vascular SMCs, but not bronchial smooth muscle cells (Saboor et al. 2016). The authors considered these nestin-positive vascular SMCs to be rather de-differentiated and in a state of changing their phenotype from contractile to synthetic (Nguyen et al. 2013; Muto et al. 2007). This unique characteristic of nestin-expressing vascular SMCs that contrasts the lack of nestin in other SMC types within the same organ was previously shown for the testis (Davidoff et al. 2004).

However, functional studies in ArKO mice using organ bath revealed only a subtle genotype-related increase in electrical field stimulation- and noradrenaline-induced contractility of the prostate (Gray et al. 2007). These findings together with the massive downregulation of PKG I in peri-glandular SMCs within the prostate presented in the present study suggest that prostatic contractility in these mice needs to be ensured by pathways different from PKG I such as the MAPK/ERK pathway (Pfeifer et al. 2014; Kinkade et al. 2008). It might be

interesting to investigate whether spontaneous contractility of the ArKO mice would remain unchanged.

5.4.3 Testosterone deficiency-induced regulation of the cGMP pathway in humans

In order to validate our previous findings of the rodent ventral prostate, cell culture experiments in human prostatic interstitial cells served as a reliable model to investigate possible hormone-induced effects on the cGMP pathway. SMC characteristics of these cells were confirmed by the expression of smooth muscle actin as well as PDE5 and PKG I. Both proteins are typically found in cells with contractile phenotype even so some of the larger investigated cells lacked PDE5 expression which could theoretically indicate a transformation into (myo-) fibroblasts of those cells. Another study on cultured human prostatic stromal cells investigated fibroblast-to-myofibroblast *trans*-differentiation in more detail, which is considered to be the major mechanism in BPH (Zenzmaier et al. 2012; Tuxhorn et al. 2002a). Addition of TGF β 1 mediated *trans*-differentiation of these stromal cells to a rather contractile phenotype, being indicated by an increase of smooth muscle actin as seen in Western blot and qPCR. The proportion of *trans*-differentiated cells was diminished by pre-incubation with the PDE5 inhibitor tadalafil but not by pre-incubation with the PKG inhibitor KT2358 (Zenzmaier et al. 2010). Furthermore, it could be shown that PDE5 inhibition by tadalafil reduced proliferation of prostate-derived fibroblasts. It would be interesting to validate these findings using the human prostatic interstitial cells of the present study.

Experiments on human prostatic interstitial cells in the present study however, focused on the influence of testosterone on important cGMP pathway components using qPCR. In this regard, testosterone-induced downregulation of smooth muscle actin, PDE5 and PKG I were shown on a mRNA level and confirmed protein data from Western blot experiments of castrated rats previously discussed in this study (see 5.4.2). The incubation time of 24 hours with testosterone provided enough time for the cells to mediate protein synthesis by gene transcription and translation. In theory, it is presumed that testosterone action, likewise to other steroid hormones is able to freely cross the plasma membrane to enter the cytoplasm and bind to the androgen receptor (Hiipakka and Liao 1998; Beato 1989). This in turn, leads to an activation of the bound androgen receptor which acts as transcription factor for DNA response elements in the gene promoters of the target protein (Costello and Franklin 2002) such as PDE5 or PKG I. Finally, activation of transcription and subsequent protein synthesis would lead to the observed upregulation of PDE5 and PKG I protein within the prostatic SMCs

(Heinlein and Chang 2002). Genomic action is assumed when latency between hormone exposure and the observed response is no shorter than the time it takes to trigger gene transcription followed by protein synthesis (Foradori et al. 2008). Duration for gene transcription is estimated for several hours after hormone exposure, followed by at least 7.5 min of transcription with some additional time for mRNA translation into proteins, their posttranslational modification and final accumulation (Cato et al. 2002; Cato et al. 1988; Groner et al. 1983). Apart from that, non-genomic pathways may also play a role in the realization of hormone-induced upregulation of cGMP pathway components. In contrast to genomic actions, hormone-induced non-genomic pathways are assumed to take only seconds to minutes to initiate measurable responses (Leach et al. 2014; Pi et al. 2010). Numerous studies describing interactions between such non-genomic pathways and intracellular signaling molecules such as mitogen-activated protein kinases (ERK1, ERK2) or a cross-talk with other factors (e.g. glucocorticoid receptor) were published (Oliver et al. 2013; Bonaccorsi et al. 2004; Castoria et al. 1999; Göttlicher et al. 1998).

Apart from PDE5 and PKG I, the cGMP-generating enzyme sGC was analyzed in addition. More precisely, the catalytic active sGC exists as heterodimer always containing one α and one β subunit (Denninger and Marletta 1999). Two isoforms of sGC ($\alpha_1\beta_1$ and $\alpha_2\beta_1$) are described to show catalytic enzyme activity (Korkmaz et al. 2018). The α_1/β_1 heterodimer is assumed to be the most abundant form (Mergia et al. 2003; Garbers 1992). sGC uses NO as its substrate to bind to the heme in the β_1 subunit and induces conversion of GTP into cGMP (Krumenacker et al. 2004). As already discussed in case of aromatase mouse models (see 5.4.2), sGC expression seems to be not influenced by testosterone treatment, when targeting its β_1 subunit by Western blot analysis. Studies on androgen-sensitive prostatic cancer cells (LNCaP) also demonstrated no testosterone regulation of the weakly expressed β_1 subunit on a protein and mRNA level (Cai et al. 2007). This study showed only α_1 subunit to be regulated by testosterone. It would be interesting to repeat these experiments using the human prostatic interstitial cells from the present study with special focus on the α_1 subunit of sGC. In contrast, Müller et al. (2011) found sGC expression remarkably increased in Western blot analysis using an antibody for the β_1 subunit of sGC after Leydig cell depletion by injection of the compound ethane dimethane sulfonate (EDS). However, differences in expression between α_1 and β_1 subunits of sGC were also shown in studies of breast cancer cells which might have importance in the development of hormone-dependent cancers (Mónica and Antunes 2018; Postovit et al. 2002).

5.5 SMC proliferation in BPH tissue

BPH (benign prostatic hyperplasia) is described as a net increase in cell number within the prostatic interstitial stroma (Wu et al. 2008; Djavan et al. 2002). The histological diagnosis of BPH is characterized by unregulated proliferation of connective tissue, SMCs and glandular epithelium within the transition zone and periurethral aspect of the prostate (Patel and Parsons 2014). However, the pathophysiology underlying the development of BPH is highly complex and insufficiently understood (Shi et al. 2018).

The present study showed visible proliferation in interstitial SMCs of human BPH tissue samples from the transition zone after transurethral resection of the prostate. Proliferative activity was also detected in nuclei of the glandular epithelium in the rat and human prostate with even higher prevalence of this cell type. The cellular pathology of BPH includes varying proportions of epithelium, fibrous connective tissue as well as SMCs and is most commonly found as adenomyofibromatous subtype while pathologists usually do not subclassify BPH histologically because of the wide variation in composition (Kirby 2005).

Moreover, an increased hyperplastic growth of prostatic SMCs contributes to urethral obstruction and voiding symptoms in BPH (Shi et al. 2018). In this regard, it is assumed that different proliferative potential of stromal cells between transition zone and adjoining regions of the prostate is crucial for the development of BPH (Foster 2000).

Taken together, these findings demonstrate the limitation of our knowledge about the underlying mechanisms of BPH development. Further investigations are therefore absolutely essential, in which CLARITY could help to extend our knowledge.

6 Summary

Prostatic enlargement due to benign prostatic hyperplasia (BPH) and/or prostate cancer are ubiquitous in aging men. While prostate cancer represents the sixth leading cause for cancer-related death worldwide, BPH is known to result in urinary retention and recurrent infections which adversely influences the quality of life among older men. Although inhibitors of the cGMP-hydrolyzing enzyme phosphodiesterase 5 (PDE5) are now regularly used for the treatment of BPH, detailed information about their cellular localization and function within the prostate is missing.

In prostate tissue of mouse, rat and man, PDE5 was shown to be highly expressed in interstitial and vascular smooth muscle cells (SMCs) but not in epithelial cells of the gland. The newly established CLARITY approach helped to improve our understanding of the prostatic architecture on a three-dimensional level and allowed highly precise reconstructions of the arrangement of PDE5-expressing SMCs. Moreover, this method demonstrated that the interstitial periglandular SMCs in rat prostate are arranged tighter around the glands than in the human prostate. Spontaneous contractions of these SMCs were visualized by the use of time lapse-imaging in both, rodents and men. Addition of the PDE5 inhibitor sildenafil resulted in a significant reduction of the contractile frequency in both tissues. In rat prostate, spontaneous contractility was only observed in terminal prostatic glands but not in proximal ducts.

The regulatory role of sex hormones on the cGMP pathway within prostatic SMCs was another important aspect of this study. In rat, androgen deprivation was induced via castration which increased the expression of prostatic cGMP pathway components considerably. Using estrogen-deficient aromatase knockout (ArKO) and -overexpressing (AROM⁺) mice, we found only glandular but not vascular smooth muscle cells affected by changes of hormone levels. These findings were consistent even in the human prostate by culturing of isolated prostatic interstitial cells as mRNA expression of cGMP pathway components increased with decreased concentrations of testosterone pretreatment.

Data, showing relevant PDE5 effects and their androgen-dependent regulation might be helpful to clarify whether PDE5 inhibitors as new therapeutics aspects for BPH are only effective in case of reduced testosterone levels.

7 Zusammenfassung

Die Vergrößerung der Prostata in Folge einer benignen Prostatahyperplasie (BPH) oder Prostatakarzinoms ist bei Männern im hohen Alter weit verbreitet. Während Prostatakarzinome eine der häufigsten Ursachen für tödlich verlaufende Krebserkrankungen darstellen, beeinträchtigt BPH die Lebensqualität älterer Männer erheblich durch Folgeschäden, wie Harnverhalt und wiederkehrende Infektionen. Obwohl Inhibitoren des cGMP hydrolysierenden Enzyms Phosphodiesterase5 (PDE5) nun auch routinemäßig zur Behandlung von BPH eingesetzt werden, fehlen noch immer detaillierte Informationen über Lokalisation und Funktion in der Prostata.

In Gewebeproben der Prostata von Mäusen, Ratten und humanen Spendern konnte die PDE5-Expression in glatten Muskelzellen des Interstitiums und der Gefäße nachgewiesen werden. Hierbei exprimierten die Epithelzellen der Prostata Drüsen jedoch kein PDE5. Ein neu entwickeltes CLARITY-Protokoll half dabei unser Verständnis der Prostataarchitektur um die dritte Dimension zu erweitern und erlaubte eine exakte Rekonstruktionen der räumlichen Anordnung PDE5-exprimierender glatter Muskelzellen. Zudem konnte mit dieser Methodik anschaulich gezeigt werden, dass in der Rattenprostata periglanduläre glatte Muskelzellen eng anliegender und kompakter um die einzelnen Drüsen angeordnet sind, im Vergleich zur humanen Prostata. Spontan auftretende Kontraktionen dieser glatten Muskelzellen konnten mittels time-lapse imaging sichtbar gemacht werden. Dabei führte die Zugabe des PDE5-Inhibitors Sildenafil zu einer signifikant reduzierten Kontraktionsfrequenz in Gewebestücken aus beiden Spezies. Bei der Ratte konnte darüberhinaus gezeigt werden, dass die Spontankontraktionen nur die Drüsenendstücke, aber nicht die Ausführungsgänge betrafen.

Die Möglichkeiten zur Regulation des cGMP-Signalwegs durch Geschlechtshormone wurde als ein weiterer wichtiger Punkt näher untersucht. In der Prostata der Ratten wurde die Androgenzufuhr durch Kastration unterbunden, was zu einem deutlichen Anstieg von cGMP-Signalwegskomponenten führte. Unter Verwendung von Mausmodellen, welche einen Aromatase-Knockout (ArKO) bzw. deren -Überexpression (AROM⁺) aufwiesen, konnte ein Einfluss durch unterschiedliche Hormonlevel auf glatte Muskelzellen gezeigt werden. Dies betraf ausschließlich glatte Muskelzellen der Drüsen und hatte keinerlei Effekt auf Gefäßmuskelzellen. Diese Ergebnisse decken sich mit Versuchen mit isolierten interstitiellen Zellen menschlicher Prostatae. Hier konnte ein Anstieg der Expression von cGMP-

Signalwegskomponenten durch Inkubation mit sinkenden Testosteronkonzentrationen gezeigt werden.

Diese Daten verdeutlichen die Androgen abhängige Regulierung von cGMP-Signalwegskomponenten in glatten Muskelzellen der Prostata, welche dabei helfen könnte, die Frage zu klären, ob PDE5-Inhibitoren als neue Therapeutika für BPH nur unter niedrigen Testosteron-Level wirksam sind.

8 Acknowledgment

First of all, I would like to mention all **rats and mice** that gave their lives to realize the present study. Furthermore, I would like to thank all **patients** from the Department of Urology, Pediatric Urology and Andrology of the Justus-Liebig-University Giessen (Head of Department: Prof. Dr. Florian Wagenlehner) that helped to clarify our understanding of prostate growth disorders by contributing to my experimental work.

I am greatly thankful to **Prof. Dr. Ralf Middendorff** for his excellent supervision. His patience and guidance helped me a lot to stay focused while balancing work and family. I also want to thank **Prof. Dr. Adriaan Dorresteyn, Prof. Dr. Gail Risbridger and Dr. Stuart Ellem** for their supervision, confidence and resources.

The present work would not have been possible without the technical support by **Andre Kaschtanow, Ingrid Schneider-Hüther, Silke Wiegand, Petra Mermer, Tania Bloch, Dr. Brindi Niranjana and Linda Teng** with special thanks to **Sabine Tasch**, my foster mother. She guided me through preparations and calculations, set my attention to a rather clean working bench and limited my frustrations with her delicious food and cooking skills.

Furthermore, I would like to thank all (post-) doctoral colleagues of my working group, in particular **Beatrix Stadler, Ansgar Reckmann, Christina Seidel, Mathias Seidensticker, Alina Töpperwein, Claudia U. Tomczyk and Andrea Mietens** for their excellent cooperation and useful creativeness. My special thanks to my bench buddy **Daniela Beyer** who formed the backbone of my work and became a close friend.

I am grateful to **Prof. Dr. Andreas Meinhardt, Prof. Dr. Kate Loveland** as well as **Pia Jürgens** who supported me as a doctoral researcher of the **International Research Training Group (IRTG)**, a collaboration between Justus-Liebig-University Giessen and Monash University. The IRTG brought me in to contact with national and international experts on the field of reproduction and with those who will surely become the next generation of these experts.

I would like to thank the team of the **Giessen Graduate Centre for the Life Sciences (GGL)**, Director: Prof. Dr. Eveline Baumgart-Vogt) for its support during my time as doctoral

researcher of the GGL, including networking with doctoral students of various working fields, improving my technical skills from basic analysis to data processing and its presentation as well as to develop later career choices.

Moreover, I would like to thank **Dr. Klemens Ekschmitt** for his guidance through the maze of statistical analysis.

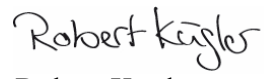
My special thanks to **Sophie Meyer** who always encouraged me in my work and brought my theoretic knowledge about reproduction to life.

Last but not least, I would like to thank my parents **Ina and Steffen Kügler** who believed in me while pushing me to finish.

9 Declaration/Selbstständigkeitserklärung

Hiermit versichere ich, die vorgelegte Thesis selbstständig und ohne unerlaubte fremde Hilfe und nur mit den Hilfen angefertigt zu haben, die ich in der Thesis angegeben habe. Alle Textstellen, die wörtlich oder sinngemäß aus veröffentlichten Schriften entnommen sind, und alle Angaben die auf mündlichen Auskünften beruhen, sind als solche kenntlich gemacht. Bei den von mir durchgeführten und in der Thesis erwähnten Untersuchungen habe ich die Grundsätze guter wissenschaftlicher Praxis, wie sie in der ‚Satzung der Justus-Liebig-Universität zur Sicherung guter wissenschaftlicher Praxis‘ niedergelegt sind, eingehalten. Gemäß § 25 Abs. 6 der Allgemeinen Bestimmungen für modularisierte Studiengänge dulde ich eine Überprüfung der Thesis mittels Anti-Plagiatssoftware.

Giessen, 21/08/2018


Robert Kügler

10 References

Alcaraz A, Hammerer P, Tubaro A, Schröder FH, Castro R (2009) Is there evidence of a relationship between benign prostatic hyperplasia and prostate cancer? Findings of a literature review. *Eur Urol* 55: 864–873

Alioua A, Huggins JP, Rousseau E (1995) PKG-I alpha phosphorylates the alpha-subunit and upregulates reconstituted GKCa channels from tracheal smooth muscle. *Am J Physiol* 268: 1057-1063

Andric SA, Janjic MM, Stojkov NJ, Kostic TS (2010) Testosterone-induced modulation of nitric oxide-cGMP signaling pathway and androgenesis in the rat Leydig cells. *Biol Reprod* 83: 434–442

Attiga FA, Fernandez PM, Weeraratna AT, Manyak MJ, Patierno SR (2000) Inhibitors of prostaglandin synthesis inhibit human prostate tumor cell invasiveness and reduce the release of matrix metalloproteinases. *Cancer Res* 60: 4629–4637

Aumüller G, Bargmann W, von Möllendorff W (1979) Prostate gland and seminal vesicles. Springer. Berlin, Germany

Baig FA, Hamid A, Mirza T, Syed S (2015) Ductal and Acinar Adenocarcinoma of Prostate. Morphological and Immunohistochemical Characterization. *Oman Med J* 30: 162–166

Beato M (1989) Gene regulation by steroid hormones. *Cell* 56: 335–344

Beech DJ (1997) Actions of neurotransmitters and other messengers on Ca²⁺ channels and K⁺ channels in smooth muscle cells. *Pharmacol Ther* 73: 91–119

Bell JR, Bernasochi GB, Varma U, Boon WC, Ellem SJ, Risbridger GP, Delbridge LMD (2014) Aromatase transgenic upregulation modulates basal cardiac performance and the response to ischemic stress in male mice. *Am J Physiol Heart Circ Physiol* 306: H1265-74

Bian K, Murad F (2014) sGC-cGMP signaling. Target for anticancer therapy. *Adv Exp Med Biol* 814: 5–13

Bianco JJ, McPherson SJ, Wang H, Prins GS, Risbridger GP (2006) Transient neonatal estrogen exposure to estrogen-deficient mice (aromatase knockout) reduces prostate weight and induces inflammation in late life. *Am J Pathol* 168: 1869–1878

- Bierhoff E, Walljasper U, Hofmann D, Vogel J, Wernert N, Pfeifer U (1997) Morphological analogies of fetal prostate stroma and stromal nodules in BPH. *Prostate* 31: 234–240
- Birukov KG, Stepanova OV, Nanaev AK, Shirinsky VP (1991) Expression of calponin in rabbit and human aortic smooth muscle cells. *Cell Tissue Res* 266: 579–584
- Bistulfi G, Affronti HC, Foster BA, Karasik E, Gillard B, Morrison C, Mohler J, Phillips JG, Smiraglia DJ (2016) The essential role of methylthioadenosine phosphorylase in prostate cancer. *Oncotarget* 7: 14380–14393
- Bonaccorsi L, Marchiani S, Muratori M, Forti G, Baldi E (2004) Gefitinib ('IRESSA', ZD1839) inhibits EGF-induced invasion in prostate cancer cells by suppressing PI3 K/AKT activation. *J Cancer Res Clin Oncol* 130: 604–614
- Böttcher R, Kweldam CF, Livingstone J, Lalonde E, Yamaguchi TN, Huang V, Yousif F, Fraser M, Bristow RG, van der Kwast T, Boutros PC, Jenster G, van Leenders GJLH (2018) Cribriform and intraductal prostate cancer are associated with increased genomic instability and distinct genomic alterations. *BMC Cancer* 18: 8
- Bowes C, Li T, Danciger M, Baxter LC, Applebury ML, Farber DB (1990) Retinal degeneration in the rd mouse is caused by a defect in the beta subunit of rod cGMP-phosphodiesterase. *Nature* 347: 677–680
- Bowman CJ, Barlow NJ, Turner KJ, Wallace DG, Foster PMD (2003) Effects of in utero exposure to finasteride on androgen-dependent reproductive development in the male rat. *Toxicol Sci* 74: 393–406
- Brechka H, McAuley EM, Lamperis SM, Paner GP, Vander Griend DJ (2016) Contribution of Caudal Müllerian Duct Mesenchyme to Prostate Development. *Stem Cells Dev* 25: 1733–1741
- Bruinsma SM, Zhang L, Roobol MJ, Bangma CH, Steyerberg EW, Nieboer D, van Hemelrijck M (2017) The Movember Foundation's GAP3 cohort. A profile of the largest global prostate cancer active surveillance database to date. *BJU Int*
- Cai C, Chen S-Y, Zheng Z, Omwancha J, Lin M-F, Balk SP, Shemshedini L (2007) Androgen regulation of soluble guanylyl cyclase α 1 mediates prostate cancer cell proliferation. *Oncogene* 26: 1606–1615
- Carson CC, Rosenberg M, Kissel J, Wong DG (2014) Tadalafil - a therapeutic option in the management of BPH-LUTS. *Int J Clin Pract* 68: 94–103

- Castoria G, Barone MV, Di Domenico M, Bilancio A, Ametrano D, Migliaccio A, Auricchio F (1999) Non-transcriptional action of oestradiol and progestin triggers DNA synthesis. *EMBO J* 18: 2500–2510
- Cato AC, Skroch P, Weinmann J, Butkeraitis P, Ponta H (1988) DNA sequences outside the receptor-binding sites differently modulate the responsiveness of the mouse mammary tumour virus promoter to various steroid hormones. *EMBO J* 7: 1403–1410
- Cato ACB, Nestl A, Mink S (2002) Rapid actions of steroid receptors in cellular signaling pathways. *Sci STKE* 2002: re9
- Chakrabarty B, Dey A, Lam M, Ventura S, Exintaris B (2015) Tamsulosin modulates, but does not abolish the spontaneous activity in the guinea pig prostate gland. *Neurourol Urodyn* 34: 482–488
- Chapple CR (2004) Pharmacological therapy of benign prostatic hyperplasia/lower urinary tract symptoms. An overview for the practising clinician. *BJU Int* 94: 738–744
- Chapple CR, Crowe R, Gilpin SA, Gosling J, Burnstock G (1991) The innervation of the human prostate gland--the changes associated with benign enlargement. *J Urol* 146: 1637–1644
- Chen H, Ge R-S, Zirkin BR (2009) Leydig cells. From stem cells to aging. *Mol Cell Endocrinol* 306: 9–16
- Chen Z, Chen N, Shen P, Gong J, Li X, Zhao T, Liao B, Liu L, Liu Z, Zhang X, Liu J, Peng Z, Chen X, Xu M, Gui H, Zhang P, Wei Q, Zhou Q, Zeng H (2015) The presence and clinical implication of intraductal carcinoma of prostate in metastatic castration resistant prostate cancer. *Prostate* 75: 1247–1254
- Christ GJ, Andersson K-E (2007) Rho-kinase and effects of Rho-kinase inhibition on the lower urinary tract. *Neurourol Urodyn* 26: 948–954
- Christensen BW (2018) Canine Prostate Disease. *Vet Clin North Am Small Anim Pract* 48: 701–719
- Chung K, Deisseroth K (2013) CLARITY for mapping the nervous system. *Nat Methods* 10: 508–513
- Chung K-S, Cheon S-Y, An H-J (2015) Effects of resveratrol on benign prostatic hyperplasia by the regulation of inflammatory and apoptotic proteins. *J Nat Prod* 78: 689–694

- Cornwell TL, Pryzwansky KB, Wyatt TA, Lincoln TM (1991) Regulation of sarcoplasmic reticulum protein phosphorylation by localized cyclic GMP-dependent protein kinase in vascular smooth muscle cells. *Mol Pharmacol* 40: 923–931
- Costello LC, Franklin RB (2002) Testosterone and prolactin regulation of metabolic genes and citrate metabolism of prostate epithelial cells. *Horm Metab Res* 34: 417–424
- Costello LC, Franklin RB (2016) A comprehensive review of the role of zinc in normal prostate function and metabolism; and its implications in prostate cancer. *Arch Biochem Biophys* 611: 100–112
- Crawford ED, Eisenberger MA, McLeod DG, Spaulding JT, Benson R, Dorr FA, Blumenstein BA, Davis MA, Goodman PJ (1989) A controlled trial of leuprolide with and without flutamide in prostatic carcinoma. *N Engl J Med* 321: 419–424
- Cunha GR (1994) Role of mesenchymal-epithelial interactions in normal and abnormal development of the mammary gland and prostate. *Cancer* 74: 1030–1044
- Cunha GR, Donjacour AA, Cooke PS, Mee S, Bigsby RM, Higgins SJ, Sugimura Y (1987) The endocrinology and developmental biology of the prostate. *Endocr Rev* 8: 338–362
- Da Silva MHA, Costa WS, B Sampaio FJ, de Souza DB (2018) The corpus cavernosum after treatment with dutasteride or finasteride. A histomorphometric study in a benign prostatic hyperplasia rodent model. *Asian J Androl*
- Dai X, Fang X, Ma Y, Xianyu J (2016) Benign Prostatic Hyperplasia and the Risk of Prostate Cancer and Bladder Cancer. A Meta-Analysis of Observational Studies. *Medicine (Baltimore)* 95: e3493
- Davidoff MS, Middendorff R, Enikolopov G, Riethmacher D, Holstein AF, Müller D (2004) Progenitor cells of the testosterone-producing Leydig cells revealed. *J Cell Biol* 167: 935–944
- Deninno MP, Andrews M, Bell AS, Chen Y, Eller-Zarbo C, Eshelby N, Etienne JB, Moore DE, Palmer MJ, Visser MS, Yu LJ, Zavadoski WJ, Michael Gibbs E (2009) The discovery of potent, selective, and orally bioavailable PDE9 inhibitors as potential hypoglycemic agents. *Bioorg Med Chem Lett* 19: 2537–2541
- Denninger JW, Marletta MA (1999) Guanylate cyclase and the .NO/cGMP signaling pathway. *Biochim Biophys Acta* 1411: 334–350
- Djavan B, Remzi M, Erne B, Marberger M (2002) The pathophysiology of benign prostatic hyperplasia. *Drugs Today* 38: 867–876

- Dorresteyn AWC (1990) Quantitative analysis of cellular differentiation during early embryogenesis of *Platynereis dumerilii*. *Roux Arch Dev Biol* 199: 14–30
- Dreef HC, van Esch E, Rijk EPCT de (2007) Spermatogenesis in the cynomolgus monkey (*Macaca fascicularis*). A practical guide for routine morphological staging. *Toxicol Pathol* 35: 395–404
- Ellem SJ, Wang H, Poutanen M, Risbridger GP (2009) Increased endogenous estrogen synthesis leads to the sequential induction of prostatic inflammation (prostatitis) and prostatic pre-malignancy. *Am J Pathol* 175: 1187–1199
- El-Mezgueldi M (1996) Calponin. *The International Journal of Biochemistry & Cell Biology* 28: 1185–1189
- Exintaris B, Nguyen D-TT, Dey A, Lang RJ (2006) Spontaneous electrical activity in the prostate gland. *Auton Neurosci* 126-127: 371–379
- Exintaris B, Nguyen D-TT, Lam M, Lang RJ (2009) Inositol trisphosphate-dependent Ca stores and mitochondria modulate slow wave activity arising from the smooth muscle cells of the guinea pig prostate gland. *Br J Pharmacol* 156: 1098–1106
- Ferlay J, Shin H-R, Bray F, Forman D, Mathers C, Parkin DM (2010) Estimates of worldwide burden of cancer in 2008. *Globocan 2008. Int J Cancer* 127: 2893–2917
- Fibbi B, Morelli A, Vignozzi L, Filippi S, Chavalmane A, de Vita G, Marini M, Gacci M, Vannelli GB, Sandner P, Maggi M (2010) Characterization of phosphodiesterase type 5 expression and functional activity in the human male lower urinary tract. *J Sex Med* 7: 59–69
- Fiedler B, Feil R, Hofmann F, Willenbockel C, Drexler H, Smolenski A, Lohmann SM, Wollert KC (2006) cGMP-dependent protein kinase type I inhibits TAB1-p38 mitogen-activated protein kinase apoptosis signaling in cardiac myocytes. *J Biol Chem* 281: 32831–32840
- Filippi S, Morelli A, Sandner P, Fibbi B, Mancina R, Marini M, Gacci M, Vignozzi L, Vannelli GB, Carini M, Forti G, Maggi M (2007) Characterization and functional role of androgen-dependent PDE5 activity in the bladder. *Endocrinology* 148: 1019–1029
- Fisher CR, Graves KH, Parlow AF, Simpson ER (1998) Characterization of mice deficient in aromatase (ArKO) because of targeted disruption of the *cyp19* gene. *Proc Natl Acad Sci U S A* 95: 6965–6970
- Foradori CD, Weiser MJ, Handa RJ (2008) Non-genomic actions of androgens. *Front Neuroendocrinol* 29: 169–181

- Foster CS (2000) Pathology of benign prostatic hyperplasia. *Prostate Suppl* 9: 4–14
- Francis JC, Swain A (2017) Prostate Organogenesis. *Cold Spring Harb Perspect Med*
- Francis SH, Busch JL, Corbin JD, Sibley D (2010) cGMP-dependent protein kinases and cGMP phosphodiesterases in nitric oxide and cGMP action. *Pharmacol Rev* 62: 525–563
- Francis SH, Corbin JD (1994) Structure and function of cyclic nucleotide-dependent protein kinases. *Annu Rev Physiol* 56: 237–272
- Fukuda Y, Imoto M, Koyama Y, Miyazawa Y, Hayakawa T (1996) Demonstration of noradrenaline-immunoreactive nerve fibres in the liver. *J Int Med Res* 24: 466–472
- Gacci M, Andersson K-E, Chapple C, Maggi M, Mirone V, Oelke M, Porst H, Roehrborn C, Stief C, Giuliano F (2016) Latest Evidence on the Use of Phosphodiesterase Type 5 Inhibitors for the Treatment of Lower Urinary Tract Symptoms Secondary to Benign Prostatic Hyperplasia. *Eur Urol* 70: 124–133
- Garbers DL (1992) Guanylyl cyclase receptors and their endocrine, paracrine, and autocrine ligands. *Cell* 71: 1–4
- Gerhardt H, Betsholtz C (2003) Endothelial-pericyte interactions in angiogenesis. *Cell Tissue Res* 314: 15–23
- Ghofrani HA, Osterloh IH, Grimminger F (2006) Sildenafil. From angina to erectile dysfunction to pulmonary hypertension and beyond. *Nat Rev Drug Discov* 5: 689–702
- Giuliano F, Ückert S, Maggi M, Birder L, Kissel J, Viktrup L (2013) The mechanism of action of phosphodiesterase type 5 inhibitors in the treatment of lower urinary tract symptoms related to benign prostatic hyperplasia. *Eur Urol* 63: 506–516
- Göttlicher M, Heck S, Herrlich P (1998) Transcriptional cross-talk, the second mode of steroid hormone receptor action. *J Mol Med* 76: 480–489
- Gray KT, Short JL, Simpson ER, Ventura S (2007) The effects of targeted deletion of the aromatase enzyme on prostatic contractile responses to noradrenaline in mice. *J Endocrinol* 195: 495–502
- Green SM, Mostaghel EA, Nelson PS (2012) Androgen action and metabolism in prostate cancer. *Mol Cell Endocrinol* 360: 3–13

- Groner B, Ponta H, Beato M, Hynes NE (1983) The proviral DNA of mouse mammary tumor virus. Its use in the study of the molecular details of steroid hormone action. *Mol Cell Endocrinol* 32: 101–116
- Haaga JR, Exner A, Fei B, Seftel A (2007) Semiquantitative imaging measurement of baseline and vasomodulated normal prostatic blood flow using sildenafil. *Int J Impot Res* 19: 110–113
- Habert R, Brignaschi P (1991) Developmental changes in in vitro testosterone production by dispersed Leydig cells during fetal life in rats. *Arch Androl* 27: 65–71
- Hayashi N, Sugimura Y, Kawamura J, Donjacour AA, Cunha GR (1991) Morphological and functional heterogeneity in the rat prostatic gland. *Biol Reprod* 45: 308–321
- Haynes JM, Cook A-LM (2006) Protein kinase G-induced activation of K(ATP) channels reduces contractility of human prostate tissue. *Prostate* 66: 377–385
- Hayward SW, Cunha GR (2000) The Prostate. Development and Physiology. *Radiologic Clinics of North America* 38: 1–14
- Heinlein CA, Chang C (2002) Androgen receptor (AR) coregulators. An overview. *Endocr Rev* 23: 175–200
- Hennenberg M, Stief CG, Gratzke C (2014) Prostatic α 1-adrenoceptors. New concepts of function, regulation, and intracellular signaling. *Neurourol Urodyn* 33: 1074–1085
- Hiipakka RA, Liao S (1998) Molecular mechanism of androgen action. *Trends Endocrinol Metab* 9: 317–324
- Hofmann F, Feil R, Kleppisch T, Schlossmann J (2006) Function of cGMP-dependent protein kinases as revealed by gene deletion. *Physiol Rev* 86: 1–23
- Huggett J, Dheda K, Bustin S, Zumla A (2005) Real-time RT-PCR normalisation; strategies and considerations. *Genes Immun* 6: 279–284
- Ichihara I, Kallio M, Pelliniemi LJ (1978) Light and electron microscopy of the ducts and their subepithelial tissue in the rat ventral prostate. *Cell Tissue Res* 192: 381–390
- Imperato-McGinley J, Binienda Z, Gedney J, Vaughan ED (1986) Nipple differentiation in fetal male rats treated with an inhibitor of the enzyme 5 alpha-reductase. Definition of a selective role for dihydrotestosterone. *Endocrinology* 118: 132–137

- Ittmann M (2017) *Anatomy and Histology of the Human and Murine Prostate*. Cold Spring Harb Perspect Med
- Jazbutyte V, Stumpner J, Redel A, Lorenzen JM, Roewer N, Thum T, Kehl F (2012) Aromatase inhibition attenuates desflurane-induced preconditioning against acute myocardial infarction in male mouse heart in vivo. *PLoS ONE* 7: e42032
- Jesik CJ, Holland JM, Lee C (1982) An anatomic and histologic study of the rat prostate. *Prostate* 3: 81–97
- Juilfs DM, Soderling S, Burns F, Beavo JA (1999) Cyclic GMP as substrate and regulator of cyclic nucleotide phosphodiesterases (PDEs). *Rev Physiol Biochem Pharmacol* 135: 67–104
- Kaplan SA (2008) Current role of alpha-blockers in the treatment of benign prostatic hyperplasia. *BJU Int* 102 Suppl 2: 3–7
- Kaplan SA (2009) Side Effects of alpha-Blocker Use. Retrograde Ejaculation. *Rev Urol* 11: S14-8
- Kellokumpu-Lehtinen P (1985) Development of sexual dimorphism in human urogenital sinus complex. *Biol Neonate* 48: 157–167
- Keravis T, Lugnier C (2012) Cyclic nucleotide phosphodiesterase (PDE) isozymes as targets of the intracellular signalling network. Benefits of PDE inhibitors in various diseases and perspectives for future therapeutic developments. *Br J Pharmacol* 165: 1288–1305
- Kimura K, Tsuzuki T, Kato M, Saito AM, Sassa N, Ishida R, Hirabayashi H, Yoshino Y, Hattori R, Gotoh M (2014) Prognostic value of intraductal carcinoma of the prostate in radical prostatectomy specimens. *Prostate* 74: 680–687
- Kinkade CW, Castillo-Martin M, Puzio-Kuter A, Yan J, Foster TH, Gao H, Sun Y, Ouyang X, Gerald WL, Cordon-Cardo C, Abate-Shen C (2008) Targeting AKT/mTOR and ERK MAPK signaling inhibits hormone-refractory prostate cancer in a preclinical mouse model. *J Clin Invest* 118: 3051–3064
- Kirby RS (2005) *Textbook of benign prostatic hyperplasia*, 2nd edn. Taylor & Francis. London, UK
- Knoblauch S, True L. (2011) *Male Reproductive System*. (In: Dintzis, Suzanne M.; Treuting, Piper M.: *Comparative Anatomy and Histology - A Mouse and Human Atlas*), 1st edn. Academic Press. Oxford, UK

- Korkmaz Y, Roggendorf HC, Siefer OG, Seehawer J, Imhof T, Plomann M, Bloch W, Friebe A, Huebbers CU (2018) Downregulation of the α 1- and β 1-subunit of sGC in Arterial Smooth Muscle Cells of OPSCC Is HPV-Independent. *J Dent Res*: 22034518774531
- Kreipke CW, Rafols JA (2009) Calponin control of cerebrovascular reactivity. Therapeutic implications in brain trauma. *J Cell Mol Med* 13: 262–269
- Krumenacker JS, Hanafy KA, Murad F (2004) Regulation of nitric oxide and soluble guanylyl cyclase. *Brain Research Bulletin* 62: 505–515
- Kügler R, Mietens A, Seidensticker M, Tasch S, Wagenlehner FM, Kaschtanow A, Tjahjono Y, Tomczyk CU, Beyer D, Risbridger GP, Exintaris B, Ellem SJ, Middendorff R (2018) Novel imaging of the prostate reveals spontaneous gland contraction and excretory duct quiescence together with different drug effects. *FASEB J*: fj201700430R
- Leach DA, Need EF, Trotta AP, Grubisha MJ, DeFranco DB, Buchanan G (2014) Hic-5 influences genomic and non-genomic actions of the androgen receptor in prostate myofibroblasts. *Mol Cell Endocrinol* 384: 185–199
- Lee C, Sensibar JA, Dudek SM, Hiipakka RA, Liao ST (1990) Prostatic ductal system in rats. Regional variation in morphological and functional activities. *Biol Reprod* 43: 1079–1086
- Lee C-L, Kuo H-C (2017) Pathophysiology of benign prostate enlargement and lower urinary tract symptoms. Current concepts. *Ci Ji Yi Xue Za Zhi* 29: 79–83
- Lee DI, Zhu G, Sasaki T, Cho G-S, Hamdani N, Holewinski R, Jo S-H, Danner T, Zhang M, Rainer PP, Bedja D, Kirk JA, Ranek MJ, Dostmann WR, Kwon C, Margulies KB, van Eyk JE, Paulus WJ, Takimoto E, Kass DA (2015) Phosphodiesterase 9A controls nitric-oxide-independent cGMP and hypertrophic heart disease. *Nature* 519: 472–476
- Lee SN, Chakrabarty B, Wittmer B, Papargiris M, Ryan A, Frydenberg M, Lawrentschuk N, Middendorff R, Risbridger GP, Ellem SJ, Exintaris B (2017) Age Related Differences in Responsiveness to Sildenafil and Tamsulosin are due to Myogenic Smooth Muscle Tone in the Human Prostate. *Sci Rep* 7: 10150
- Lepor H, Shapiro E, Bowsher RR, Henry DP (1990) Determination of norepinephrine levels in the adult human prostate. *J Urol* 144: 1263–1266
- Lepor H, Tang R, Shapiro E (1993) The alpha-adrenoceptor subtype mediating the tension of human prostatic smooth muscle. *Prostate* 22: 301–307

- Li X, Nokkala E, Yan W, Streng T, Saarinen N, Wärrä A, Huhtaniemi I, Santti R, Mäkelä S, Poutanen M (2001) Altered structure and function of reproductive organs in transgenic male mice overexpressing human aromatase. *Endocrinology* 142: 2435–2442
- Lin C-S, Albersen M, Xin Z, Namiki M, Muller D, Lue TF (2013) Phosphodiesterase-5 expression and function in the lower urinary tract. A critical review. *Urology* 81: 480–487
- Lincoln TM (1983) cGMP-dependent protein kinase. *Meth Enzymol* 99: 62–71
- Liu N, Mei L, Fan X, Tang C, Ji X, Hu X, Shi W, Qian Y, Hussain M, Wu J, Wang C, Lin S, Wu X (2016) Phosphodiesterase 5/protein kinase G signal governs stemness of prostate cancer stem cells through Hippo pathway. *Cancer Lett* 378: 38–50
- Liu S, Mansour MN, Dillman KS, Perez JR, Danley DE, Aeed PA, Simons SP, Lemotte PK, Menniti FS (2008) Structural basis for the catalytic mechanism of human phosphodiesterase 9. *Proc Natl Acad Sci U S A* 105: 13309–13314
- Liu Z, Khalil RA (2018) Evolving mechanisms of vascular smooth muscle contraction highlight key targets in vascular disease. *Biochem Pharmacol* 153: 91–122
- Lowsley OS (1912) The development of the human prostate gland with reference to the development of other structures at the neck of the urinary bladder. *Am. J. Anat.* 13: 299–349
- Lythgoe C, McVary KT (2013) The use of PDE-5 inhibitors in the treatment of lower urinary tract symptoms due to benign prostatic hyperplasia. *Curr Urol Rep* 14: 585–594
- Madar S, Brosh R, Buganim Y, Ezra O, Goldstein I, Solomon H, Kogan I, Goldfinger N, Klocker H, Rotter V (2009) Modulated expression of WFDC1 during carcinogenesis and cellular senescence. *Carcinogenesis* 30: 20–27
- Marinese D, Patel R, Walden PD (2003) Mechanistic investigation of the adrenergic induction of ventral prostate hyperplasia in mice. *Prostate* 54: 230–237
- Marker PC, Donjacour AA, Dahiya R, Cunha GR (2003) Hormonal, cellular, and molecular control of prostatic development. *Dev Biol* 253: 165–174
- McAllister-Lucas LM, Sonnenburg WK, Kadlecsek A, Seger D, Trong HL, Colbran JL, Thomas MK, Walsh KA, Francis SH, Corbin JD (1993) The structure of a bovine lung cGMP-binding, cGMP-specific phosphodiesterase deduced from a cDNA clone. *J Biol Chem* 268: 22863–22873
- McNeal J (1990) Pathology of benign prostatic hyperplasia. Insight into etiology. *Urol Clin North Am* 17: 477–486

- McPherson SJ, Hussain S, Balanathan P, Hedwards SL, Niranjana B, Grant M, Chandrasiri UP, Toivanen R, Wang Y, Taylor RA, Risbridger GP (2010) Estrogen receptor-beta activated apoptosis in benign hyperplasia and cancer of the prostate is androgen independent and TNFalpha mediated. *Proc Natl Acad Sci U S A* 107: 3123–3128
- McPherson SJ, Wang H, Jones ME, Pedersen J, Iismaa TP, Wreford N, Simpson ER, Risbridger GP (2001) Elevated androgens and prolactin in aromatase-deficient mice cause enlargement, but not malignancy, of the prostate gland. *Endocrinology* 142: 2458–2467
- McVary KT, Razzaq A, Lee C, Venegas MF, Rademaker A, McKenna KE (1994) Growth of the rat prostate gland is facilitated by the autonomic nervous system. *Biol Reprod* 51: 99–107
- Medina P, Segarra G, Vila JM, Domenech C, Martínez-León JB, Lluch S (2000) Effects of sildenafil on human penile blood vessels. *Urology* 56: 539–543
- Mergia E, Russwurm M, Zoidl G, Koesling D (2003) Major occurrence of the new alpha2beta1 isoform of NO-sensitive guanylyl cyclase in brain. *Cell Signal* 15: 189–195
- Miah S, Catto J (2014) BPH and prostate cancer risk. *Indian J Urol* 30: 214–218
- Mietens A, Tasch S, Stammler A, Konrad L, Feuerstacke C, Middendorff R (2014) Time-lapse imaging as a tool to investigate contractility of the epididymal duct--effects of cGMP signaling. *PLoS ONE* 9: e92603
- Mónica FZ, Antunes E (2018) Stimulators and activators of soluble guanylate cyclase for urogenital disorders. *Nat Rev Urol* 15: 42–54
- Müller D, Mukhopadhyay AK, Davidoff MS, Middendorff R (2011) Cyclic GMP signaling in rat urinary bladder, prostate, and epididymis. Tissue-specific changes with aging and in response to Leydig cell depletion. *Reproduction* 142: 333–343
- Murray F, MacLean MR, Pyne NJ (2003) An assessment of the role of the inhibitory gamma subunit of the retinal cyclic GMP phosphodiesterase and its effect on the p42/p44 mitogen-activated protein kinase pathway in animal and cellular models of pulmonary hypertension. *Br J Pharmacol* 138: 1313–1319
- Muto A, Fitzgerald TN, Pimiento JM, Maloney SP, Teso D, Paszkowiak JJ, Westvik TS, Kudo FA, Nishibe T, Dardik A (2007) Smooth muscle cell signal transduction. Implications of vascular biology for vascular surgeons. *J Vasc Surg* 45 Suppl A: A15-24
- Nguyen AT, Gomez D, Bell RD, Campbell JH, Clowes AW, Gabbiani G, Giachelli CM, Parmacek MS, Raines EW, Rusch NJ, Speer MY, Sturek M, Thyberg J, Towler DA, Weiser-

- Evans MC, Yan C, Miano JM, Owens GK (2013) Smooth muscle cell plasticity. Fact or fiction? *Circ Res* 112: 17–22
- Nguyen D-TT, Dey A, Lang RJ, Ventura S, Exintaris B (2011) Contractility and pacemaker cells in the prostate gland. *J Urol* 185: 347–351
- Nicholson TM, Ricke WA (2011) Androgens and estrogens in benign prostatic hyperplasia. Past, present and future. *Differentiation* 82: 184–199
- Nikolova S, Guenther A, Savai R, Weissmann N, Ghofrani HA, Konigshoff M, Eickelberg O, Klepetko W, Voswinckel R, Seeger W, Grimminger F, Schermuly RT, Pullamsetti SS (2010) Phosphodiesterase 6 subunits are expressed and altered in idiopathic pulmonary fibrosis. *Respir Res* 11: 146
- Oh S-J, Kim KM, Chung Y-S, Hong E-K, Shin SY, Kim SJ (2003) Ion-channel currents of smooth muscle cells isolated from the prostate of guinea-pig. *BJU Int* 92: 1022–1030
- Oliver VL, Poulios K, Ventura S, Haynes JM (2013) A novel androgen signalling pathway uses dihydrotestosterone, but not testosterone, to activate the EGF receptor signalling cascade in prostate stromal cells. *Br J Pharmacol* 170: 592–601
- Olumi AF, Grossfeld GD, Hayward SW, Carroll PR, Tlsty TD, Cunha GR (1999) Carcinoma-associated fibroblasts direct tumor progression of initiated human prostatic epithelium. *Cancer Res* 59: 5002–5011
- Ousset M, van Keymeulen A, Bouvencourt G, Sharma N, Achouri Y, Simons BD, Blanpain C (2012) Multipotent and unipotent progenitors contribute to prostate postnatal development. *Nat Cell Biol* 14: 1131–1138
- Parsons JK (2010) Benign Prostatic Hyperplasia and Male Lower Urinary Tract Symptoms. Epidemiology and Risk Factors. *Curr Bladder Dysfunct Rep* 5: 212–218
- Patel ND, Parsons JK (2014) Epidemiology and etiology of benign prostatic hyperplasia and bladder outlet obstruction. *Indian J Urol* 30: 170–176
- Peak TC, Richman A, Gur S, Yafi FA, Hellstrom WJG (2016) The Role of PDE5 Inhibitors and the NO/cGMP Pathway in Cancer. *Sex Med Rev* 4: 74–84
- Peixoto CA, Gomes FODS (2015) The role of phosphodiesterase-5 inhibitors in prostatic inflammation. A review. *J Inflamm (Lond)* 12: 54
- Peuler JD, Phelps LE (2015) Sildenafil does not enhance but rather attenuates vasorelaxant effects of antidiabetic agents. *J Smooth Muscle Res* 51: 22–36

- Pfeifer K, Schaub C, Domsch K, Dorresteyn A, Wolfstetter G (2014) Maternal inheritance of twist and analysis of MAPK activation in embryos of the polychaete annelid *Platynereis dumerilii*. *PLoS ONE* 9: e96702
- Pi M, Parrill AL, Quarles LD (2010) GPRC6A mediates the non-genomic effects of steroids. *J Biol Chem* 285: 39953–39964
- Picut CA, Ziejewski MK, Stanislaus D (2018) Comparative Aspects of Pre- and Postnatal Development of the Male Reproductive System. *Birth Defects Res* 110: 190–227
- Pizzuto DA, Müller J, Mühlematter U, Rupp NJ, Töpfer A, Mortezaei A, Nagel H, Kranzbühler B, Eberli D, Burger IA (2018) The central zone has increased ⁶⁸Ga-PSMA-11 uptake. "Mickey Mouse ears" can be hot on ⁶⁸Ga-PSMA-11 PET. *Eur J Nucl Med Mol Imaging* 45: 1335–1343
- Postovit L-M, Adams MA, Lash GE, Heaton JP, Graham CH (2002) Oxygen-mediated regulation of tumor cell invasiveness. Involvement of a nitric oxide signaling pathway. *J Biol Chem* 277: 35730–35737
- Prins GS, Lindgren M (2015) Accessory Sex Glands in the Male. (In: Plant, T M; Zeleznik, A J: *Knobil and Neill's Physiology of Reproduction*), 4th edn. Elsevier Science. Burlington, USA
- Prins GS, Marmer M, Woodham C, Chang W, Kuiper G, Gustafsson JA, Birch L (1998) Estrogen receptor-beta messenger ribonucleic acid ontogeny in the prostate of normal and neonatally estrogenized rats. *Endocrinology* 139: 874–883
- Qian C-N, Takahashi M, Kahnoski RJ, Teh BT (2003) Effect of sildenafil citrate on an orthotopic prostate cancer growth and metastasis model. *J Urol* 170: 994–997
- Ricke WA, McPherson SJ, Bianco JJ, Cunha GR, Wang Y, Risbridger GP (2008) Prostatic hormonal carcinogenesis is mediated by in situ estrogen production and estrogen receptor alpha signaling. *FASEB J* 22: 1512–1520
- Risbridger GP, Bianco JJ, Ellem SJ, McPherson SJ (2003) Oestrogens and prostate cancer. *Endocr Relat Cancer* 10: 187–191
- Roehrborn CG (2004) Lower urinary tract symptoms, benign prostatic hyperplasia, erectile dysfunction, and phosphodiesterase-5 inhibitors. *Rev Urol* 6: 121–127
- Roehrborn CG (2008) Pathology of benign prostatic hyperplasia. *Int J Impot Res* 20 Suppl 3: S11-8

Roehrborn CG, Schwinn DA (2004) Alpha1-adrenergic receptors and their inhibitors in lower urinary tract symptoms and benign prostatic hyperplasia. *J Urol* 171: 1029–1035

Rommerts FFG, Teerds KJ, Hoogerbrugge JW (1988) In vitro effects of ethylene-dimethane sulfonate (EDS) on Leydig cells. Inhibition of steroid production and cytotoxic effects are dependent on species and age of rat. *Mol Cell Endocrinol* 55: 87–94

Roskoski R (2015) A historical overview of protein kinases and their targeted small molecule inhibitors. *Pharmacological Research* 100: 1–23

Ross MH, Pawlina W (2016) *Histology. A text and atlas : with correlated cell and molecular biology*, 7th edn. Wolters Kluwer. Philadelphia, USA

Saboor F, Reckmann AN, Tomczyk CUM, Peters DM, Weissmann N, Kaschtanow A, Schermuly RT, Michurina TV, Enikolopov G, Müller D, Mietens A, Middendorff R (2016) Nestin-expressing vascular wall cells drive development of pulmonary hypertension. *Eur Respir J* 47: 876–888

Sampson N, Untergasser G, Plas E, Berger P (2007) The ageing male reproductive tract. *J Pathol* 211: 206–218

Schlossmann J, Feil R, Hofmann F (2003) Signaling through NO and cGMP-dependent protein kinases. *Ann Med* 35: 21–27

Seftel AD (2005) Testosterone regulates PDE5 expression and in vivo responsiveness to tadalafil in rat corpus cavernosum. *J Urol* 174: 657–658

Sensibar JA, Pruden SJ, Kasjanski RZ, Rademaker A, Lee C, Grayhack JT, Kozlowski JM (1999) Differential growth rates in stromal cultures of human prostate derived from patients of varying ages. *Prostate* 38: 110–117

Shapiro E, Becich MJ, Hartanto V, Lepor H (1992) The relative proportion of stromal and epithelial hyperplasia is related to the development of symptomatic benign prostate hyperplasia. *J Urol* 147: 1293–1297

Shaw A, Attia S, Bushman W (2008) Prostate stromal and urogenital sinus mesenchymal cell lines for investigations of stromal-epithelial interactions. *Differentiation* 76: 599–605

Shi Y-F, Yu D-J, Jiang C-Y, Wang X-J, Zhu Y-P, Zhao R-Z, Lv Z, Sun X-W (2018) TRAF6 regulates proliferation of stromal cells in the transition and peripheral zones of benign prostatic hyperplasia via Akt/mTOR signaling. *Prostate* 78: 193–201

- Somlyo AP, Somlyo AV (2000) Signal transduction by G-proteins, rho-kinase and protein phosphatase to smooth muscle and non-muscle myosin II. *J Physiol (Lond)* 522 Pt 2: 177–185
- Somlyo AP, Wu X, Walker LA, Somlyo AV (1999) Pharmacomechanical coupling. The role of calcium, G-proteins, kinases and phosphatases. *Rev Physiol Biochem Pharmacol* 134: 201–234
- Spring-Mills E, Hafez ESE (1980) Male accessory sex glands. Biology and pathology. Elsevier/North-Holland Biomedical Press. Amsterdam, Netherlands
- Tong YC, Hung YC, Lin SN, Cheng JT (1996) The norepinephrine tissue concentration and neuropeptide Y immunoreactivity in genitourinary organs of the spontaneously hypertensive rat. *J Auton Nerv Syst* 56: 215–218
- Torre LA, Bray F, Siegel RL, Ferlay J, Lortet-Tieulent J, Jemal A (2015) Global cancer statistics, 2012. *CA Cancer J Clin* 65: 87–108
- Townsley MI (2012) Structure and composition of pulmonary arteries, capillaries, and veins. *Compr Physiol* 2: 675–709
- Tulis DA (2017) Novel protein kinase targets in vascular smooth muscle therapeutics. *Curr Opin Pharmacol* 33: 12–16
- Tuxhorn JA, Ayala GE, Smith MJ, Smith VC, Dang TD, Rowley DR (2002a) Reactive stroma in human prostate cancer. Induction of myofibroblast phenotype and extracellular matrix remodeling. *Clin Cancer Res* 8: 2912–2923
- Tuxhorn JA, McAlhany SJ, Dang TD, Ayala GE, Rowley DR (2002b) Stromal cells promote angiogenesis and growth of human prostate tumors in a differential reactive stroma (DRS) xenograft model. *Cancer Res* 62: 3298–3307
- Tyekucheva S, Bowden M, Bango C, Giunchi F, Huang Y, Zhou C, Bondi A, Lis R, van Hemelrijck M, Andrén O, Andersson S-O, Watson RW, Pennington S, Finn SP, Martin NE, Stampfer MJ, Parmigiani G, Penney KL, Fiorentino M, Mucci LA, Loda M (2017) Stromal and epithelial transcriptional map of initiation progression and metastatic potential of human prostate cancer. *Nat Commun* 8: 420
- Uckert S, Kütke A, Jonas U, Stief CG (2001) Characterization and functional relevance of cyclic nucleotide phosphodiesterase isoenzymes of the human prostate. *J Urol* 166: 2484–2490

- Uckert S, Oelke M, Stief CG, Andersson K-E, Jonas U, Hedlund P (2006) Immunohistochemical distribution of cAMP- and cGMP-phosphodiesterase (PDE) isoenzymes in the human prostate. *Eur Urol* 49: 740–745
- Uckert S, Sormes M, Kedia G, Scheller F, Knapp WH, Jonas U, Stief CG (2008) Effects of phosphodiesterase inhibitors on tension induced by norepinephrine and accumulation of cyclic nucleotides in isolated human prostatic tissue. *Urology* 71: 526–530
- Ückert S, Waldkirch ES, Merseburger AS, Kuczyk MA, Oelke M, Hedlund P (2013) Phosphodiesterase type 5 (PDE5) is co-localized with key proteins of the nitric oxide/cyclic GMP signaling in the human prostate. *World J Urol* 31: 609–614
- van Asseldonk B, Barkin J, Elterman DS (2015) Medical therapy for benign prostatic hyperplasia. A review. *Can J Urol* 22 Suppl 1: 7–17
- van der Staay FJ, Rutten K, Bärfacker L, Devry J, Erb C, Heckroth H, Karthaus D, Tersteegen A, van Kampen M, Blokland A, Prickaerts J, Reymann KG, Schröder UH, Hendrix M (2008) The novel selective PDE9 inhibitor BAY 73-6691 improves learning and memory in rodents. *Neuropharmacology* 55: 908–918
- Wang G, Jacquet L, Karamariti E, Xu Q (2015a) Origin and differentiation of vascular smooth muscle cells. *J Physiol (Lond)* 593: 3013–3030
- Wang L, Zhang X, Wang G, Visweswariah SS, Lin G, Xin Z, Lue TF, Lin C-S (2015b) Lobe-specific expression of phosphodiesterase 5 in rat prostate. *Urology* 85: 703.e7-13
- Wang L, Zoetemelk M, Chitteti BR, Ratliff TL, Myers JD, Srour EF, Broxmeyer H, Jerde TJ (2015c) Expansion of prostate epithelial progenitor cells after inflammation of the mouse prostate. *Am J Physiol Renal Physiol* 308: F1421-30
- Wang W, Chen Z-X, Guo D-Y, Tao Y-X (2018) Regulation of prostate cancer by hormone-responsive G protein-coupled receptors. *Pharmacol Ther*
- Wang X, Kruithof-de Julio M, Economides KD, Walker D, Yu H, Halili MV, Hu Y-P, Price SM, Abate-Shen C, Shen MM (2009) A luminal epithelial stem cell that is a cell of origin for prostate cancer. *Nature* 461: 495–500
- Watts K, Li J, Magi-Galluzzi C, Zhou M (2013) Incidence and clinicopathological characteristics of intraductal carcinoma detected in prostate biopsies. A prospective cohort study. *Histopathology* 63: 574–579
- Wedel B, Garbers D (2001) The guanylyl cyclase family at Y2K. *Annu Rev Physiol* 63: 215–233

- Wen S, Chang H-C, Tian J, Shang Z, Niu Y, Chang C (2015) Stromal androgen receptor roles in the development of normal prostate, benign prostate hyperplasia, and prostate cancer. *Am J Pathol* 185: 293–301
- Wen X-H, Dizhoor AM, Makino CL (2014) Membrane guanylyl cyclase complexes shape the photoresponses of retinal rods and cones. *Front Mol Neurosci* 7: 45
- Wistuba J, Schrod A, Greve B, Hodges JK, Aslam H, Weinbauer GF, Luetjens CM (2003) Organization of seminiferous epithelium in primates. Relationship to spermatogenic efficiency, phylogeny, and mating system. *Biol Reprod* 69: 582–591
- Wolfe L, Corbin JD, Francis SH (1989) Characterization of a novel isozyme of cGMP-dependent protein kinase from bovine aorta. *J Biol Chem* 264: 7734–7741
- Wolfertstetter S, Huettner JP, Schlossmann J (2013) cGMP-Dependent Protein Kinase Inhibitors in Health and Disease. *Pharmaceuticals (Basel)* 6: 269–286
- Wong YC, Wang XH, Ling MT (2003) Prostate development and carcinogenesis. *Int Rev Cytol* 227: 65–130
- Wu Q, Shi J, Chen L, Wang C-Y, Park I, Lee C, Zhang J (2008) Regulation of proliferation and differentiation of prostatic stromal cells by oestradiol through prostatic epithelial cells in a paracrine manner. *BJU Int* 101: 497–502
- Yamada S, Tanaka C, Kimura R, Kawabe K (1994) Alpha1-adrenoceptors in human prostate. Characterization and binding characteristics of alpha1-antagonists. *Life Sciences* 54: 1845–1854
- Yamamura H, Hirano N, Koyama H, Nishizawa Y, Takahashi K (2007) Loss of smooth muscle calponin results in impaired blood vessel maturation in the tumor-host microenvironment. *Cancer Sci* 98: 757–763
- Yao Q, Renault M-A, Chapouly C, Vandierdonck S, Belloc I, Jaspard-Vinassa B, Daniel-Lamazière J-M, Laffargue M, Merched A, Desgranges C, Gadeau A-P (2014) Sonic hedgehog mediates a novel pathway of PDGF-BB-dependent vessel maturation. *Blood* 123: 2429–2437
- Zeng J, He R-Q, Mo W-G, Peng Z-G, Ma J, Zhong J-C, Mo C-H, Qin M-J, Hu X-H (2018) Inflammatory myofibroblastic tumor of the prostate after transurethral resection of the prostate with negative expression of anaplastic lymphoma kinase. A case report. *Sao Paulo Med J*: 0

- Zenzmaier C, Kern J, Sampson N, Heitz M, Plas E, Untergasser G, Berger P (2012) Phosphodiesterase type 5 inhibition reverts prostate fibroblast-to-myofibroblast trans-differentiation. *Endocrinology* 153: 5546–5555
- Zenzmaier C, Sampson N, Pernkopf D, Plas E, Untergasser G, Berger P (2010) Attenuated proliferation and trans-differentiation of prostatic stromal cells indicate suitability of phosphodiesterase type 5 inhibitors for prevention and treatment of benign prostatic hyperplasia. *Endocrinology* 151: 3975–3984
- Zhan X, Li D, Johns RA (1999) Immunohistochemical evidence for the NO cGMP signaling pathway in respiratory ciliated epithelia of rat. *J Histochem Cytochem* 47: 1369–1374
- Zhang H, Frederick JM, Baehr W (2014) Unc119 gene deletion partially rescues the GRK1 transport defect of Pde6d (-/-) cones. *Adv Exp Med Biol* 801: 487–493
- Zhang W, Zang N, Jiang Y, Chen P, Wang X, Zhang X (2015) Upregulation of Phosphodiesterase type 5 in the Hyperplastic Prostate. *Sci Rep* 5: 17888

11 Publications, talks and posters

11.1 Paper

Kügler R, Mietens A, Seidensticker M, Tasch S, Wagenlehner FM, Kaschtanow A, Tjahjono Y, Tomczyk CU, Beyer D, Risbridger GP, Exintaris B, Ellem SJ, Middendorff R. 2018. **Novel imaging of the prostate reveals spontaneous gland contraction and excretory duct quiescence together with different drug effects.** FASEB journal: official publication of the Federation of American Societies for Experimental Biology: fj201700430R.

11.2 Talk

Kügler R. **PDE5 regulation in the prostate: relax your way to prostatic health.** 10th Annual Conference of the International Giessen Graduate Centre for the Life Sciences 2017. Sept 27-28. Giessen

11.3 Poster

Seidensticker M, Kügler R, Mietens A, Tasch S, Wagenlehner FM, Risbridger G, Exintaris B, Ellem S.J, Middendorff R. **Visualization of PDE5 inhibitor effects in prostate tissue: no evidence for disturbances of ejaculation.** 10th Annual Conference of the International Giessen Graduate Centre for the Life Sciences 2017. Sept 27-28. Giessen

Kügler R, Müller D, Tasch S, Tjahjono Y, Kaschtanow A, Mietens A, Wagenlehner FM, Ellem S, Risbridger G, Middendorff R. **PDE5 in smooth muscle cells of the prostate: different regulation in glands and vasculature.** 9th Annual Conference of the International Giessen Graduate Centre for the Life Sciences 2016. Sept 20-21. Giessen

Kügler R, Müller D, Tasch S, Tjahjono Y, Kaschtanow A, Mietens A, Wagenlehner FM, Ellem S, Risbridger G, Middendorff R. **Androgen-dependent regulation of cGMP pathways in a subpopulation of prostatic smooth muscle cells.** 110th Annual Meeting of the Anatomic Society 2015. Sept 23-25. Würzburg